Chem Soc Rev

REVIEW ARTICLE

View Article Online
View Journal | View Issue

Cite this: *Chem. Soc. Rev.*, 2014, **43**, 7681

Mesoporous materials for clean energy technologies

Noemi Linares,[a] Ana M. Silvestre-Albero,[b] Elena Serrano,[a] Joaquín Silvestre-Albero*[b] and Javier García-Martínez*[a]

Received 29th November 2013

DOI: 10.1039/c3cs60435g

www.rsc.org/csr

Alternative energy technologies are greatly hindered by significant limitations in materials science. From low activity to poor stability, and from mineral scarcity to high cost, the current materials are not able to cope with the significant challenges of clean energy technologies. However, recent advances in the preparation of nanomaterials, porous solids, and nanostructured solids are providing hope in the race for a better, cleaner energy production. The present contribution critically reviews the development and role of mesoporosity in a wide range of technologies, as this provides for critical improvements in accessibility, the dispersion of the active phase and a higher surface area. Relevant examples of the development of mesoporosity by a wide range of techniques are provided, including the preparation of hierarchical structures with pore systems in different scale ranges. Mesoporosity plays a significant role in catalysis, especially in the most challenging processes where bulky molecules, like those obtained from biomass or highly unreactive species, such as CO_2 should be transformed into most valuable products. Furthermore, mesoporous materials also play a significant role as electrodes in fuel and solar cells and in thermoelectric devices, technologies which are benefiting from improved accessibility and a better dispersion of materials with controlled porosity.

1. Introduction

Renewable energy technologies hold the promise to meet the increasing energy demands of a 7 billion people planet without depleting our natural resources and compromising the quality of our environment.[1] Despite the significant growth of clean energy technologies observed in recent years, they are still far from reaching their full potential as in many cases they suffer from low yields, high cost, material scarcity, poor robustness, or challenging scalability.

Many of these challenges are being overcome thanks to the ingenuity and creativity of chemists, materials scientists and nanotechnologists, who are developing new materials and reinventing old ones by modifying their structure, size, morphology, surface chemistry and porosity.[2–4] Among the material science contributions which are providing some of the most significant advances in energy applications, we are covering here the development and role of mesoporosity, highlighting both new techniques to introduce controlled mesoporosity in solids and their application in a wide range of energy technologies.

Porous solids are ubiquitous due to their many advantages such as a large surface area, an enhanced accessibility and the ability to anchor different chemical functionalities on their surface. The use of molecular and supramolecular templates, especially surfactants, has been one of the most successful strategies for the production of materials with a controlled porosity.[5] Since the discovery of MCM-41, a myriad of surfactant-templated solids has populated the research efforts of many groups, dealing with their synthesis, characterization and application. Some of the main advantages of this methodology are: their versatility, robustness, simplicity and ability to produce very complex and interconnected porous structures. Sol–gel chemistry techniques are typically used in combination with different surfactants to produce a wide variety of porous metal oxides. Both soft templates, such as surfactant and polymers and hard templates such as carbon and metal oxides and carbonates which can be burned-off or easily dissolved at a certain pH, have being extensively used to introduce controlled mesoporosity in a wide variety of solids. The combination of these strategies has yielded new hierarchical materials whose unique porous structures provide significant advantages, many of them described in this review.[6]

The control and/or modification of the surface chemistry of porous materials is a critical step in the synthesis of advanced materials for energy applications.[7] The right surface polarity is

[a] *Laboratorio de Nanotecnología Molecular, Departamento de Química Inorgánica, Universidad de Alicante, Ap. 99, E-03080 Alicante, Spain. E-mail: j.garcia@ua.es; Fax: +34965903454; Tel: +34965903400x2372*

[b] *Laboratorio de Materiales Avanzados, Departamento de Química Inorgánica-Instituto Universitario de Materiales, Universidad de Alicante, Ap. 99, E-03080 Alicante, Spain. E-mail: joaquin.silvestre@ua.es; Fax: +34965903454; Tel: +34965909350x2226*

needed for the good wettability of the electrode with the electrolyte solution, and for the good contact between the catalyst and the reaction solution. In other cases, more complex surface modification is needed. For example, the introduction of complex chemical species, such as dyes, on the surface of nanoparticles, is typically carried out in the preparation of dye-sensitized solar cells.

More recently, a novel strategy has been described to introduce a wide variety of chemical functionalities in porous solids, ranging from metal complexes to nanoparticles, clusters and homogenous catalysts. This has been possible thanks to the combination of surfactant-template and sol–gel chemistry techniques.[8] Ranging from gains in accessibility, a higher surface area and enhanced yields to improved selectivity, the precise control over the pore structure and surface chemistry of mesoporous materials is having a major impact on the performance of a wide range of energy technologies, as described in some detail in this review.

Noemi Linares

Noemi Linares obtained her PhD Degree in 2010 at the Molecular Nanotechnology Lab in the University of Alicante (Spain), under the supervision of Prof. García-Martínez. After her dissertation, she moved to Florence (Italy) for a postdoctoral fellow at the ICCOM-CNR, where she was working under the ITN NANO-HOST on the immobilization of homogeneous catalysts in nanostructured materials, mainly for the synthesis of fine-chemicals under flow conditions. In May 2013, she came back to the Molecular Nanotechnology Lab to work on the synthesis of nanostructured solids with different functionalities incorporated in their structure, mainly for energetic applications (H_2 storage, water-gas shift reaction, biomass valorization).

Ana M. Silvestre-Albero

Ana M. Silvestre Albero obtained her PhD Degree in 2010 working on the preparation and characterization of Pt catalysts supported on micro-mesoporous materials to ethanol combustion reaction in the group of Prof. Rodríguez-Reinoso. Since 2012, she has been working as a researcher at the University of Alicante. Her research interests include the preparation and characterization of micro-mesopores materials, environmental pollution control, CO_2 storage, the catalytic epoxidation reaction and catalytic combustion of VOCs. She is the co-author of more than 20 peer-reviewed manuscripts.

Elena Serrano

Elena Serrano obtained her PhD in 2006 at the University of Basque Country (Spain) working on the nanostructuration of functional materials. She carried out her post-doctoral activity in collaboration with Arkema at the National Institute of Applied Sciences (INSA) at Lyon (France). In 2009, she joined the Molecular Nanotechnology Lab at the University of Alicante as a Research Fellow. Her current research interests are in the area of new synthetic pathways to prepare heterogeneous catalysts by the self-assembly of functional materials (metal nanoparticles, metal complexes, etc.), based on silica and titania materials for photocatalytic applications, where she has published extensively.

Joaquín Silvestre-Albero

Joaquín Silvestre-Albero, born 1976, studied chemistry in Alicante, Spain, where he completed his PhD thesis in 2003 in the group of Prof. Rodríguez-Reinoso. Then, he spent one-year in the group of Prof. Corma at ITQ, Valencia (Spain), and two more years at the Fritz-Haber-Institute, Berlín (Germany), in the group of Prof. Freund. In 2006, he moved back to the University of Alicante where he is now Associate Professor for Inorganic Chemistry. His interests range from materials science, adsorption processes, nanotechnology, heterogeneous catalysis and nanomedicine. His scientific work has been published in more than 75 peer-reviewed manuscripts, 4 book chapters and several patent applications have been filled in the last few years. Joaquín Silvestre-Albero has received several awards including the Alexander von Humboldt Stiftung. He has been Visiting Professor at the Vienna University of Technology (Austria), Universidad de los Andes (Colombia) and Universidad Nacional de San Luis (Argentina).

2. New mesoporous materials with unique properties

2.1. Nanostructured mesoporous materials

Twenty years after the pioneering work of Mobil's research on the synthesis and characterization of a new class of porous materials, the M41S family,[9] the literature about mesoporous materials has proliferated explosively. Since the early nineties, when the first Kresge *et al.*[9a] article was published, the investigations into mesoporous materials have continuously grown resulting in a new independent research area, closely related to zeolites and microporous materials. Proof of the interest that nanostructured mesoporous materials now generate can be found in the number of publications in this field: 6000 papers included the words *mesoporous materials* in the 'Web of Science' database in the year 2012, besides the numerous special issues, conferences, books and patents, that every year add to the accumulated knowledge of the subject. For all these reasons, it is clear that in this section we can only give a short summary of mesoporous materials, emphasizing the benefit that these materials can bring to renewable related technologies. For a more in-depth examination of the synthesis of mesoporous materials, readers are kindly directed to ref. 10–16 and to the themed issue about Mesoporous Materials that *Chemical Society Reviews* recently published to coincide with the 20th anniversary of this new material family.[17]

According to IUPAC, mesoporous materials are those possessing pore dimensions between 2 and 50 nm. That is, between micropores and macropores in size (the Greek prefix meso- means 'in between').[18] Initially, the aim of developing these materials was to overcome the '1 nm restriction' that the use of zeolites imposes.[5]

Javier García-Martínez

Javier García-Martínez is the Director of the Molecular Nanotechnology Lab at the University of Alicante, Spain. He has published extensively in the areas of nanomaterials, catalysis and energy and is the inventor of more than 25 patents. His latest books are Nanotechnology for the Energy Challenge (Wiley, 2013) and The Chemical Element (Wiley, 2011). He is the founder and chief scientist of Rive Technology, Inc. (Boston, MA), a venture capital-funded Massachusetts Institute of Technology (MIT) spin-off commercializing nanostructured catalysts for energy applications. He has received the Europe Medal in 2005, the Silver Medal of the European Young Chemist Award in 2006, and the TR 35 Award from MIT's Technology Review magazine; in 2009, he was selected as a Young Global Leader. Since 2010, he has been a member of the World Economic Forum Council on Emerging Technologies. He is a Fellow of the Royal Society of Chemistry, a member of the Global Young Academy and a Bureau member of the IUPAC.

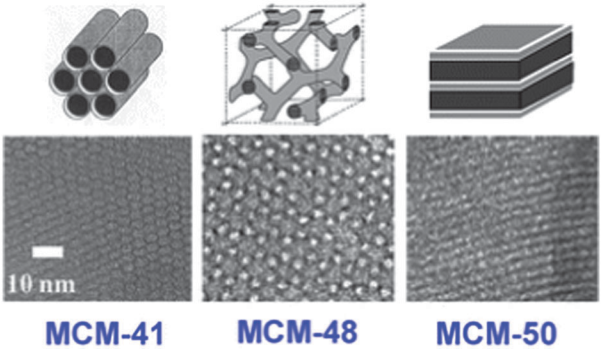

Fig. 1 Different structures of the M41S family: (top) surfactant supramolecular assemblies and (bottom) TEM images of the final materials. Reproduced from ref. 5. Copyright 2013, RSC.

Theoretically, using materials with similar features to zeolites (acidity, regular pore size, high BET surface area) but with larger pores could open the door to processing large molecules that are unable to enter into a zeolite porous framework.

The synthesis of nanostructured mesoporous solids is based on the supramolecular templating approach, where long chain organic surfactants are used as structure-directing agents (SDA) or templates. The assembly of these surfactant molecules in the presence of a silica precursor leads to a composite mesostructure during the condensation of the silica network. The subsequent removal of the surfactant gives a mesoporous material with porous systems replicating the surfactant's assembly, see Fig. 1. This method generates solids with narrow pore size distributions, high BET surface areas ($\sim$1000 $m^2\ g^{-1}$) and a tuneable pore size (depending on the surfactant used). Moreover, it can be applied to the synthesis of a great number of different solids, inorganic, organic–inorganic hybrids and organic solids.[10]

The M41S family was originally prepared employing cationic surfactants (S^+) at high pH, where the silicate species are negatively charged (I^-), and the electrostatic interaction (S^+I^-) is responsible for the silica structuration. Since the discovery of this approach, other synthetic pathways have been employed to prepare mesoporous materials in a wide range of pHs, temperatures and surfactant types (anionic (S^-), neutral (S^0/N^0)). Moreover, the mesoporous materials family has been extended from the initial silica and silica/alumina solids to a huge number of other inorganic oxides. Some examples of these types of material, along with the synthetic pathways employed for their structuration, are shown in Table 1.

Even if these materials did not accomplish the task for which they were initially conceived, which was to replace zeolites in different applications (mainly in petrochemistry), since they do not have the high catalytic activity of zeolites or their hydrothermal stability, the applications in which mesoporous materials are currently used have become countless. They are used in catalysis (as catalysts or supports), adsorption, pollutant remediation, sensors, drug delivery systems and, more related to the present review topic, photocatalysis, solar cells, fuel cells and batteries.[10] The flexibility of the templating methods permits the synthesis of materials with a controlled

Table 1 The synthetic pathways of different inorganic nanostructured materials: interaction types, examples and references

Surfactant type	Interaction type	Inorganic solids	Ref.
Cationic S^+	S^+I^-	SiO_2: M41S	9
		WO_3	19
		Sb_2O_5	19*a*
		SnS_2	19*a*, 20
	$S^+X^-I^+$	SiO_2: SBA-1, SBA-2, SBA-3	19*a*, 21
		SnO_2	22
		$ZnPO_4$	19*a*
Anionic S^-	S^-I^+	Mg, Al, Ga, Mn, Fe, Co, Ni, Zn, Pb oxides	19*a*
	$S^-M^+I^-$	Silica: AMS (using a co-structure directing agent)	23
		ZnO, Al_2O_3	19*a*
Neutral N^0/S^0	S^0I^0	HMS	24
		ZrO_2	25
		SnO_2	26
		CdS, CdSe, SnS_2, Sb_2S_3	27
	$(S^0H^+)(X^-I^+)$	SiO_2: SBA-15	28
		TiO_2, ZrO_2, Al_2O_3, Nb_2O_5, Ta_2O_5, WO_3, HfO_2, SnO_2, and mixed oxides	29
	N^0I^0	SiO_2: MSU-X	30
		γ-Al_2O_3	31

pore size and structure, controlled wall compositions and highly interconnected surface areas, all of which allow the optimisation of the material for the specific application required.

In energy related devices, nanostructured materials have attracted much attention because of their unique properties compared to bulk materials.[10] Especially relevant is the case of mesoporous transition metal oxides, which can confine d-electrons to the walls between the pores, endowing such materials with unusual magnetic, electrochemical and optical properties.[15,32] For example, mesoporous SnO_2 materials show a drastic reduction of dielectrics compared to bulk SnO_2 and these unique optical and electrical properties can extend their applications to gas sensors, optoelectronics and as electrodes in solid-state ionic devices.[33] Mesoporous TiO_2 presents a much higher photocatalytic activity due to its higher surface area;[34] mesoporous $Nb_2O_5{\cdot}nH_2O$ shows improved efficiency for the hydrolysis of cellobiose than super-microporous and bulk $Nb_2O_5{\cdot}nH_2O$;[35] mesoporous versions of α-Fe_2O_3 exhibit enhanced lithium-ion storage capabilities and excellent cycling stabilities.[36] These are not isolated cases, there are many other examples where the incorporation of mesoporosity in an inorganic solid brings new (or improved) properties that can expand the traditional applications of the material and make them, in many cases, ideal for energy technologies.[7] This will be thoroughly discussed in the following sections.

2.2. Hierarchical materials

Hierarchical porous materials contain porous systems at two or three different scales in an ordered structure with interconnectivity between the pores. Interest in this kind of materials is growing rapidly due to their practical potential in different areas from nanoscience to catalysis, separation, electronics, optics, opto-electronics, energy, environmental and life science.[37]

In the catalytic field, these materials can improve the performance of materials with only one type of porosity. For example, the incorporation of mesoporosity in zeolites, usually with micropores <1 nm, improves the diffusion of compounds within their pores and the size of molecules that can be catalyzed.[38] This is a subject of enormous interest, mainly due to the improvements in fluid catalytic cracking (FCC) that can be obtained from the incorporation of mesoporosity into zeolites, while maintaining their other features. Different reviews in this topic can be found elsewhere.[39] In summary, two main approaches have been employed to incorporate mesopores into zeolites: (1) top-down techniques that involve the removal of one of the two main components of zeolites, *i.e.* silica (*e.g. via* desilication by treatment in alkaline solutions)[40] or alumina (*e.g. via* dealumination by steaming at high temperatures or by chemical treatments),[41] and (2) bottom-up procedures that utilize soft[42,43] or hard[44] templates (*e.g.* surfactants, inorganic sacrificial materials, *etc.*). Fig. 2 shows a scheme of the different synthetic approaches to prepare mesoporous zeolites.

Regardless of the preparation method, the improved diffusion and accessibility to active sites of mesoporous zeolites results in higher catalytic activities and longer lifetimes than traditional microporous zeolites.[39a] Moreover, the incorporation of mesoporosity increases the selectivity of primary products, due to the shortening of contact time. Ying and García-Martínez have patented,[45] published[46] and more recently commercialized,[47,48] the first

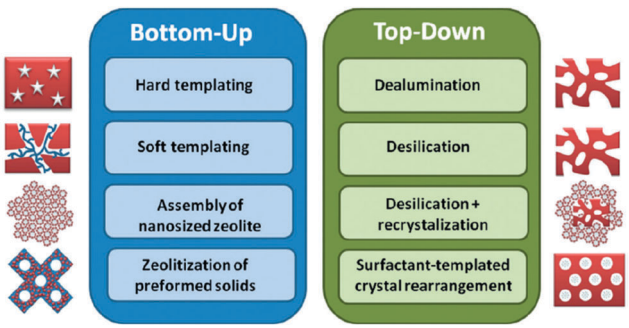

Fig. 2 Different synthetic approaches to prepare hierarchical zeolites. Reproduced with permission from ref. 48. Copyright 2013, Wiley-VCH.

method to introduce mesoporosity into Y zeolites with low Si/Al ratios, which are relevant to catalytic cracking, based on a new top-down approach using surfactant-templated crystal rearrangement, see Fig. 2. The mesostructured zeolite Y demonstrated excellent hydrothermal stability, which is critical to such applications. The testing of FCC catalysts made from mesostructured zeolite Y showed a significantly improved selectivity in product yields (more transportation fuels, *i.e.* gasoline and light cycle oil (LCO), and less coke, dry gases and uncracked residues).

With regard to renewable energy, these hierarchical zeolites can be very useful in bio-oil upgrading. Bio-oils produced from the pyrolysis of biomass are very inexpensive renewable liquid fuels. However, the fuel quality of the bio-oils is inferior to that of petroleum-based fuels and, in order to be used as replacements or supplements for fossil diesel or gasoline, they require upgrading treatment.[49] This is mainly due to the high oxygen and unsaturated content that these fuels present which, consequently, causes a low stability over time and a low heating value.[50]

The hydro-processing of bio-oil reduces both the oxygen and unsaturated content, making hydrodeoxygenation a promising method for bio-oil upgrading.[51] As in FCC, the upgrading of bio-oil in zeolites can be limited by the zeolite restricted pore size (<1 nm) since the process involves bulky reactants products.[52] With this in mind, Fang and co-workers[53] recently prepared a mesoporous ZSM-5 with wormhole like intracrystalline mesopore channels by a bottom-up approach using a dual template. That is, the typical microporous template for ZSM-5, tetrapropylammonium hydroxide (TPAOH), and a mixture of mesoporous templates such as, octyldimethyl-ammonium chloride (TPOAC) and cetyl trimethylammonium bromide (CTAB). The mesoporous zeolite was used to support Pt and its catalytic performance was evaluated in a dibenzofuran hydrodeoxygenation reaction, as a model bio-oil compound. This hierarchical material showed a better catalytic performance than Pt/ZSM-5 and Pt/Al_2O_3 due to the combination of a high acidity and easily accessible mesopore channels.

On another scale, the incorporation of macropores into mesoporous architectures also minimises diffusion barriers and may enhance the distribution of the active sites during catalyst preparation.[39a] The synthetic procedures of macro/mesoporous materials involve: (1) the combination of a supermolecular assembly of amphiphilic polymers or surfactants with second surfactant systems or with macrotemplates such as solid particles, liquid drops and air bubbles or (2) a single templating method combined with a supplementary chemical or physical method (chemical etching, chemical modification, physical deposition, and physical leaching, *etc.*).[54]

There are multiple instances where the use of macro/mesoporous materials enhances the catalytic properties of the material. Certain organic transformations of hierarchical materials result in more active and selective processes than their mesoporous counterparts. Some representative examples include single-site Ti-containing hierarchical macro/mesoporous silica, which displays higher catalytic activities for the epoxidation of linear α-olefins compared to Ti-containing mesoporous silica without macropores (the reaction rate is enhanced with increasing alkyl chain length of linear α-olefins).[55] Pd supported on macro/mesoporous TiO_2 monolith (7 nm mesopores and 2.5 μm macropores) exhibits better productivity (twice as good) and excellent durability in catalytic hydrogenation reactions under continuous flow conditions than its mesoporous counterpart (7 nm mesoporous). This is probably due to a smaller pressure drop, a higher mass transfer and more uniform residence time for reactants throughout the hierarchical material.[56] Finally, SAPO-34, a microporous alumina phosphate silicate zeolite, can be synthesised in a monolith form with 4 nm mesopores and bimodal 1 and 6 μm macropores, and shows a higher catalytic activity and stability than the conventional SAPO-34 in the catalytic conversion of methanol to light olefins.[57]

This enhancement in the performance of hierarchical materials holds true for other properties as well. For example, since macropores have comparable dimensions to the wavelength of visible and UV light, their incorporation into porous materials can aid light scattering within them.[39a] As a result, greater light scattering and harvesting can amplify the photocatalytic efficiency, a fact which has been proven in different studies. For instance, hierarchical materials with flower-like morphologies (see Fig. 3), made up of mesoporous located within the nanosheets, and larger macro/mesoporous in the spacing between consecutive nanosheets, have been synthesized for photocatalytic applications. These solids have demonstrated superior photocatalytic activities, when compared with homologous mesoporous materials.

In Fig. 3, a 3D *in situ* N-doped $(BiO)_2CO_3$ flower-like architecture is shown. This material was proved to be an efficient photocatalyst in the removal of NO in indoor air under both visible light and UV irradiation, with a higher activity than the material in particulate form.[58] Other examples of the photocatalytic enhancement in hierarchical materials are, a TiO_2 with a chrysanthemum-like morphology which has recently been reported to have a higher photoactivity for the degradation of methylene blue than the same material after grinding,[59] and macro/mesoporous ZnO double-pyramids synthesised by an ultrasound-assisted approach that present a better photocatalytic activity in the degradation of organic dyes than irregular ZnO.[60]

Another application in which hierarchical materials have shown a superior performance over other morphologies is in energy storage technologies. Low density, ultraporous 3D nanoarchitectures combine a high surface area for heterogeneous reactions with a continuous and hierarchical porous network for rapid molecular flux. They therefore present the appropriate electronic, ionic,

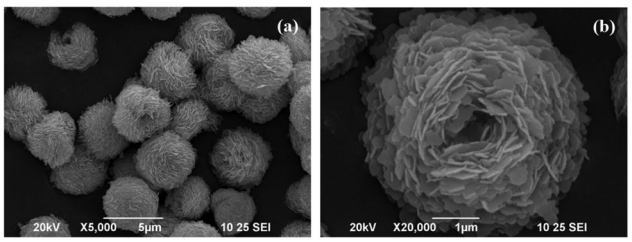

Fig. 3 SEM images of bismuth subcarbonate with a flower-like morphology. Reproduced from ref. 58*b* with permission from The Royal Society of Chemistry.

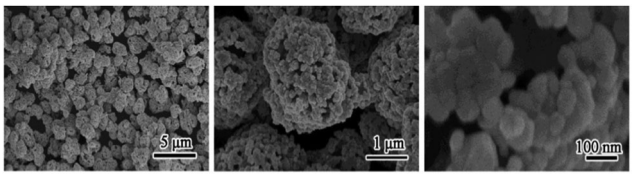

Fig. 4 The SEM images of porous NiO hollow microspheres at different magnifications. Reprinted with permission from ref. 63. Copyright 2013, Elsevier.

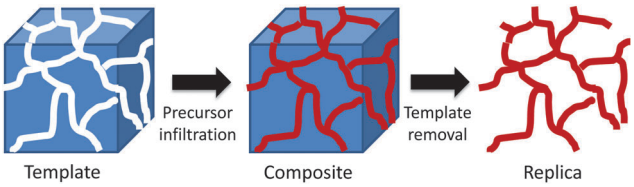

Fig. 5 A schematic representation of the nanocasting pathway using a 3D-interconnected hard template.

and electrochemical requirements for, among other uses, Li-ions batteries, supercapacitors and solar thermal storage systems. Excellent reviews about hierarchical materials for energy conversion and storage[61] and specifically for lithium batteries,[62] have recently been published.

Regarding Li-ion batteries (LIBs), their desired performance characteristics can have opposing requirements with the micro/nano-structure of electrodes. This problem can be solved using hierarchically designed electrodes, tailored to satisfy these conflicting requirements. For instance, novel porous NiO hollow microspheres prepared by an ultrasound-assisted template-free route and composed of loosely packed nanoparticles with diameters around 30–80 nm, see Fig. 4, showed an enhanced electrochemical performance when evaluated as an anode material for LIBs. Their good lithium-storage performance can be attributed to their unique porous architecture, which provides the structural flexibility for volume change and the routes for fast Li^+ diffusion.[63]

Many other hierarchical materials have been used in energy storage applications; indeed it is one of the most interesting applications of such materials. Transition-metal oxides have exhibited a high capacity for reversible lithium storage[64] while structured carbon materials show an excellent performance as supercapacitor electrodes.[65] The impressive potential of hierarchical materials in energy storage devices will be carefully reviewed later on.

2.3. Nanocasted mesoporous materials

Whilst their attractions are obvious, there are some limitations to the use of soft templates for the synthesis of transition metal mesoporous oxides. The hydrolysis and condensation of transition metal alkoxides is not as easy to control as that of silicon alkoxides. For this reason, non-siliceous mesoporous materials prepared *via* direct templating show, in most cases, low order, low crystallinity and poor stability.[66] One strategy that can overcome these limitations is nanocasting. Nanocasting is a procedure where nanoscale moulds are used to prepare solids replicating those moulds. Fig. 5 shows a schematic representation of the nanocasting procedure. A 3D-interconnected porous solid is used as a hard template and the desired material is synthesised in its porous system using a suitable precursor and the necessary chemistry. Once the solid is prepared, the removal of the hard template gives the required porous material as a negative replica of the initial template. For a more comprehensive revision of the synthetic methods and applications of these nanocasted solids, readers are directed to ref. 67.

Following this approach, and with the appropriate experimental conditions, the nanocasting of carbons and metal oxides into meso- and macro/mesoporous silicas has been extensively studied, while nanocasting of metals is less common.[68] Nanocasting offers a different way to prepare mesoporous and hierarchical materials, but the applications of the resulting materials are the same as have been mentioned above. Next some examples of nanocasted mesoporous solids used for energy applications are shown.

As has been already mentioned, structured porous carbons are one of the most interesting materials for energy storage. Their excellent chemical, mechanical and thermal stability, coupled with good conductivity and a high surface area, makes them ideal electrode materials for supercapacitors or batteries. A typical application of hierarchically porous carbon in LIBs was shown by Stein and co-workers (Fig. 6).[69] They used a two-step procedure to synthesise hierarchically structured carbon monoliths. Firstly, a hierarchical silica monolith was prepared using poly(methyl methacrylate) (PMMA) colloids as templates for the macropores and silicate/poly(oxyethylene) surfactant solutions as precursors for the mesoporous walls. Once calcined, the macro/mesoporous silica monolith was used as a silica template to produce carbon monoliths with similar structural hierarchy by a nanocasting procedure. The resulting carbon monoliths maintained the open, interconnected macropore structure of the preform and the mesoporosity of the skeleton, which provided a high surface area >1200 $m^2\ g^{-1}$ to the material. Next, more graphitic, nitrogen-doped carbon was introduced into the mesopores *via* CVD, producing a monolithic nanocomposite material, 3DOM/m C/C (not shown in Fig. 6). This composite material was more resistant to forming a solid–electrolyte interface layer and had a greater lithium capacity at high charge and discharge rates, when compared to the same material without template mesopores and walls consisting only of amorphous carbon.

Regarding transition metal oxides, among the different oxides studied, cobalt oxide has demonstrated an excellent electrochemical performance in terms of specific capacity and

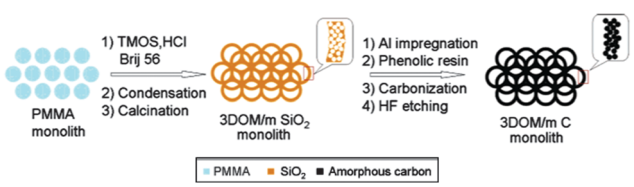

Fig. 6 A diagram of the synthesis procedure of the 3D ordered carbon monolith. Reprinted with permission from ref. 69. Copyright 2006, American Chemical Society.

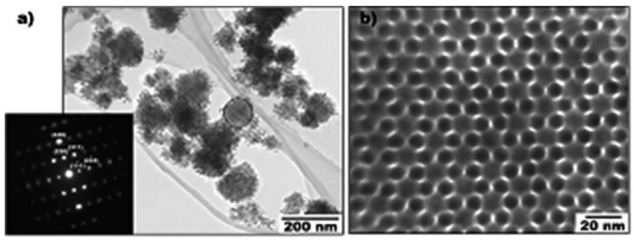

Fig. 7 TEM images at low (a) and high (b) magnifications of KIT-6 mesoporous Co_3O_4, showing highly ordered mesopores. The inset is the corresponding SAED pattern of the circled zone. Reprinted with permission from ref. 72. Copyright 2010, Wiley-VCH.

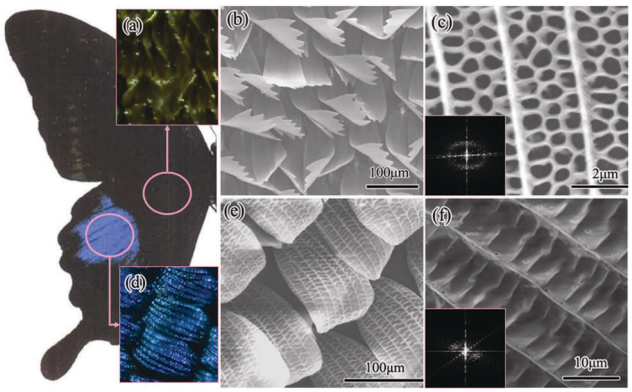

Fig. 8 Nature picture and low-magnification optical microscopy, low-magnification FE-SEM images and high-resolution FE-SEM images showing the wing of the blue male (a–c) and black male (d–f). The insets in the lower left-hand (c, f) corner show the two-dimensional, logarithmic Fourier power spectra of square areas selected from the images. Reprinted with permission from ref. 77. Copyright 2009, American Chemical Society.

cyclability.[64] Using two different hard templates, KIT-6 cubic mesoporous silica and SBA-15 hexagonal mesoporous silica, Wang *et al.* have recently prepared two highly ordered mesoporous Co_3O_4 materials replicating the previous cubic and hexagonal silica structures. These two solids showed ferromagnetic ordering even at room temperature, due to the geometric confinement of antiferromagnetic order within nanoparticles. The KIT-6 mesoporous Co_3O_4 electrode delivered a lithium storage capacity of 1760 mA h g^{-1} at a current rate of 50 mA h g^{-1}, which is similar to what has been previously reported for porous Co_3O_4 nanotubes and nanoneedles.[70] During 100 cycles, the electrode maintained a reversible capacity above 1100 mA h g^{-1}, which is higher than the theoretical capacity of Co_3O_4 (890 mA h g^{-1}). It can be attributed to the high surface area and interconnected porous structures, providing extra active sites for Li^+ storage.[71] Differing from other morphologies like powders, where the specific capacity decreases when the current density is increased, these mesoporous electrodes exhibited almost the same specific capacity, 300 mA h g^{-1}, at high and low current densities.

The extraordinary performance (long-term cyclability and high-current performance) of these mesoporous Co_3O_4 materials should be attributed to the highly ordered mesoporous structure (see Fig. 7), in which the electrolyte can easily diffuse into the mesopores.[72]

2.4. Biomimetic mesoporous materials

Over the past decade, bioentity immobilisation has opened up a new way to explore the potential energy applications for the integration of biological systems into electronic devices: chiefly in biofuel and the mitigation of CO_2 for environmental purposes. For an intensive study of this approach, the readers' attention is drawn to the outstanding review published by the group of Prof. Meunier in 2011.[73]

The term 'biomimetic', coined by Otto H. Schmitt in 1969, refers to the process of comprehending and applying biological principles to man-made design.[74] Later, IUPAC defined 'biomimetic' as 'a compound that mimics a biological material in its structure or function,' and additionally, as 'a laboratory procedure designed to imitate a natural chemical process'.[75]

There are numerous examples of the potential of biomimetic materials in different applications, including biology, medicine, aerospace, energy, *etc.* As far as energy conversion, capture and storage applications are concerned, biotemplated materials, mostly with hierarchical structures (see Section 2.2), show great promise. Su *et al.* recently reviewed the state of the art of applications of hierarchically structured porous materials in energy conversion and storage.[61] In this section, characteristic examples of biomimetic mesoporous materials for renewable energy will be put forward.

Much effort has been devoted to extending the use of TiO_2 under sunlight irradiation, including by the biomimetic route. Accordingly, hierarchical macro-mesoporous titania obtained from biotemplates such as plant leaves or butterfly wings has been reported to enhance light harvesting and photocatalytic hydrogen production, as well as showing promising properties as a photoanode for solar cells and dye sensitised solar cells (DSSCs).[61,76–79] An example of this was recently reported by Zhang *et al.*, who synthesised a new photoanode-titania based structure for DSSCs, inspired by butterfly wing scales (Fig. 8).[76]

Continuing with titania and DSSCs, diatoms are also promising biotemplates for the biomimetic fabrication of nanostructured materials and devices. Diatoms produce different regular 3D silica structures with nanometre to micrometre dimensions. These structures have been used as biosupports, generating new hierarchical materials by coating them with titania layers giving an enhanced electrical output of experimental DSSCs.[80,81]

But the potential applications of hierarchical biotemplated materials are not restricted to the DSSC field. Hierarchical macro–mesoporous wood-templated NiO,[82] Fe_3O_4,[83] manganese oxide,[84] chromium oxides,[85] alumina;[86] as well as diatomaceous earth-templated carbon[87] and mesoporous biocarbon-coated $Li_3V_2(PO_4)$[88] have all been synthesised as promising candidates for carbon electrodes in LIBs.

Besides hierarchical biotemplated materials, metal–organic framework materials (MOFs), which will be discussed in the following section, are ideal candidates for building biomimetic systems due to their extremely high surface area and chemical tuneability. Zhou *et al.*[89] recently published an excellent review on MOFs as biomimetic catalysts. Their review focuses on

implanting biomimetic active sites into stable MOFs. Maspoch *et al.*[90] highlighted the advances in the synthesis of metal–biomolecule frameworks (MBioFs). In any case, these approaches are focused far away from the concept which is discussed herein, of 'biomimetic' materials as sacrificial templates for energy applications.

2.5. Hybrid mesoporous materials

Previous sections are devoted to the synthetic methods and properties of mesoporous/nanostructured/hierarchical materials for potential applications in clean energy technology. In general they owe their promise to (i) their high surface area, needed for efficient electrochemical reactions in fuel cells and Li-ion batteries, as well as for attaching a broad spectrum of sensitizers, both organic and inorganic to DSSC and quantum-dot sensitized solar cells; and (ii) their improved diffusion, *i.e.* a fast electrolyte-surface diffusion of the electrochemically active materials in solar cells, fuel cells and batteries, and a shorter solid state diffusion path for the Li ions in batteries.[7]

Usually, the incorporation of active sites into mesoporous materials is essential to their application and thus the success of the synthetic route will determine the efficiency of the solid when used in a device. The role of the incorporation of functionality into mesoporous solids, and of mesoporosity itself, in device performance in fuel cells is highlighted in Section 4.1. Additionally, the use of mesoporous hybrid TiO_2, SiO_2, SnO_2 and ZnO-based materials for clean photocatalytic energy technologies and for mesoporous advanced solar cells will be carefully discussed in Sections 3.7 and 4.2, respectively. This section, on the other hand, will seek to summarise existing synthetic strategies for obtaining hybrid mesoporous solids, for the aforementioned applications. Examples of materials which have already found uses in these areas are given as an illustration.

Most of the techniques for the incorporation of functionality in mesoporous solids are based on post-synthetic treatments of preformed solids, which usually lead to a partial blocking of the mesoporosity and a poor control of the location and geometry of the active phase. Traditionally, supported oxide catalysts have been prepared by ion exchange, wet impregnation, deposition–precipitation or chemical vapour deposition. More efficient post-synthetic techniques are atomic layer deposition and grafting. The latter technique also includes so-called organometallic grafting, using $L_nM[O_2P(O^tBu)_2]_m$ or $L_nM[OSi(O^tBu)_3]_m$ (L_n = alkoxide, amide, alkyl ligands) as organometallic precursors that, having been cleaved thermolytically, are able to react with hydroxyl groups of the surface of the oxide support.[91,92]

More recently, a new strategy has been developed to introduce a wide range of functionalities in mesoporous materials: the so-called 'sol–gel coordination chemistry' (Fig. 9).[8]

Inspired by periodic mesoporous organosilica (PMO) hybrid materials, this approach is based on the *in situ* incorporation of chemical functionality through its co-condensation with the metal oxide precursor during the sol–gel process. The corresponding metal complex or nanoparticle is modified with terminal trialkoxysilane groups for its co-condensation with a silica source

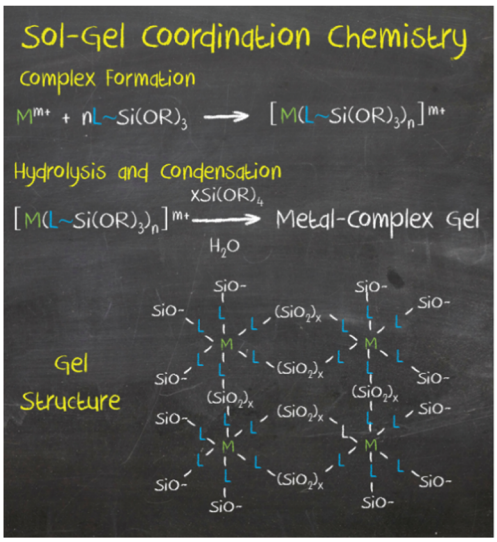

Fig. 9 Sol–gel coordination chemistry, an approach developed for the synthesis of hybrid mesoporous materials through the *in situ* incorporation of chemical functionalities into the framework of silica and organosilica porous materials. Reprinted with permission from ref. 8. Copyright 2013, Wiley-VCH.

and in the presence of an adequate surfactant. In this manner, mesoporous hybrid materials containing a wide variety of functionalities, including metal nanoparticles, metal complexes, clusters, organic molecules and dyes, as well as other homogeneous catalysts have been synthesised. In addition to silica, other mesoporous solids such as PMO and TiO_2 have been used as supports. In all cases, it has been proved that higher surface areas and enhanced yields are possible with this method, as well as precise control over the pore structure and surface chemistry of mesoporous materials.[93,94]

As an example of a hybrid mesoporous material with applications in energy-related technologies, mesoporous titania is the most common material used as the working electrode (WE) in DSCCs, and it is usually prepared by post-synthetic methods; the TiO_2 is synthesised by using hard-template or soft-template approaches, and the dye is usually incorporated by the impregnation and/or immersion of TiO_2 in a solution of the complex to incorporate, by interactions between the carboxylic groups of the metal complex with the TiO_2 surface.[7,34] Different examples of the above hybrid porous titania and its performance are given in Sections 3.7 and 4.3.

As far as the sol–gel coordination chemistry approach is concerned, Rico-Santacruz *et al.*[93] recently reported the synthesis of a novel hybrid mesoporous titania–N3 dye with high organic content (up to 50%) and a surface area of *ca.* 250 $m^2\ g^{-1}$, without the need of surfactants (and calcinations), using only water and ethanol as a solvents. This method allows for overcoming the drawbacks of traditional titania, keeping the textural properties of unmodified titanias but with a considerable improvement of the photocatalytic properties in comparison with both the unmodified one and the one prepared by the grafting of the dye on the pre-existing mesoporous titania.[93b]

2.5.1. Mesoporous metal–organic framework (MOF) materials. A special class of hybrid organic–inorganic porous materials with

Table 2 The textural and structural properties of some mesoporous MOFs. Adapted from ref. 95 and 97

Family	Name	Pore apertures (nm)	Surface area (m^2 g^{-1}) BET	Surface area (m^2 g^{-1}) Langmuir	Pore volume (cm^3 g^{-1})	Type N_2 isotherm[b]	Structure type[b,c]	Ref.
IRMOF	IRMOF-12/14	2.45	—	1750/1936	0.61/0.69		3D channel	100
	IRMOF-16	2.9	1910	—				100
	IRMOF-74-IX	9.8	1760	—	3.30	Type IV		112
MesoMOF-1-HX		2.2 × 2.6, 3.85	685	—	500–730[a]	Type IV	3D channel	101
MIL	MIL-100	1.2, 2.5 × 2.9	—	3100	1.16	Mainly type I	Cage	104
	MIL-101	1.4 × 1.6, 2.9 × 3.4	4100	5900	2.01	Type I with secondary uptakes		105*a*
	MIL-101_NDC	1.8 × 2.0, 3.9, 4.6	2100	—	—	Type I with secondary uptakes		105*b*
ZIF	ZIF-95	0.37, 2.5 × 1.4	1050	1240	0.43	Mainly type I	Cage	109
	ZIF-100	0.35, 3.56	600	770	0.37			
UMCM	UMCM-1	1.4 × 1.7, 2.4 × 2.9	4160	—		Type I with secondary	1D channel	103
	UMCM-2	2.6 × 3.2	5200	6060	2.32	uptakes[c]/type IV[b]	Cage	108
PCN	PCN-61	2.3, 1.5, 1.3	3000	3500	1.36	Type I with secondary uptakes	Cage	111
	PCN-66	2.6, 1.6, 1.3	4000	4000	1.63			
JUC	JUC-48	2.5 × 2.8	629	880	0.19	Mainly type I	1D channel	102
MOF	MOF-210	2.69 × 4.83	6240	10 400	3.60	Type IV	Cage	115
NU	NU-109E		7010	—	3.75	Type IV	Cage	113
	NU-100	1.34, 1.54, 2.74	6143	—	2.82			114
	NU-110E		7140	—	4.40	Type IV		113

[a] STP units. [b] Data from ref. 3. [c] Data from ref. 1.

potential applications in energy technologies is that of the metal–organic framework materials (MOFs). Porous materials are often classified as two groups: inorganic and carbon-based materials. MOFs represent a family of materials that bridges these two classes of porous materials.[95–97] This emerging class of materials, sometimes called porous coordination polymers (PCPs), are thus organic–inorganic hybrid solids with infinite, uniform framework structures built from organic linkers and inorganic building blocks, that exhibit micro- to meso-sized cavities and/or open channels, which are arranged regularly in a crystal lattice.[95–97]

The combination of their gas storage/capture performance at room temperature with the simplicity of their synthesis makes MOFs ideal candidates for clean energy technologies. The most relevant parameter for those applications is the surface area per volume ratio as well as their stability.[96–98] Non-mesoporous MOF-5 has one of the highest reported values of surface area per volume ratio, *ca.* 2200 m^2 cm^{-3}.[98] Despite such high surface to volume ratios, pores larger than 2 nm are required to expand the application of MOFs, to areas such as macromolecular catalysis or separation. Thus, the expansion of these structures into the mesoporous range could herald the MOFs' coming of age in the industry.[96,97,99]

Mesoporous metal–organic framework is a term denoting MOFs with pores ranging between 2 and 50 nm, as defined by IUPAC for other mesoporous materials. However, the pores of these novel solids encompass not only channels but also the cavities of the material. Thus few mesoporous MOFs have a type IV isotherm.[97] Adsorption in these materials is governed by the size of the accessible channel into the pore, *i.e.* micropores with the typical type I isotherm. A second uptake then takes place in which microporous windows open to mesoporous cages, leading to type I isotherms with a second uptake in most cases, as shown in Table 2.[97]

In 2012 Cui *et al.*[95] published a tutorial review which covers new advances in the field of mesoporous metal–organic framework (mesoMOFs). The review covers the design and synthesis of mesoMOFs, their porosity activation and surface modification, as well as their potential applications in storage and separation, catalysis, drug delivery and imaging. It is accepted that novel mesoMOF materials can be synthesised following different strategies, although the solvothermal technique is the most common.

As an example, Fig. 10 shows the synthesis of a mesoporous MOF through surfactant-assisted synthesis, as an efficient soft-templating approach to mesoporous silicates.

Zhou *et al.* classified mesoporous MOFs as five different types: those with 3D channels; those with 1D channels; mesoporous ZIFs (from zeolite imidazolate frameworks) with large cavities; mesoporous MOFs based on supramolecular templates

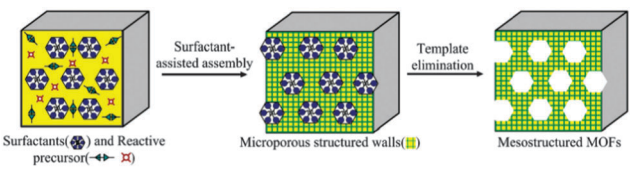

Fig. 10 A schematic representation of the surfactant-assisted synthesis of mesoporous MOF particles from microporous MOFs. Reproduced from ref. 95. Copyright 2012, RSC.

and lastly, mesoporous MOFs with large cavities, the final group being the most common type of MOFs found.[97a] Cui *et al.*[95] further reduced this classification to four types: cage-type mesoMOFs (including ZIFs), channel-type mesoMOFs (including 1D and 3D MOFs), chiral mesoMOFs and mesoporous particles of MOFs. For a more in-depth examination of the synthesis, properties and applications of these novel materials, readers are directed to ref. 95–97 and 99. Herein, we will show just a few examples of mesoMOFs with potential applications in clean energy technologies.

The first mesoporous MOF was reported in 2002 by Yaghi *et al.*[100] Named IRMOF-16, it is a 3D MOF which belongs the IRMOF family (isoreticular MOF-5), whose structure consists of ZnO_4 tetrahedra and a long organic linker ([1,1′:4′,1″-terphenyl]-4,4″-dicarboxylic acid, TPDC).

IRMOF-16 exhibited a high capacity for methane storage (240 cm^3 STP per g at 298 K and 36 atm.) and an extremely low density, 0.21 g cm^{-3}. It possesses a percentage free volume of 91.1%, much higher than some of the most open zeolites, such as faujasite, and similar to silica xerogel and aerogels.[97–100] Since then, numerous mesoporous MOFs have been synthesised,[101–115] the most representative of which are summarised in Table 2.

For example, Zhou *et al.*[101] reported the first example of a mesoporous MOF exhibiting a type IV adsorption–desorption isotherm, mesoMOF-1, by using TATAB (4,4′,4″-*s*-triazine-1,3,5-triyltri-*p*-aminobenzoate) as an organic linker and acids (HX, X = F, Cl, Br) to stabilise the meso-channels (mesoMOF-HX). Yaghi *et al.*[109] synthesised ZIF-95 and ZIF-100, two mesoporous MOFs that can selectively capture CO_2 from several different gas mixtures with methane, CO or nitrogen, at room temperature.

Recently, the same laboratory expanded the original phenylene unit of MOF-74 to prepare a series of mesoporous materials, namely IRMOF-74-I to IX, with pore apertures ranging from 1.4 to 9.8 nm, the latter figure being the highest ever reported in the literature.[112] Farha *et al.*[113] synthesised two mesoporous MOFs, NU-109 and NU-110 (Northwestern University), with BET areas *ca.* 7010–7140 m^2 g^{-1}. These BET values are the highest of any porous materials reported to date, even superseding the area of the previously synthesised NU-100[114] and MOF-210 (see Fig. 11).[115]

The surface area of a football pitch is about 7000 square metres, which means that every gram of the last four mesoporous MOFs has almost the same surface area as a football pitch. MOF-210 and NU-100 exhibited hydrogen adsorption as high as 7.9 to 9.0 wt% at 56 bar. The former is increased up to 15 wt% at 80 bar (Fig. 11)[114,115]. These values are higher than the targets of the U.S. Department of Energy (DOE) for hydrogen adsorption −5.5 wt% and 40 g l^{-1} of volume capacity at a operating temperature of −40 °C to 60 °C under a maximum delivery pressure of 100 atm.[116] Mercedes-Benz has already deployed MOF hydrogen fuel tanks in a fuel cell-powered demonstration model, the F125.[117]

These are just a few examples of the possible application of these mesoporous materials in clean energy technologies, as shown in Fig. 12. The use of these novel materials in clean energy technologies, including catalysis, will be discussed in the following sections.

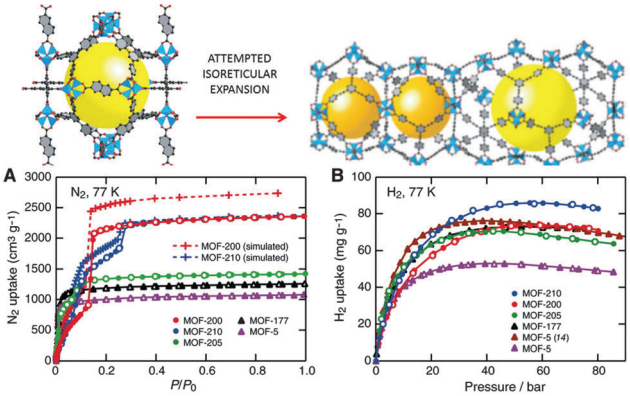

Fig. 11 (Up) The attempted isoreticular expansion of MOF-205 leads to MOF-210, and (bottom) the low-pressure N_2 isotherms (A) and high-pressure H_2 isotherms at 77 K (B) of MOF-5, -177, -200, -205, and -210. Reprinted with permission from ref. 115. Copyright 2009. American Association for the Advancement of Science.

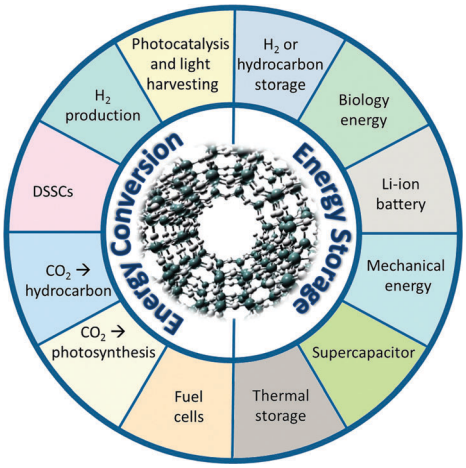

Fig. 12 The illustration of the potential applications of porous materials in energy conversion and storage. Adapted from ref. 61. Copyright 2012, Wiley-VCH.

3. Mesoporous catalysts for clean energy technologies

3.1. Biofuels production and upgrading with mesoporous catalysts

3.1.1. First and second generation biofuels. Biomass is considered by experts as the only sustainable source with the potential to displace petroleum in the production of chemical and liquid transportation fuels. Biofuels (*e.g.* biodiesel, bioethanol and biogas) produced from renewable sources could help to reduce the burning of fossil fuels and lower CO_2 emissions. Their mitigation of global warming comes from the fact that CO_2 released in burning biofuels equals the CO_2 tied up by the plants during photosynthesis and, consequently, does not increase net CO_2 in the atmosphere.

From a plethora of biofuels, bioethanol and biodiesel alone have been commercialised worldwide for transportation uses. The Directive 2003/30/EC on the promotion of the use of biofuels

or other renewable fuels established for state members of the European Union a goal of 5.75% share of renewable energy in the transport sector for 2010, this share rising to a minimum of 10% in every member state in 2020 (Directive 2009/28/EC). Biofuels must contribute to CO_2 reductions of 50% by 2017. Other countries, including the U.S., Canada, Japan and Australia have adopted similar policies for the use of biofuels over the next few years. At this point it is important to highlight that the EU is the world leader in the production of biodiesel (European demand in biodiesel could increase up to 10 million tons per year by 2010) whereas the US is the biggest ethanol producer worldwide.

Among the different biomass sources, edible biomass feedstocks (*e.g.* sugars, starches and vegetable oils) were initially proposed for the large scale production of biofuels or biochemical compounds, the so-called ''first generation'' biofuels. However, important concerns arise about the impact of edible feedstock on biodiversity and land use (possible deforestation), as well as their high production cost and competition with food crops (there is a strong argument that increases in food prices are due in part to this competition between food and fuel).[118] Newer biofuels, the so-called ''second generation'' biofuels, offer the potential to avoid the aforementioned drawbacks of edible biomass resources. Non-edible biomass resources (*e.g.* lignocellulosic feedstocks) could achieve a sustainable production of fuels and chemicals without affecting food supplies or forcing extensive changes in land use. Additionally, second generation biofuels are expected to be superior in terms of energy balance, land requirement and competition with food crops, and greenhouse gas emission reduction.

In order to evaluate the possible use of biomass derivatives in the production of biofuels in a biorefinery, the US DOE has selected so-called platform molecules, which include organic acids (*e.g.* succinic acid, lactic acid, *etc.*), polyols (*e.g.* glycerol, sorbitol, *etc.*) and others (*e.g.* bioethanol, furans, *etc.*). The processing of these renewable biomass derivatives in a biorefinery requires the design of new catalytic strategies taking into account the fact that these biomass derivatives exhibit a rich surface chemistry (high degree of oxygenated groups), are water-soluble, highly reactive and have low volatility, when compared to conventional petrochemical feeds (these systems must be designed for aqueous-phase processing in mild conditions). The processing of biomass feedstocks in biorefineries is seen as a challenging procedure, with multiple steps, because of the complex chemical composition of the feedstocks. Chemical processes using inorganic acid and base catalysts play a crucial role, for example the trans-esterification of vegetable oils with methanol in the production of biodiesel, or the hydrolysis of cellulose to fermentable sugars, *etc.* However, homogenous acid or base catalysts have significant drawbacks, mainly associated with the neutralisation and separation of catalysts from the reaction products. In this sense, the design of new solid catalysts with a proper porous structure can be envisaged as a promising alternative not only in terms of the processing and production cost (recovery and reuse of the solid catalyst at the end of the reaction) but also for the control of the reaction pathways in the production of the new biofuels from biomass.

In the following sections we will focus on some mesostructured materials which are envisaged to be promising candidates for the biomass conversion processes, both for first and second generation biofuels production, as well as the conversion of platform molecules to value-added products. The presence of complex reaction intermediates in biorefineries will make mesoporous materials extremely important as catalyst supports, able to control the preferred reaction pathways *via* pore diameter.

3.1.2. Catalytic strategies for the processing biomass feedstocks and its derivatives

3.1.2.1. Bioethanol processing. Ethanol is usually converted by the fermentation of edible-biomass aqueous sugars. Bioethanol produced from biomass is included as an additive in the formulation of gasoline in low concentrations (*e.g.* E5–15) due to the limitations of current spark-ignition engines. High-concentration blends (*e.g.* E85) will require newly designed engines, designed as flexible-fuel vehicles (FFVs). Besides being used as an additive or as a fuel, bioethanol has enormous potential as a chemical feedstock to produce renewable hydrogen *via* steam reforming or chemicals (*e.g.* ethylene, acetaldehyde, acetic acid, *etc.*) A number of reactions, dehydration, dehydrogenation, oxidation and so on, might be used in this case. These processes require the design of proper catalysts with porous structures, acid–base properties and thermal/catalytic stability under harsh temperature conditions.

One of the main conversion processes for bioethanol concerns the production of C_3 derivatives such as propene oxide, acrylonitrile and polypropene. Conventional catalysts like zeolites and metal oxides come with the dual caveat of a low catalytic activity and lifetime. Although the shape selectivity in acidic zeolites favour the formation of C_3 and C_4 derivatives, coke formation gives rise to strong deactivation processes.[119–121] Recent studies from Iwamoto *et al.* using Ni-MCM41 materials have shown that mesoporous silica materials exhibit an improved stability towards coke formation together with a higher water resistance under reaction conditions compared to conventional zeolites.[122] Although the selectivity to C_3 and C_4 derivatives is low on these mesoporous systems, the selectivity increases for low space-velocity. A similar low selectivity towards higher hydrocarbons (C_5–C_{12} derivatives) has been reported for H-ZSM-5 nanocrystals deposited on Al-MCM-41.[123] While conventional ZSM-5 exhibits a significant selectivity towards liquid hydrocarbons, mesoporous H-ZSM-5/Al-MCM-41 led to the formation of ethylene with a 100% ethanol conversion.

Another important reaction involving ethanol is steam reforming to carbon dioxide and hydrogen. Traditionally this reaction has been performed using noble metal catalysts (*e.g.* Pt, Rh, Pd) and transition metals (Co and Ni) supported on oxide supports (Al_2O_3, MgO, SiO_2, CeO_2, *etc.*).[124–127] Unfortunately, these catalysts have two important problems, their deactivation owing to coke formation, and the low selectivity to hydrogen (the main reaction products being unwanted carbon monoxide, acetaldehyde, acetone and methane). An improved performance in terms of the catalytic activity and selectivity to hydrogen has been observed in mesostructured materials. Their controllable pore size allows the accommodation of small size metal nanoparticles (large metal ensembles are related with coke deposition

and nanofibers growth). In this manner, Gac and co-workers described an improved catalytic behaviour using a Co_3O_4/MCM-48 catalyst synthesised by the nanocasting approach.[128] Mesoporous Co–Si catalysts exhibit an ethanol conversion of 100% at 420 °C with a hydrogen selectivity higher than 80%. A high selectivity for hydrogen (above 70%) was reported by Carrero and co-workers on Cu–Ni/SBA-15 catalysts although at a slightly higher reaction temperature (600 °C).[129] The metal content, metal particle size, Ni/Cu ratio and the preparation conditions (Cu/Ni framework species or deposited metal nanoparticles) have been proposed to define the final hydrogen selectivity. Interestingly, both the hydrogen selectivity and catalyst lifetime can be highly improved in mesoporous Cu–Ni/SBA-15 catalysts by incorporating basic promoters such Ca and Mg (0–20 wt%) that inhibit ethanol dehydration to ethylene and subsequent coke formation.[130] More examples of ethanol steam reforming with mesoporous catalysts can be found later on, in the hydrogen production section.

3.1.2.2. Catalytic strategies to produce biodiesel. It is hoped that in the near future, biofuels will begin to mitigate the large consumption (and side-effects) of petroleum-based fuels for transportation. Biodiesel represents a major candidate for achieving this end. Biodiesel is a mixture of fatty acid methyl esters (FAME) produced by the trans-esterification of triglycerides with an alcohol (*e.g.* methanol), using a homogeneous acid or base catalyst. Different heterogeneous catalysts (basic zeolites, alkaline earth metal oxides and hydrotalcites) have been evaluated for the trans-esterification of vegetable oils as replacements for the current homogenous base catalysts.[131] CaO has been the most widely tested base catalyst for the trans-esterification of various vegetable oils such as soybean, rapeseed and sunflower oils.[132,133]

Microporous solid catalysts (titanosilicate ETS and zeolite β) were unable to carry out mass transfer adequately; giving rise to their poor catalytic performance compared to non-porous solid catalysts. Indeed non porous examples, such as Amberlyst-15 and Nafion NR50, exhibit a promising catalytic activity compared to homogenous catalysts. Similarly, Suppes and co-workers studied the trans-esterification of soybean oil with methanol using a series of zeolites and metal catalysts.[134] The catalytic measurements show that zeolite ETS-10 gives a higher conversion than the zeolite-X catalysts, the increase being attributed to the higher basicity and improved intra-crystalline diffusion afforded by ETS-10's larger pore diameter. In general, zeolites performed better than metal oxides and also homogenous catalysts in the trans-esterification of soybean oil.

Taking into account the aforementioned diffusional limitations when dealing with high molecular weight reactants, mesoporous silica materials could have an advantage over microporous zeolites in the production of biodiesel because the mass transfer resistance and diffusion limitations can be significantly reduced. Indeed, the deposition of calcium oxide on different mesoporous silicas (SBA-15 and MCM-41) gave rise to improved catalysts for the trans-esterification of sunflower oil and castor oil with methanol.[135] A sample containing 14 wt% CaO on SBA-15 was the most active catalyst, reaching a conversion as high as 95% with sunflower oil (after 5 h of reaction) and 65% for castor oil (after 1 h). Interestingly, these catalysts showed no lixiviation of the active phase under the reaction conditions, in contrast to commercial CaO.

Li and co-workers investigated mesoporous silicas (MCM-41, KIT-6 and SBA-15) loaded with MgO as a base catalyst, for the transesterification of a blended vegetable oil with ethanol to produce biodiesel.[136] Among all catalysts, MgO-impregnated SBA-15 exhibited the highest catalytic activity for the production of biodiesel, achieving a conversion as high as 96% within 5 h. Similarly, Abdullah and co-workers achieved very active catalysts by the deposition of potassium on SBA-15 using conventional impregnation methods. The K/SBA-15 catalyst attained an optimum biodiesel yield of *ca.* 87% at 70 °C. The excellent performance of these systems was attributed to a high surface area, tuneable mesopore size and high thermal stability.[137] Corma and co-workers performed the glycerolysis of triolein and rapeseed oil using different base catalysts such as mesoporous Cs-MCM41, Cs-sepiolite and hydrotalcites. The final catalytic activity was defined by the strength of the basic sites and not by the porous structure.[138] The final conversion achieved was as high as 92% for hydrotalcite, *versus* 26% on mesoporous Cs-MCM41, with a high selectivity to monoolein (78% and 46%, respectively).

Despite the excellent results reported in the literature for heterogeneous acidic or basic catalysts in biodiesel production processes, their catalytic performance is still far from that of the conventional catalysts (NaOH, H_2SO_4, *etc.*). Furthermore, heterogeneous base catalysts are still very sensitive to the free fatty acid (FFA) content in the oil. Consequently, the design of new porous catalysts is required, bearing in mind not only the acid or basic site strength but also the available active surface and tolerance to high FFA content oil at mild reaction conditions. Another method in biodiesel processing where mesoporous catalysts may be desirable is the use of coproduced glycerol for the synthesis of oxygenated fuel components. This is described in the next section.

3.1.2.3. Glycerol conversion. One of the main by-products of biodiesel production by the trans-esterification of vegetable oils (and residual oils and fats), is glycerol. The valorisation of this highly versatile molecule into valuable chemicals, using greener catalytic processes, presents several alternatives: (i) glycerol esterification with acetic acid or trans-esterification with methyl acetate to obtain glycerol triacetate (triacetin),[139–142] (ii) glycerol etherification with different aryl/alkyl alcohols to produce a wide variety of substitute ethers,[139] (iii) glycerol oxidation with an oxygen donor substrate to produce glyceric and glycolic acids as major products,[139,143,144] and (iv) glycerol dehydration on solid acid catalysts to give acrolein and hydroxyacetone.[145]

Where glycerol esterification and etherification are concerned, the number of studies dealing with the effect of mesoporosity is rather scarce. These reactions are traditionally performed using solid acid catalysts, and the selectivity towards the different reaction products (mono-, di- and tri-esters or the corresponding ethers) is highly sensitive to the reaction conditions (substrate/acid or alcohol ratio, reaction time, amount of catalysts, *etc.*), the acid strength of the support and the presence of microwave

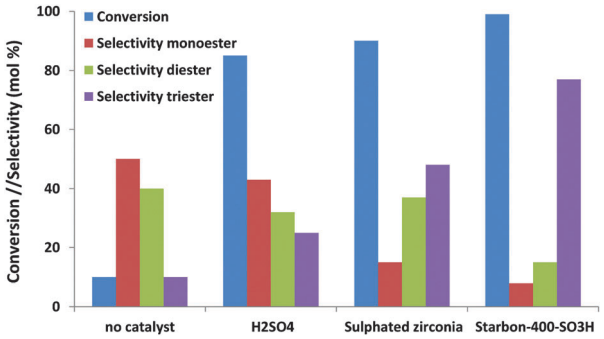

Fig. 13 The catalytic activity and selectivity of different solid acids in the esterification of glycerol with acetic acid.

radiation.[134–137] Di- and tri- derivatives are valuable petrol fuel additives which give enhanced viscosity properties when blended with diesel fuel or antiknocking properties when added to gasoline. Interestingly, Luque and co-workers confirmed the considerable effect of the pore size not only on the final conversion but also on the selectivity towards different reaction products.[139] As can be observed in Fig. 13, the mesoporous Starbon acid catalyst exhibits an improved catalytic activity compared to traditional solid acid catalysts (*e.g.* sulfated zirconia) with an unprecedented high selectivity to the triacetylglycerol. A similar improvement in terms of the conversion values (95%) and selectivity was observed for mesoporous Starbon acid carbon in the etherification of glycerol with a high selectivity to the monoether in the 1-position compared to the monoether in the 2-position (5/1).[139] Using sulfonic-acid functionalised mesostructured materials (SBA-15), Melero and co-workers found that glycerol conversion in the esterification of glycerol, to yield acetylated derivates, was higher with acetic acid than conventional acid catalysts. The total conversion reached by mesoporous materials was *ca.* 90% with over 80% selectivity to diacetylglycerol and triacetylglycerol. Significantly, the reaction activity was highly sensitive to the acid strength of the sulfonic acid groups: propylsulfonic < arenesulfonic < fluorosulfonic.[142]

For the selective liquid-phase oxidation of glycerol, noble-metal supported catalysts have been much investigated for their catalytic activity and selectivity. Using molecular oxygen as an oxidant, carbon-supported Pt and Pd nanoparticles have demonstrated a good catalytic activity, as well as selectivity for glyceric acid.[146,147] The nature of the metal nanoparticles (Pd or Pt), the pH of the reaction media and the presence of secondary species (*e.g.* Bi) exhibit a large influence not only on the catalytic activity but also on the final selectivity. The oxidation of the secondary hydroxyl group of glyceric acid to yield dihydroxyacetone was preferred under acidic conditions and after the incorporation of bismuth on platinum nanoparticles (Scheme 1).

While various studies have demonstrated the influence of the noble-metal particle size on the catalytic activity, selectivity does not seem to correlate with the size of the nanoparticles.[148–150] Indeed, Villa and co-workers confirmed that Au particle size had a negligible effect on the final selectivity when using $MgAl_2O_4$ spinels as a support and molecular oxygen as the oxidant.[151] By using spinels with a different surface compositions (Al/Mg ratio) and

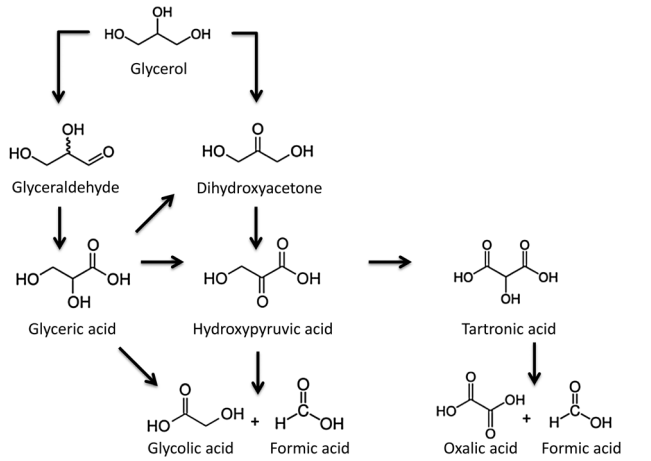

Scheme 1 Different reaction paths for the selective oxidation of glycerol.

apparent surface areas, these authors anticipated the important role of the textural and chemical properties of the support in the selectivity of the oxidation reaction.

This point was further confirmed by McMorn and co-workers[143] and Rodrigues and co-workers.[144] Apparently, wide mesopores favour the formation of partial-oxidation products (glyceric acid and glyceraldehyde) while narrow pores can lead to an easier over-oxidation of the primary products (oxalic acid and formic acid), independently of the catalyst and reaction conditions used. Indeed, the partial-oxidation products (mainly glyceraldehyde, dihydroxyacetone and glyceric acid) are the main reaction products when titania–silica materials with a large pore size (up to 15 nm) are used. It would seem that narrow micropores favour slow diffusion of the reaction products, giving rise to over-oxidation reactions, while an increase in the pore size decreases diffusion limitations, and partially oxidised products are observed.

The effect of the pore size on the final selectivity is clearly illustrated in Fig. 14 using Au nanoparticles supported in different carbon xerogels.[144] Whereas carbon xerogels with a

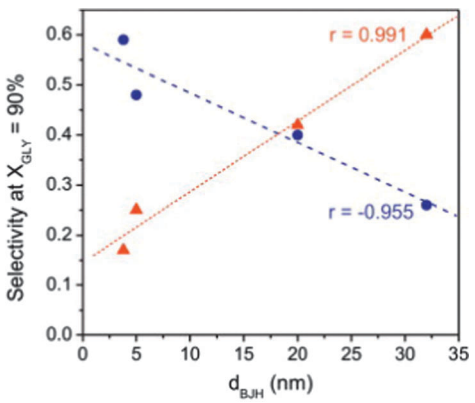

Fig. 14 Correlations between selectivities to dihydroxyacetone (DIHA – ▲) and glyceric acid (GLYCEA – ●) and the main pores size (calculated by the BJH method) for Au nanoparticles supported on mesoporous carbon supports. Reprinted with permission from ref. 144. Copyright 2012, Elsevier.

narrow pore size favour the formation of highly oxidized products (mainly glyceric acid (GLYCEA), glycolic acid and tartronic acid), an increase in the pore size diameter from 5 to 20 nm leads to a progressive shift in the product selectivity towards partially-oxidized dihydroxyacetone (DIHA).

Besides diffusion limitations, the higher selectivity towards DIHA of larger pores has been explained by the requirement of a larger void space inside the nanocavities (*e.g.* adsorption mode of the glycerol molecule). A similar observation on selectivity towards DIHA was described for Au nanoparticles supported on MWCNTs, which contained a larger proportion of mesopores than similar nanoparticles supported on a microporous activated carbon.[152]

In summary, it is clear that the liquid-phase oxidation of glycerol is highly influenced by diffusional limitations, with mesoporous materials being preferred in order to avoid undesired over-oxidation reactions.

Another reaction where the role of mesoporosity is crucial is the dehydration of glycerol to hydroxyacetone and acrolein in the presence of acidic catalysts. Using mesoporous alumino-phosphates which incorporated transition metal-ions (*e.g.* Cr(III), Cu(II) and La(III)), Liu and co-workers observed the good performance of these systems in terms of the glycerol conversion (as high as 99%) and selectivity to acrolein (*ca.* 80%).[145] Interestingly, the selectivity and conversion of glycerol was sensitive to the reaction temperature, the textural characteristics of the support and the Cr/Cu molar ratio.

3.2. Mesoporous materials in gas-to-liquid conversion

Natural gas is considered as an alternative to petroleum for the production of chemicals and as clean(er) liquid fuel. Natural gas reserves are more plentiful than those of petroleum, making the conversion of natural gas to value-added chemicals (gas to liquid (GTL) technology) an attractive proposition. There are two approaches for achieving that conversion, the direct one, from natural gas itself, and the indirectly route, *via* synthesis gas (syngas) or methanol. Of these approaches, the indirect route is the more commercialised technology. One of the main steps in the conversion of natural gas is the activation of the methane molecule using heterogeneous catalysts.

The direct conversion of natural gas involves multiple reactions, including pyrolysis – to produce hydrogen and carbon nanotubes, methane dehydro-aromatization – giving higher hydrocarbons (benzene, toluene, *etc.*), and direct oxidative conversions – to ethane, methanol and formaldehyde.[153] Concerning methane dehydroaromatization (MDA), Su and co-workers found an improvement in the conversion of methane to aromatics using Mo catalysts supported on modified HZSM-5.[154a] The unique selectivity to aromatics and the stability of the catalysts, which were derived from alkali-treated ZSM5, was attributed to the coexistence of mesopores which enhance the diffusion of the reaction products (aromatics) and inherent micropores in the zeolite that are the active sites for aromatics formation. Similar results were obtained by Chu and co-workers using an unusual hierarchical ZSM5 developed by the assembly of many French fry-like crystals using SBA-15 as the silica source.[154b] Mo nanoparticles supported on modified ZSM5 resulted in a higher methane conversion and a stronger coking-resistance compared to the conventional Mo/ZSM5 catalyst. The higher resistance to deactivation by coke formation is due, according to Martinez and co-workers, to the presence of intracrystalline mesopores that allow more coke to be formed while keeping the active sites (acidic sites) in the 10-ring channels of the zeolite active for aromatization.[155] Similarly, hierarchical mesoporous Mo/HMCM-22-HS catalysts, prepared by hard templating with carbon black, exhibit exceptional behaviour in terms of methane conversion, benzene yield and catalyst lifetime.[156]

Direct oxidative conversion of methane to methanol and formaldehyde has been widely investigated in mesoporous materials (*e.g.* MCM-41 or SBA-15) using oxide nanoparticles (MoO_x, VO_x and $FePO_4$) as the active species.[157] Compared to crystalline oxides, Wang and co-workers demonstrated that the confinement of $FePO_4$ species in ordered mesoporous silicas gives an improvement in the catalytic activity and selectivity towards HCHO. The catalytic behaviour is further improved after the incorporation of phosphorous species and the subsequent formation of the $FePO_4$ active sites.[158a] Apparently, the reducibility of the $FePO_4$ cluster was improved when embedded in mesoporous silicas, as this gave rise to a larger proportion of the lattice oxygen required for the selective oxidation reaction. Similar improvements were described by Li and co-workers with copper nanoparticles attached to mesoporous SBA-15.[158b] Using these catalysts the oxidation of methane produces formaldehyde as the main reaction product (5.6 mol HCHO mol Cu^{-1} s^{-1}) together with a small amount of carbon dioxide.

The indirect conversion of methane involves a first step to syngas followed by conversion of this syngas to the desired product (*e.g.* methanol) or the further conversion of methanol to value-added products.

For the methane reforming reaction to syngas, mesoporous catalysts have been mainly applied to control the size of the supported active species by the diameter of the pores. In this way, Ni nanoparticles supported on mesoporous nanocrystalline ZrO_2 showed a high catalytic activity and an improved lifetime under low temperatures and high carbon dioxide to methane ratios.[159]

The synthesised syngas can be converted into higher hydrocarbons or oxygenates with predominantly straight carbon chains *via* Fischer–Tropsch (FT) synthesis. The formation of hydrocarbons *via* FTS is a surface-catalysed polymerisation reaction which proceeds *via* a modified carbene mechanism on bifunctional catalysts, *i.e.* active species (Fe, Co, *etc.*) for FTS supported on acidic zeolites. However, the lack of sufficient external surface area makes the use of mesoporous materials very attractive due to the high metal loading required. Mesoporous materials allow an optimum dispersion of the active species together with improved transport properties which increase the selectivity towards liquid hydrocarbons.[160a–c]

Sartini and co-workers compared the catalytic behaviour of Co/mesoH-ZSM5 catalysts in FTS with conventional Co/SiO_2.[160d] After 140 h of reaction, the former was twice as active and three times more selective to the C_5–C_{11} fraction with a large content of unsaturated hydrocarbons.

With regard to the synthesis of methanol *via* the hydrogenation of carbon monoxide, van den Berg *et al.* compared the catalytic performance of a supported copper catalyst, Cu/ZnO/MCM48, with the typical copper catalyst, the former having a fourfold higher surface area and a fivefold higher copper content. According to these authors, the formation of confined nanocrystalline ZnO species on the mesoporous channels of MCM-48 prior to copper impregnation is of major importance to achieve a large catalytic activity.[161a,b]

Methanol dehydration to dimethyl ether (DME), as a new synthetic fuel, is another interesting process to substitute diesel or liquefied petroleum gas. Traditionally, methanol dehydration has been performed over acidic catalysts such as zeolites. However, the microporous nature of zeolites does not allow a proper diffusion of DME causing a fast loss of activity and selectivity. Tang *et al.* reported a micro-mesoporous ZSM-5/MCM-41 composite molecular sieve prepared by combining a microporous zeolite silica source with nano self-assembly methods for the catalytic dehydration of methanol to DME.[162a] The synthesised catalyst showed an excellent catalytic behaviour, with a methanol conversion of 86.6%, a selectivity to DME of 100% and a long catalyst lifetime better than the parent ZSM-5 catalyst. Similarly, Cho and co-workers reported a higher methanol conversion, lower selectivity to hydrocarbons and a slower deactivation for mesoporous LTA zeolites compared to the conventional CaA microporous zeolite.[162b] Unfortunately, the selectivity to DME was larger in the conventional CaA zeolite.

Another important process for methanol concerns its conversion to hydrocarbons and gasoline (methanol to hydrocarbon MTH and methanol to gasoline MTG). These processes play an important role in the conversion of biomass, coal, natural gas and CO_2 to liquid hydrocarbon fuels which can be tuned to produce gasoline-rich or olefin-rich products depending on the catalyst and the reaction conditions. The reactions are catalysed by shape-selective solid acid catalysts, such as zeolites. Due to the limited growth of the hydrocarbon chains inside the zeolite cavities as a result of steric hindrance, nanozeolites have been proposed as a potential replacement to avoid the aforementioned drawbacks. In this sense, nanoscale HZSM5 crystals have shown a higher activity, a lower coke content and a better stability in the conversion of methanol to hydrocarbons compared to conventional, larger zeolitic crystals.[163a]

Another approach to minimize kinetic limitations is the use of mesoporous catalysts. Bjorgen and co-workers studied the methanol to gasoline reaction on HZSM5 zeolite chemically treated with NaOH to develop mesoporosity.[163b] The catalyst lifetime increased by a factor of 3.3 on the desilicated zeolites and the selectivity towards the gasoline fraction (C_{5+}) was increased by 1.7. It seems that the hydrogen transfer reaction was faster in the modified samples and led to more aromatic and paraffinic compounds in the product. A similar improvement in the catalyst lifetime was reported by Kim and co-workers using a series of mesoporous MFI zeolites during the methanol to hydrocarbon conversion.[163c] While the catalyst's activity is related to the acid site density, the catalyst's stability (deactivation rate) correlates with its mesoporosity.[163d,e] Mesoporous catalysts exhibit an improved stability due to the faster removal of products with a shorter diffusion path-length and lower coke formation in the conversion of methanol to gasoline-range hydrocarbons.

3.3. The catalytic production of hydrogen

Interest in hydrogen production has grown inexorably in recent times. Some reviews have been published on this topic.[164–167] As it is known, hydrogen has emerged as a strategic clean energy carrier for both transportation and stationary applications. It is considered to be one of the best alternative fuels due to its abundance and non-polluting nature when used in fuel cells. In fact, hydrogen conversion in fuel cells efficiently generates energy, producing water as the only residue.[168,169] Hydrogen is the most abundant element in the universe and it is also the major constituent of Earth. However, it does not occur in a significant amount as a free H_2 molecule, but it is mainly found in the form of water or biomass. Nowadays, nearly 95% of the total hydrogen supply is produced from fossil fuels, mainly by methane steam reforming. However, applications of hydrogen in the transportation sector or to regulate the generation of renewable electricity are still a hot research topic, because of the techno-economical limitations and competition with other technologies. Catalytic technologies are expected to play an essential role in enhancing the yield and the energy efficiency. Ordered mesoporous materials are starting to play a significant role in the development of new types of catalyst for the production of clean hydrogen from different sources and through a variety of routes. The production of hydrogen can be achieved following 4 methods: (i) steam reforming of biomass, (ii) catalytic decomposition of methane, (iii) catalytic decomposition of ammonia and (iv) photocatalytic process. This review will show the most relevant articles related to the effect of mesoporosity on the different technologies. For more detailed information readers are referred to a recent review by Serrano *et al.*[167]

3.3.1. Steam reforming of methane. As it has been mentioned before, steam reforming of methane (SRM) is currently the most important method for hydrogen production on a commercial scale due to its high efficiency.[170] Methane is the main component of natural gas, as well as of other non-conventional fossil fuel resources. In order to obtain CO_2-free hydrogen, the possibility of coupling methane steam reforming with carbon capture and sequestration (CCS) is a promising route. Methane steam reforming is an endothermic process and is operated at high temperatures.

Transition metal-based catalysts (Ru, Rh, Ni, Ir, Pd, Pt, Co and Fe) have been used since the 1970s in steam reforming.[171,172] Ni-based catalysts have been widely used due to their low cost and high catalytic activity. However, Ni-based catalysts show high carbon deposition related to the deactivation of the catalyst. Additional efforts have been made to increase the stability of Ni-based catalysts and, using mesoporous materials as a support, a strong resistance to catalyst deactivation has been achieved.[173–175] The high surface area and mesopore uniformity of these systems seem to be the key factors behind

the superior catalytic behaviour compared to microporous catalysts.

Bang and co-workers prepared a series of mesoporous nickel–alumina xerogel catalysts by a single-step carbon-templating sol–gel method to study the steam reforming of liquefied natural gas (LNG).[176,177] They concluded that the crystallite size of metallic nickel served as an important factor in determining the catalytic activity. Later on, Bang and co-workers studied the same reaction but with a series of mesoporous alkaline earth metal-promoted nickel–alumina xerogel (M = Mg, Ca, Sr and Ba) catalysts, these were prepared by a single-step epoxide-driven sol–gel method and a subsequent incipient wetness impregnation method.[178] It was demonstrated that the exposed Ni surface area of the reduced catalysts decreased in the order of Mg > Sr > Ca > Ba, and the hydrogen production is correlated with the exposed surface area of nickel. Highly exposed nickel gives rise to higher LNG conversion and hydrogen yield. It has also been reported that high Ni exposure provides more stable catalysts towards deactivation.[179]

Recently, another steam reforming process based on ethanol has been studied for the production of hydrogen. Ethanol can be considered as a renewable source since it is produced by the fermentation of a relatively large variety of biomass types with a high carbohydrate content. As with methane reforming, Ni-based catalysts have been employed in the case of ethanol. For instance, a series of Ni catalysts supported on Al-SBA-15 mesoporous materials were studied in the context of ethanol steam reforming by Lindo and co-workers.[180] They demonstrated that the Ni/Al-SBA-15 catalysts produce larger amounts of ethylene and coke, with a slightly lower hydrogen selectivity than the Ni/SBA-15 catalysts. This result was explained by the ethanol dehydration taking place in the Ni/Al-SBA-15 acid sites, while an ethanol dehydrogenation mechanism predominates in the Ni/SBA-15 catalyst. Thus it was concluded that for steam ethanol reforming, Ni supported onto pure silica SBA-15 was a promising catalyst.

Han and co-workers used mesoporous Ni–Al_2O_3–ZrO_2 catalysts prepared using sol–gel chemistry and the results confirmed the importance of a high nickel surface area being exposed.[181–183] At the same time, Serra *et al.* studied bioethanol steam reforming on Ni-modified mordenite to see the effect of mesoporosity and the addition of alkaline metals.[184] Ni nanoparticles deposited on mesoporous mordenite show a high activity and selectivity and are resistant against coke deposition. The mesoporosity seems to be the main reason for the good performance while the addition of alkaline metals (Na) improves significantly the selectivity to hydrogen while decreasing coke deposition.

In a typical catalytic reforming reaction, hydrogen evolves at a high temperature over a Ni or noble metal-based catalysts. In order to reduce the maximum temperature for high hydrogen generation, Sn was used by Lee and co-workers[185] as a promoter for steam ethanol reforming. It was demonstrated that the addition of Sn reduces the temperature for the steam ethanol reforming with high hydrogen yield.

In addition to methane and ethanol, ethylene glycol and glycerol are considered interesting renewable sources for hydrogen production. In this case, recent work has shown the benefits of employing different types of ordered mesoporous materials as supports for the preparation of steam ethylene glycol or glycerol catalysts. Serrano and co-workers[167] analysed the effect of Pt-MCM-41 materials or Ni nanoclusters embedded in multicomponent mesoporous metal oxides. Both catalysts favour a higher hydrogen production because of their good metal dispersion. For instance, the ethylene glycol steam reforming reaction was studied with Pt nanoparticles supported on ordered mesoporous carbon by Kim and co-workers.[186] The Pt catalyst with a 3D pore structure shows a higher catalytic performance which is due to the fact that there is little metal sintering during the reaction process and more favourable transport and diffusion of the reactants and products.

3.3.2. Catalytic decomposition of methane. Yet another alternative for producing hydrogen is by the decomposition of methane in an inert atmosphere. The development of effective catalysts is one of the key factors hindering the practical viability of this process.

Metal-based catalysts have been used as an active phase for methane decomposition. However, important deactivation effects have been encountered due to coke formation. In order to mitigate these drawbacks, mesoporous materials have been proposed as promising candidates for supporting active phases in the catalytic decomposition of methane.[167] For instance, Ni dispersed within an ordered mesoporous material, consisting of partially Ce-substituted MCM-41 silica showed a higher methane conversion, as well as total selectivity for hydrogen and a high resistance to deactivation, compared with other metal-based catalysts.

Botas and co-workers have used a new class of carbonaceous materials (CMK-3 and CMK-5), which have an ordered mesoporous structure.[187,188] Their results showed that CMK-5 is an active catalyst for hydrogen production with a high stability. Carbon deposition from methane decomposition may leave the CMK-5 pores, growing towards the outside part of the catalyst particles, which avoids the total blockage of the mesopores. Recently, Jin and co-workers prepared Fe–Al_2O_3 supported on carbon materials to study the methane decomposition.[189] It has been demonstrated that the introduction of Fe and Al_2O_3 into the activated carbon decreases the surface area and pore volume, but mesopores with an average pore size around 4.5 nm are formed as an activation process. The resultant catalyst, with appropriate Fe/Al_2O_3 loading, exhibits good methane conversion and stability. Apparently, mesopores and larger pore volumes are beneficial to achieving a good dispersion of the active Fe species, giving rise to a higher catalytic activity than microporous carbon.

3.3.3. Catalytic decomposition of ammonia. Ammonia is another option for obtaining hydrogen *via* catalytic decomposition. The main advantages of this route are zero emissions of CO and CO_2, N_2 being the only co-product (it is important to highlight that although the process itself has zero emissions, the actual routes for ammonia synthesis involve hydrogen coming from the catalytic reforming of hydrocarbons with the associated CO_2 emissions). In the catalytic decomposition of ammonia, the research has been done using metal active phases like Ru, Fe, Co and Ni on a support.

As reported by Serrano and co-workers[167] the effect of mesoporosity is important to obtain a high metal dispersion and a small particle size, parameters that enhance the catalytic decomposition of ammonia. For instance, Tan and co-workers studied this reaction with Ru nanoparticles confined in the channels of ordered mesoporous alumina and magnesium oxide-modified ordered mesoporous alumina. The higher catalytic activity was attributed to the optimised nanoparticle size and the confined space provided by the channels of the mesoporous supports.[190]

3.3.4. Photocatalytic hydrogen production. Photocatalytic water splitting to form hydrogen and oxygen has attracted considerable attention as a potential means of renewable energy production with no reliance on fossil fuels and no carbon dioxide emissions.[191–194] Although TiO_2 is the most widely investigated photocatalyst for this reaction, it still provides low photocatalytic efficiency. The improvement of its photocatalytic water splitting performance can be achieved by many ways, such as doping it with metals to narrow its band gap energy, the addition of electron donors (hole scavengers) to the reaction system, and the establishment of a semiconductor mixed oxide in order to reduce the charge carrier recombination.[195]

The use of ordered mesoporous materials can provide significant advantages over conventional photocatalysts. Thus, well-defined and uniform pores are ideal to disperse the photoactive component, in the case of the as supported catalysts, and metal doping. Furthermore, with a pure mesostructured semiconductor, both a high light absorption and favourable interaction with the reagents take place simultaneously. Nevertheless, the crystallinity is important because the amorphous components are inactive in photocatalysis.[167]

TiO_2 modified with WS_2 was reported by Jing and co-workers showing that the mesoporous structure of the substrate was beneficial for a larger amount of WS_2 loading. They demonstrated the effectiveness of using mesoporous TiO_2 as the substrate and WS_2 as a sensitiser to construct an efficient and stable heterogeneous photocatalyst system responding to visible light.[196] Later on, TiO_2 modified with ZrO_2 was prepared as a mesoporous structured phase using the block co-polymer surfactants method, and was tested in the aforementioned reaction.[197] The most important results are shown in Fig. 15.

Comparing the specific hydrogen production rate shows that the synthesised mesoporous-assembled TiO_2–ZrO_2 mixed oxide photocatalyst with a specific Ti/Zr ratio provide the highest photocatalytic activity for hydrogen production compared to commercial TiO_2 photocatalysts. The mesoporous-assembled structure, with a pore diameter of around 5.6 nm, is considered to be a prime factor in increasing the photocatalytic hydrogen production. All the investigated commercial TiO_2 photocatalysts possess undesired non-mesoporous characteristics and this may lead to their comparatively low photocatalytic hydrogen production activities, because the photoactive species is less accessible to the reactant.

Dang and co-workers[198] have studied photocatalytic hydrogen production with $Cu(OH)_2$/TNTs catalysts prepared by the hydrothermal precipitation process. TNTs loaded with 8 wt% $Cu(OH)_2$ exhibit a remarkably improved activity due to the higher dispersion of $Cu(OH)_2$ onto the TNT surface compared with pure TNTs.

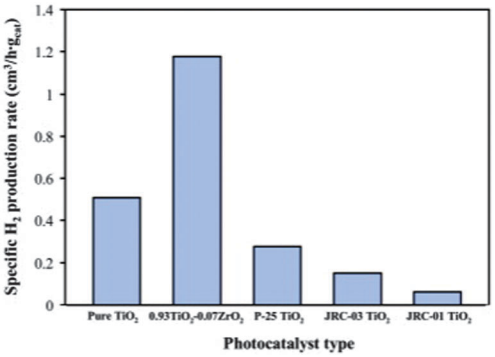

Fig. 15 The effect of the photocatalyst type on the specific H_2 production rate over the synthesised mesoporous-assembled pure TiO_2 and $0.93TiO_2$–$0.07ZrO_2$ mixed oxide photocatalysts calcined at 500 °C when compared to commercial TiO_2 photocatalysts (P25, JRC-01 Ishihara Sangyo Co., JRC-03 Ishihara Sangyo Co).

Another alternative to improve the photocatalytic activity is the incorporation of transition metal oxides into the mesoporous silica frameworks in a one-pot synthesis process. The photocatalytic mechanism in this case is based on a metal–metal charge transfer excitation, where incorporated metals act as chromophores, absorbing UV and/or visible light which leads to the formation of an excited state of charge transfer. Moreover, the high dispersion of these isolated species can lead to an increase in the conversion per centre in the case of bulk catalysts.

ZrO_2 is a promising light harvesting agent because its conduction band is located at a much higher energy level. For this reason it has been used to prepare Zr-MCM-41 to study the photocatalytic activity in water splitting. The experimental results show that the enhancements in the photocatalytic activity afforded by the Zr-MCM-41 photocatalysts could be due to the high dispersion of ZrO_2 in the amorphous wall of MCM-41.[199a] Similar results were reported using W supported on MCM-48.[199b]

Recently, Peng *et al.*[200] have prepared two sets of titania, one containing MCM-41 and the other MCM-48, as catalysts for water splitting. The photocatalytic H_2 evolution results indicate that the cubic phase MCM-48 exhibits a higher activity as the host photocatalyst than hexagonal MCM-41 materials. Moreover, it was also confirmed that tetrahedrally coordinated Ti species possess a much higher photocatalytic efficiency than the octahedral ones and that the cubic phase is a better support than the hexagonal mesoporous silica support.

Ordered mesoporous materials have significant potential for improving a variety of catalytic routes for the production of hydrogen. Some additional results related to the importance of the mesoporosity in the H_2 production can be found elsewhere.[167]

3.4. Catalytic valorisation of CO_2

Nowadays CO_2 emissions to the atmosphere are growing, owing to the higher demand for fossil fuels caused by increases in population and living standards. The European Union has set

an ambitious target to drastically reduce greenhouse gas emissions over the next few decades. In 2020 the reduction of greenhouse gas emissions should be 20% and in 2050 around 50% in Spain.[201] The need to mitigate the accumulation of CO_2 in the atmosphere requires technologies able to reduce CO_2 emission. Among the different technologies hoping to lower such emissions, the utilization of CO_2 as a building block may represent an interesting approach to obtain valuable chemicals and materials.[202–206] The most difficult task related to CO_2 conversion into organic compounds is the stability of the CO_2 molecule. In order to activate the CO_2 molecule a high quantity of energy is necessary to weaken the C–O bond. The valorisation process of CO_2 must be partnered with a renewable energy like solar energy, to supply the energy involved in the process.[207]

Traditionally, CO_2 was limited to a few processes like the synthesis of urea, salicylic acid and polycarbonates. However, nowadays the versatility of CO_2 to produce chemical products is being developed constantly, as shown in Fig. 16. Carbon dioxide reacts with hydrogen, alcohols, acetals, epoxides, amines, carbon–carbon unsaturated compounds and oxetanes in the presence of metal compounds as catalysts.[204–209]

Intensive research efforts are necessary to find new ways of functionalising carbon dioxide and to improve the selectivity of the products by new catalysts. Although most organic compounds are synthesised by homogeneous catalysis, the most important obstacle for large-scale production using this approach is the removal of the catalyst and the purity of the final products. Heterogeneous catalysis is more realistically applicable to large-scale production because it is possible to remove the catalysts and, consequently, the purity of the products is higher.

Therefore, it is vital to develop heterogeneous catalysts if CO_2 is to be converted into valuable molecules for different applications.[210]

CO_2 valorisation includes different processes like the hydrogenation of CO_2, methanol or ethanol reforming, the conversion of alkane to alkenes and the fixation of CO_2 into organic molecules.

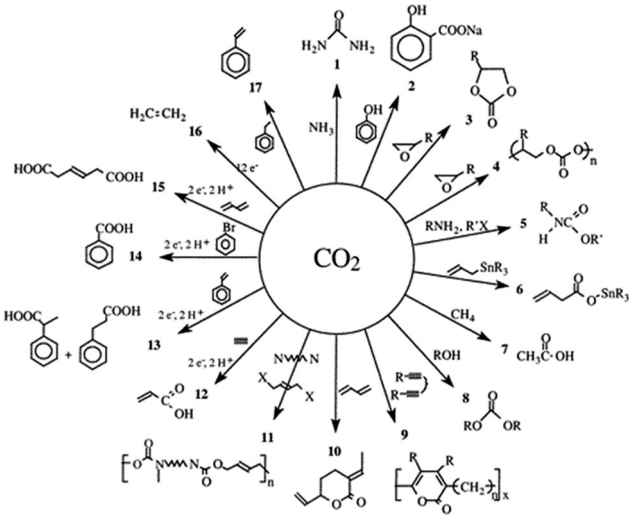

Fig. 16 The chemical transformation of CO_2. Reproduced with permission from ref. 209. Copyright 2001, American Chemical Society.

3.4.1. Hydrogenation of CO_2. One of the most interesting processes to valorise CO_2 is the hydrogenation of CO_2 to form oxygenates and/or hydrocarbons. Anything from C1-type molecules like methane or methanol to higher molecular weight alkanes, alkenes and alcohols (through C–C bond formation) are able to be produced by this process.[211] Methanol synthesis from CO_2 and H_2 has been investigated at the pilot plant stage with promising results. Methanol may be used as feedstock in fuel cells, providing a route to store energy from CO_2 and then produce electricity.[212]

Over the last two decades, the hydrogenation of CO_2 to CH_3OH has been studied in order to develop effective catalysts. At the beginning, supported precious metals (Pt or Pd) were used to study CO_2 hydrogenation. It is well established that both the support and the active phase can modify the activity and selectivity.[213–215]

Additionally, the activity can be increased by the addition of promoters like Cr_2O_3, Ga_2O_3 and ZrO_2.[206,216,217] Recently, it has been observed that the uniform pore structure of mesoporous materials may provide nano-sized uniform reaction environments which enable the stabilisation of small metal nanoparticles inside the mesopores. In this connection, it is worth mentioning that a so-called bi-functional mechanism has been proposed for CH_3OH formation from CO_2, over metal oxide-promoted Pd catalysts, where the metal oxide promoters stabilise adsorbed formate (or CO_2) species and metallic Pd-dissociated H_2 molecules simultaneously.[218] Thus, a better catalytic activity for CH_3OH formation would be expected when small Pd and metal oxide nanoparticles are incorporated inside mesocavities. In addition, if the size of the Pd nanoparticles can be controlled systematically by mesoporous materials with different pore diameters, these catalysts could also become an interesting model catalyst.

Although some research groups have already shown the use of mesoporous silica with a high activity for the hydrodesulfuration of dibenzothiophene,[219] the Fischer–Tropsch synthesis,[220] and H_2O_2 synthesis[221] as a support, its utility in the hydrogenation of CO_2 to methanol is still very limited. In 2006 Yu and co-workers studied the effect of a Ru catalyst supported on functionalised MCM-41.[222] In this study they combined the benefits of heterogeneous catalysis with the benefits of homogeneous catalysis, immobilising Ru complexes on the functionalized mesoporous MCM-41. Their results showed that MCM-41-immobilised ruthenium complexes exhibit a promising catalytic performance as heterogeneous catalysts for the synthesis of formate from CO_2 and H_2 in CO_2-expanded solvent. Later on, Kosizumi and co-workers studied the effect of nano-structured mesoporous supports and the effect of the addition of alkali/alkaline earth metal oxides on the CO_2 hydrogenation reaction.[223]

As shown in Fig. 17, mesoporosity does not guarantee good performance in CO_2 hydrogenation. This paper demonstrates that the small mesopores of MCM-41 and SBA-15 work as a template for the formation of small Pd^0 nanoparticles, leading to a higher activity for methanol formation compared to the conventional amorphous silica. Indeed, the importance of mesoporosity is related to the development of specific Pd nanoparticles rather than diffusional problems. It seems that the overall reaction for methanol formation is governed by the

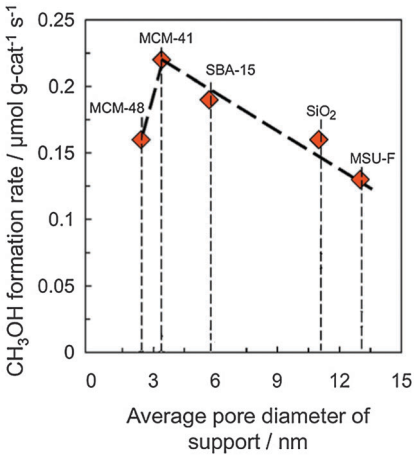

Fig. 17 The dependency of the rate of CH_3OH formation over Ca(0.4)/Pd(6) catalysts on the average pore diameter. Adapted from ref. 223. Copyright 2012, Elsevier.

surface reaction rather than diffusion on the reactants, probably due to the low reaction temperature used.

3.4.2. Dry reforming. One possibility for CO_2 valorisation concerns dry reforming to obtain syngas with a H_2/CO molar ratio of 1, which can then be used to produce hydrocarbons by the Fischer–Tropsch reaction.

This reaction has been extensively studied using mesoporous materials as a support for the active phase. Rh-based catalysts are known to have a high activity, stability and low coke formation in the CO_2 reforming of methane and the reforming of ethanol reactions.[224] Wu and Kawi studied the effect of Rh/Ce-SBA-15 as a catalyst for the CO_2 reforming of ethanol.[225] They observed that the mobility of the surface oxygen species and the Rh dispersion over the Ce/SBA-15 catalyst support were important parameters in achieving a high catalytic performance. It was demonstrated that hexagonal mesoporous SBA-15 remains intact after the CO_2–ethanol reforming reaction for 24 h at 600, 650, 700 and 750 °C. So, the 1%Rh/Ce-SBA15 catalyst is a potential commercial catalyst for CO_2 reforming with ethanol to produce syngas and hydrogen.

One important point about CO_2 reforming is the inhibition of the catalysts by carbon deposition. This coke deposition is related to the active metals and the support. Ni-based catalysts have been reported to easily deactivate due to the formation of coke. The low cost of Ni has encouraged the development of new Ni-based catalysts with an improved stability. Xu and co-workers studied the effect of an ordered mesoporous NiO–Al_2O_3 composite in the CO_2 reforming of methane.[226] It was demonstrated that ordered mesostructured catalysts can offer a high activity and long stability, by supplying much more accessible Ni active sites to the reactant and stabilising the Ni nanoparticles *via* the ''confinement effect'' during the reaction. Ni nanoparticles exist among the framework of the material, which contribute to suppressing the coke deposition.

Later on, the incorporation of MgO was evaluated in order to produce mesoporous NiO–MgO–Al_2O_3 *via* a one pot evaporation induced self-assembly (EISA) strategy.[227] The benefits of the material NiO–MgO–Al_2O_3 over NiO–Al_2O_3 were found to be a large specific surface area, a large pore volume and a favourable thermal stability. The addition of moderate amounts of Mg promotes the catalytic properties. These materials were tested over a 100 h reaction time with no loss in catalytic activity.

Furthermore, it is well known that the nature of the supports greatly affected the catalytic performance of Ni based catalysts for the catalytic reforming of methanol (CRM). Various materials such as MgO, Al_2O_3, SiO_2, CeO_2 and ZrO_2 have been investigated as a support for Ni based catalysts. Currently, different metal oxides have been developed in order to obtain materials with improved thermal stability.

In order to compare the effect of the support, Sarkar and co-workers studied the CO_2 reforming to methane, catalysed by Ni supported on SiO_2/Al_2O_3 and ZSM-5.[228] They demonstrated that mesoporous ZSM-5 as a support was more active than mesoporous SiO_2/Al_2O_3 due to the different Ni dispersion on the supports. Ni-ZSM with 5% of Ni showed 96.2% methane conversion at 800 °C in the used conditions. Consequently, mesoporous materials are important to synthesise active phase nanoparticles with good metal dispersion.

After studying the effect of Ni and Ni–Mg mesoporous materials on Al_2O_3, Xu and co-workers studied CO_2 reforming by using Ni–Ce/Zr mesoporous solids.[229] It was the mesoporous framework that endowed the mesoporous catalyst with more activity. Specifically, predominant textural properties provided more ''accessible'' Ni active centres for the gaseous reactants accounting for the higher activity. The ''confinement effect'' of the mesopores imbued the Ni nanoparticles with a higher stability. As noble metals commonly excel in coke resistance and thermal sintering, Takahashi and co-workers analysed the effect of a Pt/ZrO_2 mesoporous catalyst in the CRM reaction.[230] As previously mentioned, the presence of a mesoporous support is important to achieve good metal dispersion and to improve the resistance to coking.

Recently, the CRM reaction has been studied on different mesoporous catalysts, like Ni-SBA-15 prepared with β-cyclodextrine.[231] β-Cyclodextrine was added to increase Ni dispersion and the catalysts prepared with β-cyclodextrine were more active than their NiSBA-15 counterparts. The presence of mesopores was required in order to favour the intimate contact between the cyclodextrine and the Ni particles, thus preventing Ni sintering effects. It is known that Y can act as a promoter for catalytic reforming reactions. With this in mind, Li and co-workers studied the effect of Ni/Y-SBA15 mesoporous materials in the CRM reaction.[232] Y is a promoter of the CRM reaction by enhancing the reduction of NiO, which was attributed to the oxygen vacancies on the surface of the catalyst and the high mobility and activity of the surface oxygen species. The presence of a mesoporous support is important to achieve a good Y dispersion around the structure.

As mentioned before, CeO_2 is a good support for catalysts due to its redox properties. However, its thermal stability must be improved. Zeng and co-workers described the influence of pore distribution on the catalytic performance of an inverse CeO_2/Co_3O_4 catalyst for the CMR reaction.[233] It was demonstrated

that the CeO_2/Co_3O_4 catalyst with double pore distribution could give more active sites as well as better gas circulation channels, reducing the internal diffusion resistance and improving the catalytic performance for CH_4/CO_2 reforming. This work is in agreement with the results obtained using bimodal silica.[234] Finally, one of the latest works related to the CRM reaction has been done by Guo and co-workers, who have studied the catalytic properties and stability of cubic mesoporous $La_xNi_yO_z$/KIT-6 catalysts.[235] La_2NiO_4/KIT-6, showing the highest activity for CMR reaction at 800 °C, still retains the mesoporous structure and high surface area, which is favourable for the diffusion or adsorption of reactant molecules. During the reforming reaction, the formation of $La_2O_2CO_3$ species can maintain the balance between carbon deposition and elimination. The thermal stability of the La_2NiO_4/KIT-6 catalyst is significantly higher than that of La_2NiO_4/SBA-15 due to the stable cubic structure of the KIT-6 support.

3.4.3. Conversion of alkanes to alkenes. The conversion of alkanes into alkenes by oxidative or non-oxidative dehydrogenation is important because of the growing demand. Nakagawa and co-workers studied in 1998 the dehydrogenation of ethane by carbon dioxide over several oxides and found that gallium oxide was an effective catalyst for this reaction.[236] Takahara and Saito reported the promoting effect of CO_2 on propane dehydrogenation by Cr_2O_3 catalysts.[237] A few years ago Leth and co-workers studied the effect of Ga addition in MFI mesoporous materials on this reaction.[238] The introduction of mesoporosity into Ga-MFI zeolite leads to a significant improvement of the catalytic activity and selectivity in ethane aromatisation. This improvement was attributed to the better accessibility of the active Ga species inside the mesopores.

Taking into account the promoting effect of Cr_2O_3, Rao and co-workers studied the effect of Cr addition on different siliceous materials derived from MCM-41.[239,240] The results showed that the ethane dehydrogenation reaction depends on the chromia loading and the catalyst preparation. Cr/MCM-41 catalysts were more active than bulk Cr_2O_3, this effect being attributed to the better metal dispersion on the mesoporous material supports.

Another important process is the oxidative dehydrogenation (ODH) of propane to propene. It is known that a limited propene selectivity at higher propane conversions is linked with the propene adsorption on acid sites and their subsequent oxidation to carbon oxides. Thus, it is challenging to develop new efficient catalyst systems which can allow the production of propene with a high selectivity at a higher propane conversion. Cr catalysts were studied in the propane dehydrogenation reaction by Michorczyk and co-workers using mesoporous materials as the support.[241] In dehydrogenation reactions the higher the dispersion of the active phase, the higher the activity.

Recently, Zhang and co-workers studied the effect of ZSM-5-supported chromium oxide catalysts prepared by the incipient wetness method in the dehydrogenation of propane.[242] This study demonstrates that chromium oxide supported on an Na-type ZSM-5 with a smaller crystal size (*ca.* 400 nm) is an attractive new catalyst applicable for propane dehydrogenation to propylene with CO_2. This catalyst exhibits a substantially higher activity than chromium oxide supported on ZSM-5 with a larger crystal size (*ca.* 2 μm).

Finally, it is noteworthy to mention that the number of studies dealing with large molecules is rather scarce. As an example, Wang and co-workers prepared a series of mesoporous silica SBA-15 supported chromia catalysts and examined their catalytic properties for the ODH of ethane, propane, *n*-butane and isobutane.[243] All catalysts showed an excellent catalytic activity and the results could be explained by a combination of factors: (1) the good redox behaviour of the Cr species, (2) the formation of highly disperse mono- and polychromate domains, and (3) the formation of well-ordered mesostructured banana-like SBA-15 rods that provide a local environment favourable for the adsorption, desorption and diffusion of the reactant or product molecules. One important process is the catalytic dehydrogenation of ethylbenzene (EB) to obtain styrene. Styrene is one of the most important monomers in the petrochemical industry because of its use in the production of various polymers such as polystyrene, styrene-acrylonitrile (SAN) copolymer, styrene-butadiene rubber (SBR) and acrylonitrile-butadiene-styrene (ABS) *tert*-polymer.

Contrary to the process that uses oxygen as a strong oxidant, the dehydrogenation of ethylbenzene with CO_2 produces styrene with a much higher selectivity. Qiao and co-workers studied VO_x/MCM-41 catalysts for the EB reaction.[244] They concluded that catalysts prepared using a mesoporous support showed a higher EB conversion, which must be attributed to the better metal dispersion on the support.

3.4.4. Fixation of CO_2 into organic molecules. The synthesis of cyclic carbonates is a field of growing interest due to a wide variety of applications. In the last decade of the 20th century, many catalytic systems were developed for the insertion of carbon dioxide into oxiranes. However, these catalysts suffered from a low catalytic activity and/or selectivity, a low stability and poor separation, as well as requiring high pressure and/or high temperatures.

The functionalisation of well-ordered mesoporous solids by post-grafting techniques has been postulated as a more efficient synthetic route since it increases the efficiency for the utilisation of large pore materials. Hybrid inorganic–organic mesoporous materials based on the co-condensation of siloxane and organosiloxane precursors, in the presence of a templating surfactant solution are of interest for producing a regular and ordered architecture. Udayakumar and co-workers studied the fixation of CO_2 to allyl glycidyl ether over an ionic liquid immobilisation on MS41.[245] The results showed that the modified MS41 materials were generated with a large number of active sites, uniform pores and high surface area. The excellent activity of these materials is owed to the large number of active sites in the host system. Recently, Nelson and Adam studied the synthesis of styrene carbonate *via* the cycloaddition of CO_2 using ordered mesoporous MCM-41-Imi/Br catalysts.[246] This material promises to be a heterogeneous, environmentally friendly and active catalyst for the production of cyclic carbonates from styrene oxide. The fixation of CO_2 into three-member heterocyclic rings such as aziridine for their transformation into five-member heterocyclic rings such as oxazolidinones is important for their versatile intermediates. MCM-41 grafted with amine groups has

been reported to catalyse many organic reactions. These catalysts have a good mesoporous structure ordering, a large BET surface area and a high porosity. All these qualities are important to permit the diffusion of the molecules into the catalyst. Recently, Nale and co-workers studied the regioselective synthesis of 5-aryl-2-oxazolidinones from CO_2 and aziridines by amine functionalised MCM-41.[247] The results make it a promising material for the cyclic carbonates reaction from styrene oxide.

The efficient CO_2 valorisation process requires mesoporous catalysts containing uniformly distributed small nanoparticles. For the big size of the molecules involved in this process, mesoporous materials also help to avoid diffusional problems.

3.5. Photocatalytic energy technologies

By adsorption of light with greater photonic energy, semiconductors can generate electron–hole pairs, which initiate simultaneously oxidative and reductive reactions with surface species, before recombination. Catalysts under light irradiation, called photocatalysts, are attracting a great deal of attention, both for fundamental science and practical applications.[248] This technology can be divided into the degradation of molecules into CO_2 or the utilization of CO_2 to produce organic molecules.

3.5.1. Degradation of organic molecules. In order to solve the problems related to environmental pollution, various catalytic techniques have been investigated in the last decades. Heterogeneous photocatalysis is a popular technique that has great potential to control aqueous contaminates or air pollutants. Since the early development of this technology in the 1970s, TiO_2 has constituted the archetypical photocatalyst due to its relatively high efficiency, low cost and availability. However, during the last decade a considerable number of approaches have been adopted with the aim of increasing the surface area, porosity or the incorporation of additional components such as metals or second semiconductor phases.[249] Heterogeneous photocatalytic oxidation using TiO_2 has been widely studied and applied to degrading a variety of organic compounds.[250] However, pure titania exhibits a low adsorption ability for bulky organic pollutants, which can be improved by its deposition on inert porous supports.

During the last few years, a lot of research has been done to activate mesoporous materials with titanium oxide in order to obtain large pore catalysts allowing high diffusion rates and therefore an improved photocatalytic activity for bulky molecules.[93a,251,252] The preparation conditions such as the synthesis time and calcination temperature significantly influence the photocatalytic activity of meso–macroporous TiO_2, illustrating the role of porosity in light harvesting photocatalysis[253,254]

For instance, Saadoun and co-workers[255] tested the activity of a titania, synthesised using an ammonium salt as a hydrolysis control agent, in the oxidation reaction of formaldehyde. The results indicated that the diffusion of the reactants or products within a porous catalyst could be a rate-limiting factor. TiO_2 catalysts prepared hydrothermally showed a significantly higher efficiency than the commercial titania, Degussa P25.

Later on, Wang and co-workers[256] prepared bimodal meso–macroporous TiO_2 by a self-formation phenomenon process in the presence of surfactants. Ethylene photodegradation in the gas-phase was chosen as a probe reaction to study the photocatalytic activity. The results showed that catalysts calcined at 350 °C possess an intact macro/mesoporous structure and higher photoactivity (60% higher than of commercial P25 titania). When the calcination temperature was increased above 600 °C, the macro/mesoporous structure was destroyed and a loss in the photocatalytic activity was observed. The high photocatalytic performance of the low-temperature-calcined macro/mesoporous TiO_2 may be explained by the existence of macrochannels that increase the photoabsorption efficiency and allow the efficient diffusion of gaseous molecules. Similar results were obtained by Yu and co-workers.[257] These authors found that the hierarchical macro–mesoporous TiO_2 calcined at 300 °C had the maximum photocatalytic activity for the oxidation of acetone in the gas phase (around twice that of P25). The activity then decreased as the calcination temperature increased, due to the destruction of the macroporous structure and the decrease in the surface area.

The incorporation of supported titania within silica materials has been also proposed for improving the surface area of these materials. Hamdy and co-workers studied the incorporation of TiO_2 in a silica mesoporous material (TUD-1), to evaluate the selective light-activated oxidation of propane to acetone.[258] The results showed that nanoparticle-containing TiO_2-TUD-1 can be more selective in the photooxidation of propene to acetone than commercially available microcrystalline anatase.

Later on, Busuioc and co-workers[259] reported a post-synthesis deposition method to form crystalline titania plugs inside the mesopores of SBA-15. Anatase nanoparticles with different sizes were deposited into the SBA-15 channels, influencing the adsorption properties and photocatalytic activity. These materials exhibit an improved catalytic activity for the destruction of Rhodamine 6G under UV light irradiation.

More recently, Tasbihi and co-workers[260] studied the photocatalytic degradation of isopropanol in the gaseous medium. They catalysed the reaction with titania, incorporated in ordered (SBA-15) and disordered (KIL-2) mesoporous silica *via* the sol–gel impregnation method. The results showed that the photocatalytic activity towards the formation of acetone depends on the accessibility and number of titania nanoparticles. In the STi/SBA-15 (1/1) sample, prepared using an aqueous crystalline anatase sol with a Ti/Si ratio of 1, the loading of titania was not too high to decrease accessibility and high enough to ensure a sufficient quantity of active nanoparticles for the reaction. Therefore among all the investigated samples the photocatalytic activity (acetone formation rate) of STi/SBA-15 (1/1) was the highest. The results revealed the benefits of a mesoporous support when removing an organic contaminant from the gaseous phase.

Later on, Dong and co-workers[261] prepared 2-D hexagonal mesoporous TiO_2–SiO_2 nanocomposites consisting of anatase TiO_2 nanocrystals and amorphous SiO_2 nanoparticles, with large mesochannels and high specific surface areas. The photocatalytic degradation of different organic dyes like Methylene Blue, Safranin O, Crystal Violet, Brilliant Green, Basic Suchsin, Rhodamine-6G, Acid Fuchsin, Orange II, Reactive Brilliant Red

X3B, Acid Red 1 and Microcystin-LR was evaluated in these systems. The results showed that the samples prepared by TiO_2–SiO_2 nanocomposites exhibited an excellent degradation activity for all the contaminants, much higher than that of the P25 photocatalyst. The dyes were not only decolourised promptly but degrade readily as well. It was thus demonstrated that these catalysts had promising applications in the fast and highly efficient degradation of various organic pollutants. Recently, Rico *et al.* synthesised a mesoporous titania–organosilica material with a high surface area, (*ca.* 300 $m^2\ g^{-1}$) with excellent activity in the degradation of a commercial dye under UV light.[93a]

As far as the morphology of TiO_2 is concerned, Zhang *et al.*[262] employed highly crystalline mesoporous TiO_2 synthesised *via* the surfactant sulfuric acid carbonisation method for the degradation of Rhodamine B (RhB) under UV light irradiation. A higher photocatalytic activity was achieved than from the commercial P25, which can be attributed to the higher surface area of the ordered mesoporous TiO_2. At the same time, Zhu and co-workers[263] prepared titanium oxides with hierarchical structures using biotemplates by the sonochemical method. The calcination temperature has a strong effect on the structural reproducibility and photocatalytic activity of the replicas. It was demonstrated that a calcination temperature of 450 °C results in the best structural replication, the highest surface area, (*ca.* 58.4 $m^2\ g^{-1}$), and hence the best photocatalytic properties. TiO_2-450 showed better photocatalytic properties than P25, which could be attributed to its hierarchical interconnected structures with open and accessible pores, as well as the fine grain size and large surface area of the TiO_2 replica. Finally, He and co-workers[264] have studied the photocatalytic activity in the degradation of gaseous benzene with mesoporous TiO_2. Mesoporous anatase TiO_2 samples were prepared *via* a solvothermal method, using TBT (tetrabutyl titanate) as the Ti source and acetic acid as the solvent. The materials were studied for the degradation of gaseous benzene under UV irradiation. It was demonstrated that nano-sized TiO_2 particles prepared under optimal conditions had the largest specific surface area (two times higher than Degussa P25) and a significantly higher efficiency for benzene degradation compared to commercial P25.

Up to now, the importance of the development of mesoporous TiO_2 for photocatalytic degradation has been demonstrated. To further improve the photocatalytic activity of hierarchical porous TiO_2, several strategies based on chemical and physical concepts have been adopted. Metal doping of porous TiO_2 structures has been thought to be a good way to enhance the photocatalytic activity, while the coupling of TiO_2 with another semiconductor is another widely used approach.[192,248]

For instance, Zhou and co-workers[265] studied the effect of Fe doping on mesoporous TiO_2. The samples were prepared by the ultrasonic-induced hydrolysis reaction of tetrabutyl titanate in a ferric nitrate aqueous solution without using any template. The photocatalytic activity of the Fe-doped TiO_2 powders calcined at 400 °C was more than twice that of Degussa P25 (at an optimal atomic ratio of Fe to Ti of 0.25) for the photodegradation of acetone. The high activity of the Fe-doped TiO_2 powder can be attributed to the results of the synergetic effect of Fe-doping, the large BET specific surface area and the small crystallite size.

Recently, the doping of different metals has been used in different photocatalytic degradation reactions. As an example, Ismail[266] reported a synthesis of mesoporous PdO–TiO_2 nanocomposites, through a simple one-step sol–gel reaction, for the photooxidation of methanol in aqueous suspensions. Comparing these catalysts with Pd/aeroxide TiO_2–P25, the PdO–TiO_2 nanocomposites showed more effective and efficient photocatalytic activities for methanol oxidation to formaldehyde (4 and 2 times more than PdO–TiO_2 and Pd/TiO_2-P25, respectively). The photocatalytic results indicated that these PdO–TiO_2 nanocomposites with a mesoporous structure enable the high flux and rapid diffusion of methanol.

Additionally, Ismail[267] reported the synthesis of mesoporous Ag/TiO_2 films, where the nanoparticles are highly dispersed into TiO_2 thin films in a simple one-pot reaction, with the P123 triblock copolymer as a template. The obtained mesoporous Ag/TiO_2 films were evaluated for their photocatalytic degradation of 2-chlorophenols showing that these catalysts were more photoactive (8 times more) than the nonporous commercial photocatalyst Pilkington Glass Activ. Furthermore, the Ag/TiO_2 films were quite stable during the reaction with no significant loss of activity after 10 runs. Recently, Choina and co-workers[268] have studied the effect of Zr-doped anatase titania prepared by sol–gel and chemical vapour deposition methods in the oxidative decomposition of Ibuprofen (IBP). The obtained photocatalytic material shows a high initial activity and exhibits improved adsorption properties in aqueous solution. Both of these properties make the catalyst interesting for the decomposition of hazardous compounds like IBP, especially in a low concentration aqueous solution.

Since doping both with transition metals and lanthanide ions each has its respective advantages, it can be assumed that doping with two dopants can show a synergetic effect with an improved photocatalytic activity. For instance, Nesic and co-workers[269] prepared titanium dioxide photocatalysts co-doped with lanthanum and vanadium using a facile microwave-assisted hydrothermal method. The co-doping of vanadium contributes to the extension of absorption into the visible region. The photocatalytic activity of the samples was evaluated by the decolourisation of the textile dye Blue 52 in aqueous solutions under sun-like radiation. Compared with La singly doped TiO_2, the co-doped catalysts showed a significant improvement in photoactivity, even higher than commercially available titania P25. Although gold was recognised to be poorly active as a catalyst, when Au nanoparticles were highly dispersed on semiconductor metal oxides or hydroxides, they exhibited a good catalytic activity. Furthermore, it was expected that the encapsulation of gold nanoparticles in the MCM-41 or TiMCM-41 surface would tailor the photoresponsiveness into the visible region.

With this in mind, Kumar and co-workers[270] prepared Au/TiMCM-41 photocatalysts to study the photodegradation of methyl orange. It was demonstrated that Au/TiMCM-41 had a higher photocatalytic activity than TiMCM-41. Recently, Zhan and co-workers[271] have studied the photocatalytic degradation of

methyl orange by using $Mo/TiO_2/SiO_2$ materials. A Mo-doped, TiO_2-fumed SiO_2 composite was prepared by a feasible sol–gel method. The prepared catalysts exhibit a good photocatalytic activity under both ultraviolet and visible light irradiation for methyl orange degradation. The high surface area and high active site concentration on the composite surface are considered the key factors in this.

Yan *et al.*[272] have studied the effect of WO_3 in the photodegradation of Rhodamine B dye and phenol under simulated solar light irradiation. It is worth noting that WO_3, with a narrow band gap, is one of the most important photocatalysts. For that reason, Yan prepared a highly ordered mesoporous WO_3–TiO_2 composite material by a surfactant template-assisted evaporation-induced self-assembly process. The presence of a large quantity of mesopores in the composite system allows the diffusion of organic compounds inside the bulk material, shortening the migration distance of photogenerated charge carriers and reducing the opportunity for electron–hole recombination. The results show that both the surface area and crystallinity degree are important parameters in the photodegradation reaction.

Similar to metals, non-metals doped or deposited on TiO_2 can effectively improve its photoactivity and selectivity under visible light irradiations. The most commonly used non-metals so far investigated, in a number of studies, are C, N, F, I and S. For instance, Hu and co-workers[273] studied the effect of N doping on mesoporous TiO_2. Non-metal doping is one of the typical chemical modifications able to enhance the visible light photocatalytic activity of oxides. N-doping has been proved to be a simple and effective way to increase the visible light adsorption. N-doped mesoporous TiO_2 spheres were prepared by a dual-templating synthesis. The ordered arrays of N-doped mesoporous TiO_2 spheres showed an enhanced visible light photocatalytic activity, which could be attributed to the N doping effect, abundant ordered mesopores and a unique opal structure. Such TiO_2 sphere arrays may be promising for practical applications in the fields of environmental purification, water photoelectrolysis and dye sensitized solar cells.

Non-semiconducting metal oxides, like alumina and silica, have frequently been used for supporting photocatalysts, in order to control the product selectivity or to shift the reaction to visible light irradiation conditions. For instance, Cr–SiO_2 materials containing highly dispersed chromate species have been proved to catalyse the photo-oxidation of different olefins under visible light irradiation, with a high selectivity to partially oxidized products; while TiO_2 promoted complete decomposition.[274] Mo, Mn, Cr, Cu, Co and Ag have all been studied as metal doping photocatalysts. Rodriguez and co-workers[275] compared the photoactivity of Degussa P25 with Co–Al-MCM41 materials in the degradation of acetaldehyde using visible light and UV-visible light. The results showed that Co–Al-MCM41 with an optimum Co/Al ratio effected good photocatalytic degradation in visible light, but did not work as well as P25 in UV-visible light conditions. Similar results were obtained using Cr–Al-MCM-41 and AgBr/Al-MCM-41 catalysts.[276,277] These are thus representative examples which prove that mesoporous materials as a support have many advantages due to their large surface area, uniform pore size and accessible open frameworks.

3.5.2. Artificial photosynthesis. Artificial photosynthesis of hydrocarbons from CO_2 and water was studied by Baly and co-workers in 1921.[278] The final product, formaldehyde, was produced under visible light using colloidal uranium and ferric hydroxides as catalysts. Nowadays, with increasing CO_2 emissions ever on the mind, the artificial photosynthesis of CO_2 is an alternative for obtaining organic compounds with high value. The process is endothermic and consequently it constitutes a potential route for storing solar energy in the form of convenient liquid fuels. Under this premise, it is necessary to develop new catalysts with a high efficiency for CO_2 conversion.[279] TiO_2 is one of the most investigated photocatalysts in artificial photosynthesis. In the 1970s, Fujishima and co-workers reported photoelectrochemical water splitting and CO_2 photoreduction by TiO_2.[280,281] Later, Hwang and co-workers showed that the incorporation of Ti into mesoporous silica (Ti-SBA-15) increases the CH_4 yield by two orders of magnitude when compared to TiO_2, and the methanol yield by one order of magnitude in terms of μmol produced per gram Ti per hour.[282]

Recently, the effect of mesoporosity in artificial photosynthesis has been developed by many research groups. For instance, Frei and co-workers[283] studied the formation of formic acid as the main product over a Ti silicalite molecular sieve (TS-1), under UV light and using methanol as an electron donor. On studying the mechanism of the reaction with FTIR spectroscopy measurements they found that CO_2 splits to CO and O_2 at the excited metal-to-metal charge-transfer sites.[284] Recently, Tahir *et al.*[285] have studied photocatalytic CO_2 reduction with H_2O in the gaseous phase, using TiO_2 and indium doped TiO_2 nanoparticles in a microchannel monolith photoreactor. The results show that this photoreactor possesses a larger illuminated surface areas, higher light utilisation, an efficient adsorption–desorption process and a higher catalyst interparticle mesoporosity. All of these are key factors in improving the yield rates in a monolithic photo-reactor. They have demonstrated that well-developed mesopores, a larger surface area and a higher pore volume can enhance the molecular transportation rates of reactants and products to increase CO_2 conversion efficiency.

Another study using mesoporous silica supported Cu–TiO_2 nanocomposites and prepared by a one-pot sol–gel method shows that the high surface area mesoporous silica substrate greatly enhanced CO_2 photoreduction due to improved TiO_2 dispersion and the increased adsorption of CO_2 and H_2O on the catalyst.[286]

Until now, a large number of studies have been reported for the increased CO_2 photocatalytic conversion efficiency using various TiO_2-based photocatalysts. However, because of the wide band gap and relatively slow carrier transport of titania, the activity of TiO_2-based photocatalysts in the reduction of CO_2 with H_2O is not high enough for practical uses, especially under visible or solar light irradiation. CeO_2 is an n-type semiconductor and therefore has been used as a dopant to improve titania-based catalysts. Wang and co-workers[287] have studied the reduction of CO_2 with H_2O under simulated solar irradiation using ordered

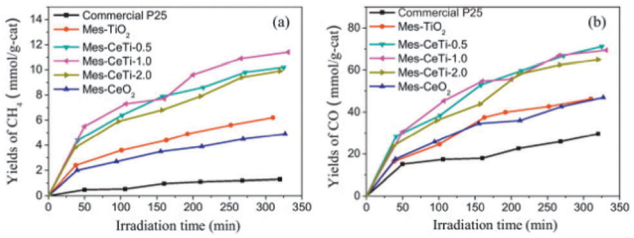

Fig. 18 The yield of CH_4 (a) and CO (b) as a function of the irradiation time over all photocatalysts. Reproduced with permission from ref. 287. Copyright 2013, Elsevier.

mesoporous CeO_2–TiO_2 composites synthesised through a nanocasting route, with ordered mesoporous SBA-15 as the template. The results are shown in Fig. 18.

It is demonstrated that the ordered mesoporous CeO_2–TiO_2 composites exhibit a higher photocatalytic activity in the photoreduction of CO_2 with H_2O under simulated solar irradiation than commercial P25. The results show that CeO_2 addition can enhance the photocatalytic efficiency of pure mesoporous TiO_2. The enhanced photocatalytic performance for these CeO_2–TiO_2 composites can be ascribed to their unique structure, which confers a variety of favourable properties. Firstly, ordered mesoporous architecture with a large surface area and 2D open-pore system makes the reactant diffusion into the bulk of the catalyst easy, and hence provides fast intraparticle molecular transfer. Secondly, the introduction of CeO_2 species into composites can effectively extend the spectral response from the UV to the visible area owing to the CeO_2-photosensitisation. Later on, Wang's group prepared ordered mesoporous Fe-doped CeO_2 catalysts by nanocasting, using ordered mesoporous SBA-15 as the template.[288] These catalysts exhibit a good photocatalytic performance in the reduction of CO_2 under simulated solar irradiation.

Another alternative to CO_2 photoreduction is the use of surface-anchored molecular catalysts that combine the advantages of homogeneous and heterogeneous catalysis.[289] For instance, Dubois *et al.*[290] have studied the photocatalytic reduction of CO_2 using Re-bby immobilised on mesoporous silica. The results show that covalent attachment through simple organic linkages is a promising strategy for immobilising molecular CO_2-reduction photocatalysts on solid-state surfaces.

4. Beyond catalysis

4.1. Novel mesoporous electrodes for fuel cell technologies

In a fuel cell, the chemical energy of a fuel and an oxidant is converted into electrochemical energy. The process involves electron transfer during the oxidation and reduction reactions with an essentially invariant electrode–electrolytic system.[291] Nowadays, there are several types of fuel cell (FC) differing, mainly, in the nature of the electrolyte. However, the basic operating principle of all types of FC is the same; see the schematic representation in Fig. 19. A fuel, *i.e.* hydrogen, is oxidised at the anode into protons and electrons, while at the

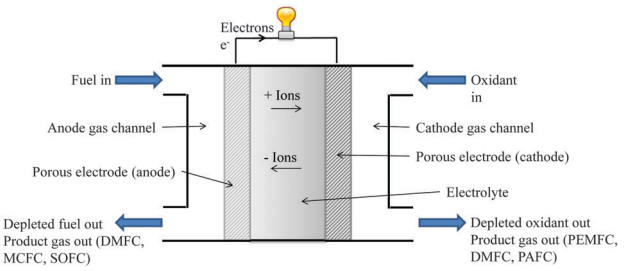

Fuel cell type	Anode reaction	Mobile Ion	Cathode reaction
AFC	$2H_2 + 4OH^- \rightarrow 4H_2O + 4e^-$	OH^-	$O_2 + 2H_2O + 4e^- \rightarrow 4OH^-$
PEMFC	$H_2 \rightarrow 2H^+ + 2e^-$	H^+	$1/2O_2 + 2H^+ + 2e^- \rightarrow H_2O$
DMFC	$CH_3OH + H_2O \rightarrow 6H^+ + 6e^- + CO_2$	H^+	$3/2O_2 + 6H^+ + 6e^- \rightarrow 3H_2O$
PAFC	$H_2 \rightarrow 2H^+ + 2e^-$	H^+	$1/2O_2 + 2H^+ + 2e^- \rightarrow H_2O$
MCFC	$H_2O + CO_3^{2-} \rightarrow 2H_2O + CO_2 + 2e^-$	CO_3^{2-}	$1/2O_2 + CO_2 + 2e^- \rightarrow CO_3^{2-}$
SOFC	$H_2 + O^{2-} \rightarrow 2H_2O + 2e^-$	O^{2-}	$1/2O_2 + 2e^- \rightarrow O^{2-}$

Fig. 19 A schematic representation showing the general operating principles of a fuel cell and the principle anode and cathode reactions, as well as the mobile ions associated with the most common fuel cell types. Adapted from ref. 296. Copyright 2011, IEEE.

cathode, oxygen is reduced to oxide species, and these then react to form water. Depending on the electrolyte, protons or oxide ions are transported through the electrolyte, which should be ion conducting but electronically insulating. Finally, electrons travel round an external circuit delivering electric power.[292] FC are classified based on the choice of fuel and electrolyte into 6 major groups:[293]

– alkaline fuel cells (AFC) utilise an aqueous potassium hydroxide (KOH) solution as the alkaline electrolyte;

– proton exchange membrane fuel cells (PEMFC) and direct methanol fuel cells (DMFC) use a polymer membrane as the electrolyte;

– phosphoric acid fuel cells (PAFC) use pure phosphoric acid as the electrolyte;

– molten carbonate fuel cells (MCFC) use a molten mixture of lithium, sodium, and potassium carbonates as the electrolyte;

– solid oxide fuel cells (SOFC) use a ceramic material as the electrolyte.

As the process is not governed by Carnot's law, fuel cells do not need high pressure or thermal gradients to obtain good efficiency, having much higher theoretical efficiencies (35–55%) than traditional combustion-based thermal energy conversion. Furthermore, they present very low levels of pollutant emission due to the absence of high pressure, high temperature a combustion chamber and the fact that air and fuel are separated.[294] Hence, FCs are cleaner and more efficient energy conversion technologies than traditional systems. However, it is necessary to point out that FCs are only classed as renewable energy systems if the fuel used is renewable (biofuels, hydrogen from wind or solar conversion of water).[295]

Regarding the use of porous materials in FCs, anodes and cathodes have to be porous in order to allow the diffusion of the fuel and the products and, moreover, the use of mesoporous supports in the active catalyst region would increase the

dispersion and stability of the catalyst (typically Pt and Pt based alloys[297]).

As reported by Sharma and Pollet,[298] an ideal support for the electrocatalyst should have: (1) a good electrical conductivity, (2) good catalyst–support interaction, (3) a large surface area, (4) a mesoporous structure enabling the ionomer and polymer electrolyte to bring the catalyst nanoparticles close to the reactants, *i.e.* to maximise the triple-phase boundary (TPB), (5) a good water handling capability to avoid flooding, (6) good corrosion resistance, and (7) easy recovery of the catalyst.

Usually, electrocatalysts in FCs have been supported in highly conductive porous carbons and different reviews have recently been published dealing with this topic.[299] Mesoporous carbons show very good properties as FC catalyst supports: high surface area, high electrical conductivity and a relatively good stability. However, carbon has the issue of its corrosion during the reaction, leading to catalyst loss and dramatically affecting the performance of the FC. For this reason, lately, non-carbonaceous-based materials have been extensively studied as electrocatalyst supports. An interesting review about non-carbon support materials for PEMFC electrocatalysts can be found elsewhere.[300]

Due to the large body of reports dealing with mesoporous supports for FC catalysts, and as the topic has been extensively reviewed in the lasts years,[291,298,301] here we only discuss the most relevant contributions published in the last year on mesoporous electrodes for PEMFC and DMFC, because they are two of the most promising systems. An extensive summary of the application of mesoporous materials in FC technology, showing last year's contributions, is shown in Table 3.

Concerning carbon based electrodes, a recent work published by Lazaro and co-workers shows the influence of different morphologies of carbon materials as electrocatalyst supports on the catalysts' performance in DAFCs.[302] Platinum catalysts supported on carbon nanofibres (CNFs), carbon nanocoils (CNCs) and ordered mesoporous carbons (CMK-3) were evaluated in the alcohol oxidation reaction, and compared with a platinum catalyst supported on Vulcan XC-72R (by the same method), and with the commercial Pt/C catalyst from E-TEK. The support material's characteristics were shown to have an influence on both the physicochemical and electrochemical properties of electrocatalysts. The highest current densities, both in methanol and ethanol oxidations, were reached with the mesoporous Pt/CMK-3 catalyst. This could be rationalised by proposing that the high electrical conductivity and ordered porous structure of the support allow better electron transfer and diffusion of the reactants and by-products, during the electrochemical reactions. In the same vein, other very recent works also demonstrate the superior performances of mesoporous catalysts over other kinds of support.[299a,303,304]

Without doubt, the most employed and studied electrodes nowadays are the ones based on carbon, see Table 3. However, as has been previously mentioned, there is a key drawback associated with the use of carbon electrodes, their corrosion with use under high potentials. This can be overcome using non-carbon catalyst supports possessing the good properties of carbon (especially high surface area and high electrical conductivity), but also being corrosion-resistant. Some of the materials developed lately include porous metal and alloys,[306] nitrides,[307] different mixed oxides,[308] as well as metal oxides.[309] As an example, DiSalvo and co-workers have developed a methodology to prepare mesoporous nitrides of Ti, Cr and Ti/Nb by ammonolysis of different oxides of those metals.[307]

Table 3 A summary of the most relevant contributions regarding mesoporous materials for PEMFC and DMFC technologies published during 2013

Materials	Structure	Preparation method	Properties and applications	Ref.
Pt/C, PtRu/C	Mesoporous	Non-ionic surfactant	Enhancement of the activity in	310–312
		Dual soft/hard templating	DAFC and PEMFC	313
		SBA-15 as hard template		302–304, 314
	Hierarchical meso/macroporous	Hard template and adjusting of the synthetic conditions		315
	Mesoporous	SBA-15 as hard template	Acid treatments to improve	315
	Micro/mesoporous	Xerogel	catalytic activity in DAFC	316
	Mesoporous	Alkylamine surfactants	Different studies/treatments to	317
		SBA-15 as hard template	enhance the ORR activity	318
	Micro/mesoporous	Derived from Mo_2C		319
Pt/M_xO_y/C,[a] Pt/TiO_xC	Mesoporous	Non-ionic surfactant	Studies of the dopant influence	320
		SBA-15 as hard template	into the electrocatalysis	321
Pt/C doped with other C structures	Mesoporous	Silicas as hard template	Enhanced electrochemical performance and long-term stability	322
PtRuIrNi/C	Hierarchical meso/macroporous	Silicas as hard template	Enhancement in activity and better electrochemical stability in DAFC	323
Pt/CrN, Pt/TiN, Pt/$Ti_{0.5}Nb_{0.5}N$	Micro/mesoporous	Ammonolysis	High tolerance to corrosion, excellent long-term stability.	307
Pt/(SiO_2/RuO_2), Pt/(TiO_2/RuO_2)	Mesoporous	Cationic surfactant	Better stability results in electrooxidation	308
Pt/M_xO_y[a]	Mesoporous	Different procedures	Alternative electrodes to the C based ones	309

[a] M = transition metal.

These nitrides showed excellent electronic conductivity and high surface area, performing very well as a result in methanol electrooxidation and the ORR in acid and alkaline media. Furthermore, they present in every case, a higher electrocatalytic stability than commercial Pt/C. Their high tolerance to corrosion makes them very promising candidates to replace carbon black as supports for fuel cell catalysts.

Finally, it is necessary to mention that, even with the great potential that FC systems show as clean energy conversion systems, there are some bottlenecks which inhibit FCs from finding a wide range of applications. Two of these bottlenecks are the poor efficiency of the oxygen reduction reaction (ORR) and the use of noble metals (mainly Pt) in the electrocatalysts, which makes the process unsustainable and/or expensive. With this in mind, Asefa and co-workers have recently published the synthesis of a metal-free electrocatalyst based on N- and O-doped mesoporous carbon for the ORR.[305] The synthesis of this novel carbon catalyst was carried out using SBA-15 as a hard template, see the schematic representation of the synthetic procedure in Fig. 20. The aforementioned N- and O-doped mesoporous carbon, was produced in two broad steps. First, polymerised mesoporous silica-supported polyaniline (PANI) was carbonised *in situ*, before the mesoporous silica template was etched away. This synthetic method also permitted the immobilisation of non-noble metals, Fe and Co, into the system. All the resulting materials showed excellent electrocatalytic activity toward the ORR. However, the metal-free, PANI-derived mesoporous carbon exhibited the highest activity, challenging conventional paradigms. This unprecedented activity of the metal-free catalyst towards the ORR can be attributed to the synergetic activities of the nitrogen and oxygen (or hydroxyl) species that were implanted in it by PANI/mesoporous silica during pyrolysis. Other very recent reports also show the possibility of using metal free catalysts in the ORR which can definitively help reduce costs in FC, avoiding the use of expensive Pt.[324]

To conclude, it is true that much work has been done over recent years on FC systems, indeed, all the references cited here were published only in 2013. However, while the results are encouraging, a lot remains to be done in order to provide materials solutions to the main deficiencies that FC technology still suffers from such as the high-cost (mainly due to the catalyst), and durability issues.

4.2. Mesoporous materials in advanced solar cells

A dye sensitised solar cell (DSSC) is a photoelectrochemical cell which generates electricity using solar power. It consists of three parts: the working electrode (WE) which contains the sensitising dye, the electrolyte, and the counter electrode (CE), see Fig. 21.

Since O'Regan and Grätzel reported the first high-efficiency DSSC in 1991,[325] this class of solar cells has emerged as a promising alternative to conventional silicon solar cells. A lot of effort has been made to increase the efficiency of the cell since that first report, reaching a top reported efficiency of 12.3% in 2011 for liquid DSC, again by the Grätzel group.[326,327] DSSCs use wide band-gap semiconductors, while the sensitisation to the solar spectrum is performed by the dye. Different materials have been tested in DSCs including SnO_2, rutile TiO_2, ZnO, anatase TiO_2, Nb_2O_5 and $SrTiO_3$. As pointed out in Section 2.5, the most commonly used material, and the one offering the best performance, is anatase TiO_2.[328] Regarding the morphology of the electrodes, mesoporous nanostructures offer interesting advantages which can improve the characteristics of both the WE and CE. Next, some selected examples will be discussed to indicate those ideal features for mesoporous WE and CE; for a broader description, readers are kindly addressed to ref. 7, 34 and 248.

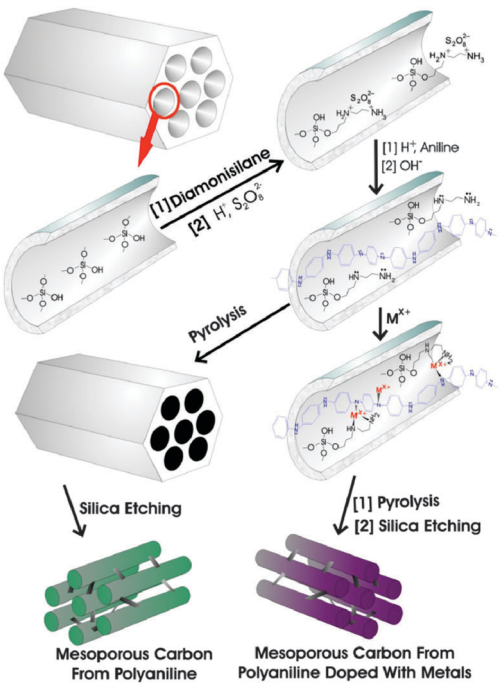

Fig. 20 The synthetic procedure of N- and O-doped mesoporous carbons with or without metal dopants by the carbonization of polymerized mesoporous silica (SBA-15)-supported polyaniline, and the subsequent etching of the SBA-15. Reprinted with permission from ref. 305. Copyright 2013, American Chemical Society.

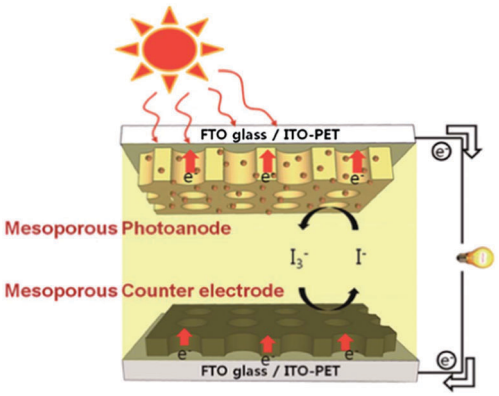

Fig. 21 A schematic representation of a dye sensitized solar cell (DSSC) showing the mesoporous working electrode and counter electrode. Reproduced from ref. 7. Copyright 2013, RSC.

The overall conversion efficiency of the WE increases with the following factors: (1) a higher dye loading which will produce a higher light harvest, (2) an efficient transport of the injected electrons from the dye molecules to the external circuit in order to decrease the back reaction with oxidised species in the electrolyte and the holes in the dye, (3) a higher porosity to improve the binding of the dye molecules and the diffusion of the electrolyte and, (4) scattering functions in the WE, which can lengthen the light pathway and therefore improve light harvesting. All these factors can be enhanced using a mesoporous electrode as the WE.[7,34,248,326,329] Herein, the two highest DSSC efficiencies reported using mesoporous hybrid titania as the WE, will be highlighted. Grätzel *et al.*[326] reported mesoscopic solar cells prepared using a mesoporous hybrid titania as the WE, a zinc porphyrin dye used as a sensitiser and a Co(II/III)tris(bipyridyl) complex as the electrolyte. The WE was made by immersing a 10 μm mesoporous TiO_2 film (5 μm thick transparent mesoporous layer + 5 μm thick scattering layer) in a solution of the dye used as the sensitiser. With this configuration, the efficiency values for these DSSC based on liquid junctions of 12.3% was achieved. More recently, the same group reported the fabrication of a solid-state mesoscopic perovskite-sensitised solar cell with an efficiency of 15% and a stability comparable to that of today's best thin-film solar cells. The cell used mesoporous anatase TiO_2 as the WE.[329]

Similarly in the CE, different studies show better performances when using mesoporous carbon (MC), with a well-developed nanostructure and high surface area, as the CE than with graphite and activated carbon.[330–335] The good performances of these inexpensive and abundant carbonaceous materials, added to their high corrosion resistance and good catalytic activity, make them very promising alternative materials for the CE. That is, replacements for the commonly used Pt catalyst, which is very active but scarce and expensive, inhibiting its large scale applications in the future.[336]

As examples, two works of Ramasamy and Lee are explained. They developed two different mesoporous carbon CEs using hard[332] and soft[333] templating approaches. An ordered mesoporous carbon (OMC) with a high surface area ($\sim$1575 $m^2 g^{-1}$) and bimodal mesoporosity (2.5 and 6.1 nm) was synthesised using a triblock copolymer, namely F127, as a structure directing agent. The DSC prepared with this OMC based CE offered an energy conversion efficiency of 7.46%, which represents a 42% enhancement over a commercial Vulcan based CE. Electrochemical impedance spectroscopy analysis reveals decreased charge transfer resistance at the OMC counter electrode–electrolyte interface, and thus an improved fill factor and energy conversion efficiency.[332] Simultaneously, the same group published a CE comprised of large-pore sized mesoporous carbon. The synthesis of this new large-pore MC involved the use of a mesocellular silica, MSU-F, as a hard template. Large-pore sized mesopores with an interconnected pore structure of sub-micron size MSU-F–C facilitated redox electrolyte penetration, and consequently most of the active surface area of the MSU-F–C carbon CE participates in the I_3^- reduction reaction. As a result, an 8.18% solar to electric energy conversion efficiency was obtained, a 21% increase in device performance compared with CMK-3 carbon (SBA-15 templated). Fig. 22 shows the characteristics of the MSU-F–C and the Nyquist plots displaying the similarity of its behaviour to Pt-based CEs.[333]

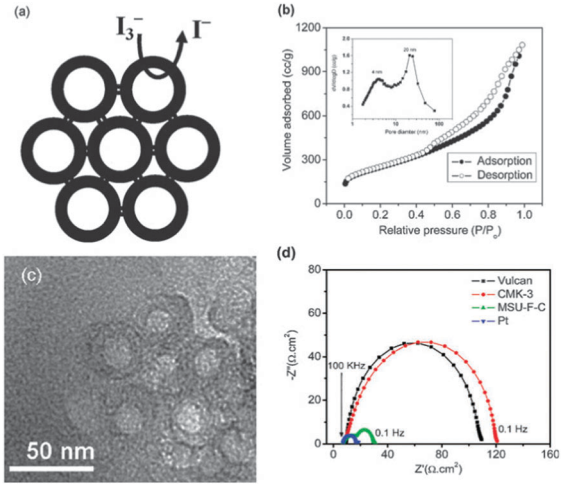

Fig. 22 (a) A schematic illustration of the facile diffusion and reduction of I_3^- ions in MSU-F–C carbon. (b) The N_2 isotherm and pore size distribution (inset) of MSU-F–C carbon. (c) High-resolution TEM image of microtomed MSU-F–C carbon. (d) Nyquist plots of various carbon electrodes and conventional Pt electrodes in a thin layer symmetric cell configuration. Reproduced from ref. 333. Copyright 2010, RSC.

4.3. Mesoporous thermoelectric materials

The thermoelectric effect is a phenomenon involving a direct energy conversion from heat into electricity (or *vice versa*). Materials showing this effect, that is, capable of directly converting temperature gradients to electric voltage and *vice versa*, are considered thermoelectric (TE) materials. These materials offer the possibility of directly converting waste thermal energy back to electricity, as well as to cool atmosphere without using harmful chemicals like CFC and/or moving parts.[337] A huge amount of waste heat is produced in both automotive and industry operations, and many of mankind's activities may be converted into useful energy using TE. As an illustration, in 2008 the US Department of Energy (DOE) reported that somewhere between 20 to 50% of industrial energy input in the US is lost as waste heat.[338] Hence, capturing and reusing this lost heat would be a valuable approach to improve the overall energy efficiency. For this reason, TE materials have been receiving increasing attention in the last few years.[339]

The energy-conversion efficiency of a TE material is evaluated by a dimensionless quantity called the figure of merit (zT), defined as $zT = S^2\sigma T/\kappa$; where S is the Seebeck coefficient (thermoelectric power, the change in voltage per unit temperature difference in a material), σ is the electrical conductivity, κ is the thermal conductivity, and T is the average temperature between the hot and the cold sides. A high electrical conductivity, a high Seebeck coefficient, and a low thermal conductivity are essential characteristics of thermoelectric materials. However, it is very difficult to control

these factors individually, because the electrical conductivity and the Seebeck coefficient have an inverse relationship. Insulators, for example, tend to have very high Seebeck coefficients, while metals usually present low values in the order of 1–10 $\mu V\ K^{-1}$. In this sense, semiconductors with Seebeck coefficients in the order of 10^2 to 10^3 $\mu V\ K^{-1}$, are ideal thermoelectric devices. Heavily doped semiconductors were found to have a comparatively good zT. G. A. Slack[340] proposed that in order to optimise the figure of merit, an ideal material should have a low lattice thermal conductivity as in a glass, and a high electrical conductivity as in a crystal, which is known as 'electron crystal, phonon glass' (ECPG). Consequently, thermoelectric materials comprise a huge family, including different materials: semimetals, semiconductors and ceramics; different crystalline forms: monocrystals, polycrystals, nanocomposites; and covering varying dimensions: from bulk to film, wire to cluster.[337] Some polymers are also showing interesting thermoelectric material properties.[341]

In this sense, nanocrystals are expected to reduce thermal conductivity because of the higher presence of boundaries than in bulk materials, and mesopores are likely to further reduce the thermal conductivity *via* crystalline wall-pore interfaces. In addition, a continuous mesostructure nanocrystalline framework can maintain a high electrical conductivity.[342] However, there are limited publications studying such porous TE materials and most of them are based on theoretical calculations.[343]

Regarding experimental studies, Park and co-workers are one of the groups that have been most active in analysing how mesoporosity and the synthetic parameters of mesoporous solids influence their thermoelectric properties. They have reported the synthesis of TiO_2[344–347] and ZnO[348,349] mesoporous films using a triblock copolymer, Pluronic-123, and a neutral surfactant, Brij-76, as porogens, respectively. In the case of TiO_2, the resistivity of mesoporous TiO_2 films increases when the surfactant concentration increases because the porosity induces a reduction in the electrical path for carriers.[347] This resistivity affects the Seebeck coefficient, which is higher for the higher concentration of surfactant. The group concludes that both porosity and pore arrangement could have an effect on the electrical conductivity of the mesoporous film. On further investigating the porosity of TiO_2 films, at different surfactant/precursor ratios and different annealing temperatures, they consolidated their previous conclusions, as well as the idea that a disordered structure also has a positive effect on the thermoelectric property of the film.[344] In the case of mesoporous ZnO films, the same trend was found, by increasing the porosity of the ZnO films, their conductivity ratio and Seebeck coefficients increased.[348] Thus, the higher the porosity of the ZnO mesoporous films, the better their thermoelectric properties. However, even if these works show interesting results about the relationship between the porosity and the enhancement of the TE properties and the growing interest that the TE properties of transition metal oxides are lately attracting for their potential future prospects,[350] the prototype TE materials in the low and high temperature ranges nowadays are Bi_2Te_3 and Si.[342] In this regard, and following on from this study, two very recent and interesting works exploring the possibilities of mesoporous Bi_2Te_3 and Si are reviewed.

Stucky and co-workers reported in 2012 the first mesoporous monolith for TE applications.[342] The monolith was prepared by a two-step procedure. First, mesoporous n-type Bi_2Te_3 powder was synthesised, using colloidal silica nanospheres (LUDOX) as a hard template. A mesoporous solid with 28 $m^2\ g^{-1}$ of BET surface area, 0.17 $cm^3\ g^{-1}$ of pore volume and an average pore size of 15 nm (consistent with the particle size of the silica nanospheres, 14 nm) was obtained. In the second step, the raw powder was hot-pressed into a mechanically stable monolith; most of the porosity in the final 3D monolith came from the synthetic mesopores of the initial Bi_2Te_3 material. The authors demonstrate that a continuous mesoporous nanocrystalline framework is highly effective for phonon scattering. The generated interfaces and boundaries which are a result of the mesoporosity, scatter phonons with a high efficiency leading to a substantially reduced thermal conductivity. When comparing with the control sample prepared without porosity, the thermal conductivities of the *meso*-Bi_2Te_3 are reduced by more than 50%. This huge reduction compensates for the loss of electrical conductivity caused by the mesopores and finally, the porous monolith presents a higher zT in the entire temperature range (300–500 K) then the fully condensed control sample. The maximum enhancement in the figure of merit (zT) is achieved in the temperature range from 400 to 500 K being over 45% higher in the porous monolith. As the authors finally conclude being 'the first reported mesoporous monolith, the mesopores in the n-type Bi_2Te_3 monolith suggest a new viable avenue for the heterostructured synthesis of efficient TE materials'.

Similar results were obtained for Fang *et al.* when studying the thermal conductivity of ordered mesoporous nanocrystalline silicon thin films.[351] In this case, two silica films were synthesised using two different diblock copolymers, namely, PB-PEO [poly(butadiene)-*b*-poly(ethylene oxide)] and PEP-PEO [poly(ethylene-propylene)-*b*-poly(ethylene oxide)]. Once the ordered mesoporous silica films are produced, they were subsequently reduced by magnesium vapor under an inert atmosphere, giving as a result a silicon film replicating the silica structure. Thermal conductivity measurements for the ordered mesoporous nanocrystalline silicon thin films from 25 to 315 K, resulted in a 3 to 5 orders of magnitude smaller thermal conductivity than that of the bulk single crystal silicon, depending on the temperature range examined. In addition, thin films templated by the PB-PEO copolymer had a smaller thermal conductivity than those templated by the PEP-PEO copolymer due to their smaller pores and increased disorder. Moreover, good agreement was found between the measured data and the model predictions.

Even if the literature regarding mesoporous materials for thermoelectric applications is scarce, the majority of the cases reported show an enhancement in the thermoelectric properties mostly coming from the reduction in thermal conductivities for the mesoporous solids regarding their dense counterparts. However, a reported model for polycrystallized Si_xGe_{1-x} alloys with a nanosized ($\approx$20 nm) interparticle porosity, shows a significant reduction in zT.[352] Consequently, it seems evident that the porosity can have a positive or negative effect on zT depending on the material composition, the effective mass of the carriers, the pore size distributions and the type of pores

(inter or intraparticulate). Therefore, a precise synthetic design is required if one wishes to improve zT by the incorporation of mesopores into a condensed matrix.

5. Conclusions

Recent advances in the synthesis of highly tuneable and complex porous structures have unlocked a wide range of opportunities in clean energy technologies, providing an improved accessibility, a higher surface area and a better dispersion of the active species. In addition to the development of controlled mesoporosity, the modification of the surface chemistry of porous materials using a wide range of techniques, from chemical grafting to the oxidation of the material surface has allowed further improvement in their performance when dealing with molecules of different polarity.

New approaches to introducing mesoporosity, as well as revisited traditional techniques, have both been reviewed highlighting the possibility of combining different approaches to produce hierarchical structures with a controlled porosity at different scales. In this regard, a wide range of nanotechnologies from surfactant-templating to nanocasting have been successfully applied in the last decades, yielding novel materials with unprecedented control over their architecture.

In many cases, mesoporous materials are used as catalysts for the transformation of clean energy sources into electricity, fuels or valuable molecules. Herein we have provided some relevant examples of the role of controlled mesoporosity in increasing the activity, but mainly the selectivity of some of the most challenging processes, including the transformation of biomass to high quality fuels, the efficient production of hydrogen or the valorisation of CO_2. However, mesoporous materials are widely used beyond catalysis, mainly as electrodes in fuel and solar cells and in thermoelectric devices. In these cases, the presence of mesoporosity significantly enhances the dispersion of the active phase and the accessibility of the electrolyte, which suggests that new advances in mesoporous materials will play a significant role in the clean production of energy in the future.

Acknowledgements

We specially thank Daniel Johnson for his invaluable help with the editing of this paper. The authors wish to thank the Spanish MINECO (Project CTQ2011-28954-C02-01) for financial support. E.S. acknowledges financial support from UA (Project GRE12-39).

Notes and references

1 (*a*) http://www.iea.org/publications/freepublications/publication/EnergyTechnologyInitiatives_2013.pdf, accessed on 15th November 2013; (*b*) http://www3.weforum.org/docs/WEF_EN_EnergyVision Report_2013.pdf, accessed on 15th November 2013; (*c*) http://www.un.org/wcm/webdav/site/sustainableenergyforall/shared/Documents/SEFA-Action%20Agenda-Final.pdf, accessed on 15th November 2013.

2 A. S. Aricò, P. Bruce, B. Scrosati, J.-M. Tarascon and W. van Schalkwijk, *Nat. Mater.*, 2005, **4**, 366–377.

3 E. Serrano, K. Li, G. Rus and J. García-Martínez, in *Nanotechnology for the Energy Challenge*, ed. J. García-Martínez, Wiley-VCH, Weinheim, Germany, 2nd edn, 2013.

4 E. Serrano, G. Rus and J. García-Martínez, *Renewable Sustainable Energy Rev.*, 2009, **13**, 2373–2384.

5 C. T. Kresge and W. J. Roth, *Chem. Soc. Rev.*, 2013, **42**, 3663–3670.

6 J. García-Martínez, in *Tomorrow's Chemistry Today*, ed. B. Pignataro, Wiley-VCH, Weinheim, Germany, 2008, ch. 3.

7 Y. Ye, C. Jo, I. Jeong and J. Lee, *Nanoscale*, 2013, **5**, 4584–4605.

8 E. Serrano, N. Linares, J. R. Berenguer and J. García-Martínez, *ChemCatChem*, 2013, **5**, 844–860.

9 (*a*) C. T. Kresge, M. E. Leonowicz, W. J. Roth, J. C. Vartuli and J. S. Beck, *Nature*, 1992, **359**, 710–712; (*b*) C. T. Kresge, M. E. Leonowicz, W. J. Roth and J. C. Vartuli, *Synthetic Mesoporous Crystalline Material*, *US Pat.*, 5,098,684, 1992; (*c*) C. T. Kresge, M. E. Leonowicz, W. J. Roth and J. C. Vartuli, *Synthetic Porous Crystalline Material, Its Synthesis*, *US Pat.*, 5,102,643, 1992.

10 N. Pal and A. Bhaumik, *Adv. Colloid Interface Sci.*, 2013, **189–190**, 21–41.

11 W. Li and D. Zhao, *Chem. Commun.*, 2013, **49**, 943–946.

12 *Introduction to Zeolite Science and Practice*, Stud. Surf. Sci. and Catal., ed. J. Čějka, H. van Bekkum, A. Corma and F. Schüth, Elsevier, Amsterdam, 2007, vol. 168.

13 R. Xu, W. Pang, J. Yu, Q. Huo and J. Chen, *Chemistry of Zeolites and Related Porous Materials*, Wiley, Singapore, 2007.

14 F. Di Renzo, A. Galarneau, P. Trens and F. Fajula, in *Handbook of Porous Solids*, ed. F. Schüth, K. S. W. Sing and J. Weitkamp, Wiley-VCH, Weinheim, 2002, pp. 1311–1395.

15 G. J. de, A. A. Soler-Illia, C. Sanchez, B. Lebeau and J. Patarin, *Chem. Rev.*, 2002, **102**, 4093–4138.

16 A. Corma, *Chem. Rev.*, 1997, **97**, 2373–2419.

17 Mesoporous Materials [Themed collection], *Chem. Soc. Rev.*, ed. B. Lebeau, A. Galarneau and M. Linden, 2013, vol. 42(9).

18 P. Behrens, *Adv. Mater.*, 1993, **5**, 127–132.

19 (*a*) Q. Huo, D. I. Margolese, U. Ciesla, D. K. Demuth, P. Feng, T. E. Gier, P. Sieger, A. Firouzi, B. F. Chmelka, F. Schüth and G. D. Stucky, *Chem. Mater.*, 1994, **6**, 1176–1991; (*b*) A. Sayari, *Stud. Surf. Sci. Catal.*, 1996, **102**, 1–46; (*c*) N. D. Hoa, N. V. Duy and N. V. Hieu, *Mater. Res. Bull.*, 2013, **48**, 440–448.

20 J. Li, L. Delmotte and H. Kessler, *Chem. Commun.*, 1996, 1023–1024.

21 Q. Huo, R. Leon, P. M. Petroff and G. D. Stucky, *Science*, 1995, **268**, 1324–1327.

22 Y. Wang, C. Ma, X. Sun and H. Li, *Microporous Mesoporous Mater.*, 2001, **49**, 171–178.

23 S. Che, A. E. Garcia-Bennett, T. Yokoi, K. Sakamoto, H. Kunieda, O. Terasaki and T. Tatsumi, *Nat. Mater.*, 2003, **2**, 801–805.

24 P. T. Tanev and T. J. Pinnavaia, *Science*, 1995, **267**, 865–867.
25 N. Ulagappan, Neeraj, B. V. N. Raju and C. N. R. Rao, *Chem. Commun.*, 1996, 2243–2244.
26 K. G. Severin, T. M. Abdel-Fattah and T. J. Pinnavaia, *Chem. Commun.*, 1998, 1471–1472.
27 Neeraj and C. N. R. Rao, *J. Mater. Chem.*, 1998, **8**, 1631–1634.
28 D. Zhao, J. Feng, Q. Huo, N. Melosh, G. H. Fredrickson, B. F. Chmelka and G. D. Stucky, *Science*, 1998, **279**, 548–552.
29 (*a*) P. Yang, D. Zhao, D. I. Margolese, B. F. Chmelka and G. D. Stucky, *Nature*, 1998, **396**, 152–155; (*b*) C. Tagusagawa, A. Takagaki, A. Iguchi, K. Takanabe, J. N. Kondo, K. Ebitani, S. Hayashi, T. Tatsumi and K. Domen, *Angew. Chem., Int. Ed.*, 2010, **49**, 1128–1132.
30 S. A. Bagshaw, E. Prouzet and T. J. Pinnavaia, *Science*, 1995, **269**, 1242–1244.
31 Z. Zhang, R. W. Hicks, T. R. Pauly and T. J. Pinnavaia, *J. Am. Chem. Soc.*, 2002, **124**, 1592–1593.
32 (*a*) P. Yang, T. Deng, D. Zhao, P. Feng, D. Pine, B. F. Chmelka, G. M. Whitesides and G. D. Stucky, *Science*, 1998, **282**, 2244–2246; (*b*) X. He and D. Antonelli, *Angew. Chem., Int. Ed.*, 2002, **41**, 214–229; (*c*) S. Yuan, Z. Zho and G. Li, *CrystEngComm*, 2011, **13**, 4709–4713.
33 D. Chandra, N. Mukherjee, A. Mondal and A. Bhaumik, *J. Phys. Chem. C*, 2008, **112**, 8668–8674.
34 J. L. Vivero-Escoto, Y.-D. Chiang, K. C.-W. Wu and Y. Yamauchi, *Sci. Technol. Adv. Mater.*, 2012, **13**, 013003.
35 K. Nakajima, T. Fukui, H. Kato, M. Kitano, J. N. Kondo, S. Hayashi and M. Hara, *Chem. Mater.*, 2010, **22**, 3332.
36 K. Brezesinski, J. Haetge, J. Wang, S. Mascotto, C. Reitz, A. Rein, S. H. Tolbert, J. Perlich, B. Dunn and T. Brezesinski, *Small*, 2011, **7**, 407–414.
37 B. L. Su, C. Sanchez and X.-Y. Yang, *Hierarchically structured porous materials: from nanoscience to catalysis, biomedicine, optics and energy*, Wiley-VCH, Weinheim, Germany, 2011.
38 J. Čějka, A. Corma and S. I. Zones, *Zeolites and Catalysis: Synthesis, Reactions and Applications*, Wiley-VCH, Weinheim, Germany, 2010.
39 (*a*) C. M. A. Parlett, K. Wilson and A. F. Lee, *Chem. Soc. Rev.*, 2013, **42**, 3876–3893; (*b*) K. Na, M. Choi and R. Ryoo, *Microporous Mesoporous Mater.*, 2013, **166**, 3–19; (*c*) L.-H. Chen, X.-Y. Li, J. C. Rooke, Y.-H. Zhang, X.-Y. Yang, Y. Tang, F.-S. Xiao and B.-L. Su, *J. Mater. Chem.*, 2012, **22**, 17381–17403; (*d*) S. Lopez-Orozco, A. Inayat, A. Schwab, T. Selvam and W. Schwieger, *Adv. Mater.*, 2011, **23**, 2602–2615; (*e*) J. Pérez-Ramírez, C. H. Christensen, K. Egeblad, C. H. Christensen and J. C. Groen, *Chem. Soc. Rev.*, 2008, **37**, 2530–2542; (*f*) K. Egeblad, C. H. Christensen, M. Kustova and C. H. Christensen, *Chem. Mater.*, 2008, **20**, 946–960.
40 (*a*) K. P. de Jong, J. Zecevic, H. Friedrich, P. E. de Jongh, M. Bulut, S. van Donk, R. Kenmogen, A. Finiels, V. Hulea and F. Fajula, *Angew. Chem., Int. Ed.*, 2010, **49**, 10074–10078; (*b*) J. Pérez-Ramírez, D. Verboekend, A. Bonilla and S. Abelló, *Adv. Funct. Mater.*, 2009, **19**, 3972–3979; (*c*) J. C. Groen, T. Bach, U. Ziese, A. M. Paulaime-van Donk, K. P. de Jong, J. A. Moulijn and J. Pérez-Ramírez, *J. Am. Chem. Soc.*, 2005, **127**, 10792–10793; (*d*) J. C. Groen, L. A. A. Peffer, J. A. Moulijn and J. Pérez-Ramírez, *Chem. - Eur. J.*, 2005, **11**, 4983–4994; (*e*) M. Ogura, S. Y. Shinomiya, J. Tateno, Y. Nara, E. Kikuchi and H. Matsukata, *Chem. Lett.*, 2000, 882–883.
41 (*a*) C.-Y. Chen and S. I. Zones, in *Zeolites and Catalysis: Synthesis, Reactions and Application*, ed. J. Čějka, A. Corma and S. I. Zones, Wiley-VCH, Weinheim, Germany, 2010, pp. 155–170; (*b*) S. van Donk, A. H. Janssen, J. H. Bitter and K. P. de Jong, *Catal. Rev. Sci. Eng.*, 2003, **45**, 297–319; (*c*) C. S. Triantafillidis, A. G. Vlessidis and N. P. Evmiridis, *Ind. Eng. Chem. Res.*, 2000, **39**, 307–319.
42 (*a*) B. Liu, C. Li, Y. Ren, Y. Tan, H. Xi and Y. Qian, *Chem. Eng. J.*, 2012, **210**, 96–102; (*b*) K. Na, C. Jo, J. Kim, K. Cho, J. Jung, Y. Seo, R. J. Messinger, B. F. Chmelka and R. Ryoo, *Science*, 2011, **333**, 328–332; (*c*) F.-S. Xiao, L. Wang, C. Yin, Y. Di, J. Li, R. Xu, D. S. Su, R. Schlogl, T. Yokoi and T. Tatsumi, *Angew. Chem., Int. Ed.*, 2006, **45**, 3090–3093; (*d*) H. Wang and T. J. Pinnavaia, *Angew. Chem., Int. Ed.*, 2006, **45**, 7603–7606; (*e*) M. Choi, H. S. Cho, R. Srivastava, C. Venkatesan, D.-H. Choi and R. Ryoo, *Nat. Mater.*, 2006, **5**, 718–723.
43 D. H. Park, S. S. Kim, H. Wang, T. J. Pinnavaia, M. C. Papapetrou, A. A. Lappas and K. S. Triantafyllidis, *Angew. Chem., Int. Ed.*, 2009, **48**, 7645–7648.
44 (*a*) J.-B. Koo, N. Jiang, S. Saravanamurugan, M. Bejblová, Z. Musilová, J. Čějka and S.-E. Park, *J. Catal.*, 2010, **276**, 327–334; (*b*) W. Fan, M. A. Snyder, S. Kumar, P.-S. Lee, W. C. Yoo, A. V. McCormick, R. L. Penn, A. Stein and M. Tsapatsis, *Nat. Mater.*, 2008, **7**, 984–991; (*c*) C. J. H. Jacobsen, C. Madsen, J. Houzvicka, I. Schmidt and A. Carlsson, *J. Am. Chem. Soc.*, 2000, **122**, 7116–7117; (*d*) H. Zhu, Z. Liu, Y. Wang, D. Kong, X. Yuan and Z. Xie, *Chem. Mater.*, 2008, **20**, 1134–1139; (*e*) C. H. Christensen, I. Schmidt, A. Carlsson, K. Johannsen and K. Herbst, *J. Am. Chem. Soc.*, 2005, **127**, 8098–8102; (*f*) Y. Tao, H. Kanoh, L. Abrams and K. Kaneko, *Chem. Rev.*, 2006, **106**, 896–910.
45 J. Y. Ying and J. García-Martínez, *US Pat.*, US 2005/0239634 A1, 2004.
46 J. García-Martínez, M. Johnson, J. Valla, K. Li and J. Y. Ying, *Catal. Sci. Technol.*, 2012, **2**, 987–994.
47 J. García-Martínez, K. Li and G. Krishnaiah, *Chem. Commun.*, 2012, **48**, 11841–11843.
48 K. Li, J. Valla and J. García-Martínez, *ChemCatChem*, 2014, **6**, 46–66.
49 S. Xiu and A. Shahbazi, *Renewable Sustainable Energy Rev.*, 2012, **16**, 4406–4414.
50 P. M. Mortensen, J.-D. Grunwaldt, P. A. Jensen, K. G. Knudsen and A. D. Jensen, *Appl. Catal., A*, 2011, **407**, 1–19.
51 T. V. Choudhary and C. B. Phillips, *Appl. Catal., A*, 2011, **397**, 1–12.
52 K. Jacobson, K. C. Maheria and A. K. Dalai, *Renewable Sustainable Energy Rev.*, 2013, **23**, 91–106.
53 Y. Wang, Y. Fang, T. He, H. Hu and J. Wu, *Catal. Commun.*, 2011, **12**, 1201–1205.

54 For a review of synthetic procedures see: X.-Y. Yang, Y. Li, A. Lemaire, J.-G. Yu and B.-L. Su, *Pure Appl. Chem.*, 2009, **81**, 2265–2307.
55 T. Kamegawa, N. Suzuki, M. Che and H. Yamashita, *Langmuir*, 2011, **27**, 2873–2879.
56 N. Linares, S. Hartmann, A. Galarneau and P. Barbaro, *ACS Catal.*, 2012, **2**, 2194–2198.
57 H. Yang, Z. Liu, H. Gao and Z. Xie, *J. Mater. Chem.*, 2010, **20**, 3227–3231.
58 (*a*) F. Dong, S. C. Lee, Z. Wu, Y. Huang, M. Fu, W.-K. Ho, S. Zou and B. Wang, *J. Hazard. Mater.*, 2011, **195**, 346–354; (*b*) F. Dong, Y. Sun, W. K. Ho and Z. Wu, *Dalton Trans.*, 2012, **41**, 8270–8284.
59 P.-C. Chen, M.-C. Tsai, M.-H. Yang, T.-T. Chen, H.-C. Chen, I.-C. Changa, Y.-C. Chang, Y.-L. Chen, I.-N. Lin, H.-T. Chiu and C.-Y. Lee, *Appl. Catal., B*, 2013, **142–143**, 752–760.
60 D. Xie, L. Chang, F. Wang, G. Du and B. Xu, *J. Alloys Compd.*, 2012, **545**, 176–181.
61 Y. Li, Z.-Y. Fu and B.-L. Su, *Adv. Funct. Mater.*, 2012, **22**, 4634–4667.
62 J. Xiao, J. Zheng, X. Li, Y. Shao and J.-G. Zhang, *Nanotechnology*, 2013, **24**, 424004.
63 D. Xie, W. Yuan, Z. Dong, Q. Su, J. Zhang and G. Du, *Electrochim. Acta*, 2013, **92**, 87–92.
64 P. Poizot, S. Laruelle, S. Grugeon, L. Dupont and J.-M. Tarascon, *Nature*, 2000, **407**, 496–499.
65 (*a*) X. Li and B. Wei, *Nano Energy*, 2013, **2**, 159–173; (*b*) Y. Zhu, S. Murali, M. D. Stoller, K. J. Ganesh, W. Cai, P. J. Ferreira, A. Pirkle, R. M. Wallace, K. A. Cychosz, M. Thommes, D. Su, E. A. Stach and R. S. Ruoff, *Science*, 2011, **332**, 1537–1541.
66 A. Walcarius, *Chem. Soc. Rev.*, 2013, **42**, 4098–4140.
67 A.-H. Lu, D. Zhao and Y. Wan, *Nanocasting: A Versatile Strategy for Creating Nanostructured Porous Materials*, RSC Publishing, Cambridge, UK, 2009.
68 (*a*) Y.-S. Hu, P. Adelhelm, B. M. Smarsly, S. Hore, M. Antonietti and J. Maier, *Adv. Funct. Mater.*, 2007, **17**, 1873–1878; (*b*) L. Yu, N. Brun, K. Sakaushi, J. Eckert and M. M. Titirici, *Carbon*, 2013, **61**, 245–253; (*c*) S. Wang, Z. Yang, H. Zhang, H. Tan, J. Yu and J. Wu, *Electrochim. Acta*, 2013, **106**, 307–311.
69 Z. Wang, F. Li, N. S. Ergang and A. Stein, *Chem. Mater.*, 2006, **18**, 5543–5553.
70 (*a*) N. Du, H. Zhang, B. D. Chen, J. B. Wu, X. Y. Ma, Z. H. Liu, Y. Q. Zhang, D. Yang, X. H. Huang and J. P. Tu, *Adv. Mater.*, 2007, **19**, 4505–4509; (*b*) X. W. Lou, D. Deng, J. Y. Lee, J. Feng and L. A. Archer, *Adv. Mater.*, 2008, **20**, 258–262; (*c*) X. W. Lou, D. Deng, J. Y. Lee and L. A. Archer, *J. Mater. Chem.*, 2008, **18**, 4397–4401.
71 L. Tian, H. L. Zou, J. X. Fu, X. F. Yang, Y. Wang, H. L. Guo, X. H. Fu, C. L. Liang, M. M. Wu, P. K. Shen and M. Q. Gao, *Adv. Funct. Mater.*, 2010, **20**, 617–623.
72 G. Wang, H. Liu, J. Horvat, B. Wang, S. Qiao, J. Park and H. Ahn, *Chem. - Eur. J.*, 2010, **16**, 11020–11027.
73 C. F. Meunier, X. Y. Yang, J. C. Rooke and B. L. Su, *ChemCatChem*, 2011, **3**, 476–488.
74 O. H. Schmitt, Some interesting and useful biomimetic transforms, *Proc. 3rd Int. Biophysics Congress*, 1969, p. 297.
75 Compendium of Chemical Terminology, 2nd ed; (the "Gold Book"), Compiled by A. D. McNaught and A. Wilkinson, Blackwell Scientific Publications, Oxford (1997), XML on-line corrected version: http://goldbook.iupac.org (2006-) created by M. Nic, J. Jirat, B. Kosata; updates compiled by A. Jenkins, ISBN 0967855098, DOI: 10.1351/goldbook, accessed on October 2013.
76 H. Zhou, X. Li, T. Fan, F. E. Osterloh, J. Ding, E. M. Sabio, D. Zhang and Q. Guo, *Adv. Mater.*, 2010, **22**, 951–956.
77 W. Zhang, D. Zhang, T. J. Fan, J. J. Gu, J. Ding, H. Wang, Q. X. Guo and H. Ogawa, *Chem. Mater.*, 2009, **21**, 33–40.
78 X. F. Li, T. X. Fan, H. Zhou, S. K. Chow, W. Zhang, D. Zhang, Q. X. Guo and H. Ogawa, *Adv. Funct. Mater.*, 2009, **19**, 45–56.
79 Z. Schnepp, W. Yang, M. Antonietti and C. Giordano, *Angew. Chem., Int. Ed.*, 2010, **49**, 6564–6566.
80 D. Losic, P. J. Evans, A. Atanacio, J. G. Mitchell and N. H. Voelcker, *J. Mater. Chem.*, 2006, **16**, 4029–4034.
81 (*a*) C. Jeffryes, T. Gutu, J. Jiao and G. L. Rorrer, *ACS Nano*, 2008, **2**, 2103–2112; (*b*) C. Jeffryes, T. Gutu, J. Jiao and G. L. Rorrer, *J. Mater. Res.*, 2008, **23**, 3255–3262.
82 Z. Liu, T. Fan and D. Zhang, *J. Am. Ceram. Soc.*, 2006, **89**, 662–665.
83 Z. Liu, T. Fan, W. Zhang and D. Zhang, *Microporous Mesoporous Mater.*, 2005, **85**, 82–88.
84 X. Li, T. Fan, Z. Liu, J. Ding, Q. Guo and D. Zhang, *J. Eur. Ceram. Soc.*, 2006, **26**, 3657–3664.
85 T. Fan, X. Li, Z. Liu, J. Gu, D. Zhang and Q. Guo, *J. Am. Ceram. Soc.*, 2006, **89**, 3511–3515.
86 J. Cao and H. Sieber, *J. Porous Mater.*, 2004, **11**, 163–172.
87 S. M. Holmes, B. E. Graniel-Garcia, P. Foran, P. Hill, E. P. L. Roberts, B. H. Sakakini and J. M. Newton, *Chem. Commun.*, 2006, 2662–2663.
88 W. He, X. Zhang, X. Du, Y. Zhang, Y. Yue, J. Shen and M. Li, *Electrochim. Acta*, 2013, **112**, 295–303.
89 Z.-Y. Gu, J. Park, A. Raiff, Z. Wei and H.-C. Zhou, *ChemCatChem*, 2014, **6**, 67–75.
90 I. Imaz, M. Rubio-Martínez, J. An, I. Solé-Font, N. L. Rosi and D. Maspoch, *Chem. Commun.*, 2011, **47**, 7287–7302.
91 S. L. Wegener, T. J. Marks and P. C. Stair, *Acc. Chem. Res.*, 2012, **45**, 206–214.
92 K. L. Fujdala and T. D. Tilley, *J. Catal.*, 2003, **216**, 265–275.
93 (*a*) M. Rico-Santacruz, A. E. Sepúlveda, E. Serrano, J. R. Berenguer, E. Lalinde and J. García-Martínez, *Spanish Pat.*, ref. 20130535, 2013; (*b*) M. Rico-Santacruz, A. E. Sepúlveda, E. Serrano, J. R. Berenguer, E. Lalinde, J. García-Martínez, unpublished results.
94 (*a*) E. Coronado, A. Ribera, J. García-Martínez, N. Linares and L. M. Liz-Marzán, *J. Mater. Chem.*, 2008, **18**, 5682–5688; (*b*) J. García-Martínez, N. Linares, S. Sinibaldi, E. Coronado and A. Ribera, *Microporous Mesoporous Mater.*, 2009, **117**, 170–177; (*c*) N. Linares, A. E. Sepulveda, M. C. Pacheco, J. Berenguer, E. Lalinde, C. Nájera and J. García-Martínez, *New J. Chem.*, 2011, **35**, 225–234; (*d*) N. Linares,

A. E. Sepulveda, J. Berenguer, E. Lalinde and J. García-Martínez, *Microporous Mesoporous Mater.*, 2012, **158**, 300–308; (*e*) A. I. Carrillo, J. García-Martínez, R. Llusar, E. Serrano, I. Sorribes, C. Vicente and J. A. Vidal-Moya, *Microporous Mesoporous Mater.*, 2012, **151**, 380–389; (*f*) M. Rico, A. E. Sepulveda, E. Serrano, S. Ruiz, J. García-Martínez, J. R. Berenguer and E. Lalinde, *Chem. Commun.*, 2012, **48**, 8883–8885; (*g*) N. Linares, E. Serrano, A. Carrillo and J. García-Martínez, *Mater. Lett.*, 2013, **95**, 93–96.

95 W. Xuan, C. Zhu, Y. Liu and Y. Cui, *Chem. Soc. Rev.*, 2012, **41**, 1677–1695.

96 J.-R. Li, J. Sculley and H.-C. Zhou, *Chem. Rev.*, 2012, **112**, 869–932.

97 (*a*) Q. R. Fang, T. A. Makal, M. D. Young and H. C. Zhou, *Comments Inorg. Chem.*, 2010, **31**, 165–195; (*b*) *Metal-organic frameworks: design and applications*, ed. L. R. MacGillivray, Wiley-VCH, 2010, ISBN 978-0-470-19556-7.

98 O. M. Yaghi, M. O'Keeffe, N. W. Ockwig, H. K. Chae, M. Eddaoudi and J. Kim, *Nature*, 2003, **423**, 705–714.

99 H. Furukawa, K. E. Cordova, M. O'Keeffe and O. M. Yaghi, *Science*, 2013, **341**, 1230444.

100 M. Eddaoudi, J. Kim, N. Rosi, D. Vodak, J. Wachter, M. O'Keeffe and O. M. Yaghi, *Science*, 2002, **295**, 469–472.

101 X. S. Wang, S. Q. Ma, D. F. Sun, S. Parkin and H. C. Zhou, *J. Am. Chem. Soc.*, 2006, **128**, 16474–16475.

102 Q. R. Fang, G. S. Zhu, Z. Jin, Y. Y. Ji, J. W. Ye, M. Xue, H. Yang, Y. Wang and S. L. Qiu, *Angew. Chem., Int. Ed.*, 2007, **46**, 6638–6642.

103 K. Koh, A. G. Wong-Foy and A. J. Matzger, *Angew. Chem., Int. Ed.*, 2008, **47**, 677–680.

104 G. Ferey, C. Serre, C. Mellot-Draznieks, F. Millange, S. Surble, J. Dutour and I. Margiolaki, *Angew. Chem., Int. Ed.*, 2004, **43**, 6296–6301.

105 (*a*) G. Ferey, C. Mellot-Draznieks, C. Serre, F. Millange, J. Dutour, S. Surble and I. Margiolaki, *Science*, 2005, **309**, 2040–2042; (*b*) A. Sonnauer, F. Hoffmann, M. Froba, L. Kienle, V. Duppel, M. Thommes, C. Serre, G. Ferey and N. Stock, *Angew. Chem., Int. Ed.*, 2009, **48**, 3791–3794.

106 (*a*) J. Juan-Alcaniz, M. G. Goesten, E. V. Ramos-Fernandez, J. Gascon and F. Kapteijn, *New J. Chem.*, 2012, **36**, 977–987; (*b*) M. R. Lohe, M. Rose and S. Kaskel, *Chem. Commun.*, 2009, 6056–6058.

107 Y. K. Park, S. B. Choi, H. Kim, K. Kim, B. H. Won, K. Choi, J. S. Choi, W. S. Ahn, N. Won, S. Kim, D. H. Jung, S. H. Choi, G. H. Kim, S. S. Cha, Y. H. Jhon, J. K. Yang and J. Kim, *Angew. Chem., Int. Ed.*, 2007, **46**, 8230–8233.

108 K. Koh, A. G. Wong-Foy and A. J. Matzger, *J. Am. Chem. Soc.*, 2009, **131**, 4184–4185.

109 B. Wang, A. P. Cote, H. Furukawa, M. O'Keeffe and O. M. Yaghi, *Nature*, 2008, **453**, 207–211.

110 L.-G. Qiu, T. Xu, Z.-Q. Li, W. Wang, Y. Wu, X. Jiang, X.-Y. Tian and L.-D. Zhang, *Angew. Chem., Int. Ed.*, 2008, **47**, 9487–9491.

111 D. Zhao, D. Yuan, D. Sun and H.-C. Zhou, *J. Am. Chem. Soc.*, 2009, **131**, 9186–9188.

112 H. Deng, S. Grunder, K. E. Cordova, C. Valente, H. Furukawa, M. Hmadeh, F. Gándara, A. C. Whalley, Z. Liu, S. Asahina, H. Kazumori, M. O'Keeffe, O. Terasaki, J. F. Stoddart and O. M. Yaghi, *Science*, 2012, **336**, 1018–1023.

113 O. K. Farha, I. Eryazici, N. C. Jeong, B. G. Hauser, C. E. Wilmer, A. A. Sarjeant, R. Q. Snurr, S. T. Nguyen, A. Ö. Yazaydın and J. T. Hupp, *J. Am. Chem. Soc.*, 2012, **134**, 15016–15021.

114 H. Furukawa, N. Ko, Y. B. Go, N. Aratani, S. B. Choi, E. Choi, A. O. Yazaydın, R. Snurr, M. O'Keeffe, J. Kim and O. M. Yaghi, *Science*, 2010, **329**, 424–428.

115 O. K. Farha, A. O. Yazaydın, I. Eryazici, C. D. Malliakas, B. G. Hauser, M. G. Kanatzidis, S. T. Nguyen, R. Q. Snurr and J. T. Hupp, *Nat. Chem.*, 2010, **2**, 944–948.

116 M. P. Suh, H. J. Park, T. K. Prasad and D.-W. Lim, *Chem. Rev.*, 2012, **112**, 782–835.

117 Mercedes-Benz F125, www.emercedesbenz.com/autos/mercedes-benz/concept-vehicles/mercedes-benz-f125-research-vehicle-technology, accessed on 20th October 2013.

118 S. N. Naik, V. V. Goud, P. K. Rout and A. K. Dalai, *Renewable Sustainable Energy Rev.*, 2010, **14**, 578–597.

119 A. G. Gayubo, A. Alonso, B. Valle, A. T. Aguayo, M. Olazar and J. Bilbao, *Chem. Eng. J.*, 2011, **167**, 262–277.

120 M. Inaba, K. Murata, M. Saito and I. Takahara, *Green Chem.*, 2007, **9**, 638–646.

121 H. Oikawa, Y. Shibata and T. Baba, *Appl. Catal., A*, 2006, **312**, 181–185.

122 M. Iwamoto, K. Kasai and T. Haishi, *ChemSusChem*, 2011, **4**, 1055–1058.

123 A. M. Varvarin, K. N. Khomenko and V. V. Brei, *Theor. Exp. Chem.*, 2011, **47**, 36–40.

124 P. D. Vaidya and A. E. Rodrigues, *Chem. Eng. J.*, 2006, **117**, 39–49.

125 S. Sá, H. Silva, L. Brandao, J. Sousa and A. Mendes, *Appl. Catal., B*, 2010, **99**, 43–57.

126 L. P. R. Profeti, E. A. Ticianelli and E. M. Assaf, *Appl. Catal., A*, 2009, **360**, 17–25.

127 C. B. Wang, C. C. Lee, J. L. Bi, J. Y. Siang, J. Y. Liu and C. T. Yeh, *Catal. Today*, 2009, **146**, 76–81.

128 W. Gac, W. Zawadzki and B. Tomaszewska, *Catal. Today*, 2011, **176**, 97–102.

129 A. Carrero, J. A. Calles and A. J. Vizcaíno, *Appl. Catal., A*, 2007, **327**, 82–94.

130 A. J. Vizcaíno, A. Carrero and J. A. Calles, *Catal. Today*, 2009, **146**, 63–70.

131 A. Sivasamy, K. Y. Cheah, P. Fornasiero, F. Kemausuor, S. Zinoviev and S. Miertus, *ChemSusChem*, 2009, **2**, 278–300.

132 S. Yan, M. Kim, S. O. Salley and K. Y. Simon Ng, *Appl. Catal., A*, 2009, **360**, 163–170.

133 D. E. López, J. G. Goodwin Jr., D. A. Bruce and E. Lotero, *Appl. Catal., A*, 2005, **295**, 97–105.

134 G. J. Suppes, M. A. Dasari, E. J. Doskocil, P. J. Mankidy and M. J. Goff, *Appl. Catal., A*, 2004, **257**, 213–223.

135 M. C. G. Albuquerque, I. Jiménez-Urbistondo, J. Santamaría-González, J. M. Mérida-Robles, R. Moreno-Tost, E. Rodríguez-Castellón, A. Jiménez-López, D. C. S. Azevedo, C. L. Cavalcante Jr. and P. Maireles-Torres, *Appl. Catal., A*, 2008, **334**, 35–43.

136 E. Li and V. Rudolph, *Energy Fuels*, 2008, **22**, 145–149.
137 A. Z. Abdullah, N. Razali and K. T. Lee, *Fuel Process. Technol.*, 2009, **90**, 958–964.
138 A. Corma, S. Iborra, S. Miquel and J. Primo, *J. Catal.*, 1998, **173**, 315–321.
139 R. Luque, V. Budarin, J. H. Clark and D. J. Macquarrie, *Appl. Catal., B*, 2008, **82**, 157–162.
140 J. Delgado, *SP Pat.*, 2,201,894, 2002.
141 R. Wessendorf, *Erdoel Kohle, Erdgas, Petrochem.*, 1995, **48**, 138–143.
142 J. A. Melero, R. van Grieken, G. Morales and M. Paniagua, *Energy Fuels*, 2007, **21**, 1782–1791.
143 P. McMorn, G. Roberts and G. J. Hutchings, *Catal. Lett.*, 1999, **63**, 193–197.
144 E. G. Rodrigues, M. F. R. Pereira and J. J. M. Orfao, *Appl. Catal., B*, 2012, **115–116**, 1–6.
145 S.-Y. Liu, C.-J. Zhou, Q. Liu, G.-C. Liu, C.-J. Huang and Z.-S. Chao, *ChemSusChem*, 2008, **1**, 575–578.
146 H. Kimura, K. Tsuto, T. Wakisaka, Y. Kazumi and Y. Inaya, *Appl. Catal., A*, 1993, **96**, 217–228.
147 R. Garcia, M. Besson and P. Gallezot, *Appl. Catal., A*, 1995, **127**, 165–176.
148 N. Dimitratos, A. Villa, C. L. Bianchi, L. Prati and M. Makkee, *Appl. Catal., A*, 2006, **311**, 185–192.
149 S. Demirel-Gülen, M. Lucas and P. Claus, *Catal. Today*, 2005, **102–103**, 166–172.
150 W. C. Ketchie, Y.-L. Fang, M. S. Wong, M. Murayana and R. J. Davis, *J. Catal.*, 2007, **250**, 94–101.
151 A. Villa, A. Gaiassi, I. Rossetti, C. L. Bianchi, L. Prati, K. van Benthem, G. M. Veith and L. Prati, *J. Catal.*, 2010, **275**, 108–116.
152 E. G. Rodrigues, M. F. R. Pereira, J. J. Delgado, X. Chen and J. J. M. Orfao, *Catal. Commun.*, 2011, **16**, 64–69.
153 M. Gharabi, F. T. Zangeneh, F. Yaripour and S. Sahebdelfar, *Appl. Catal., A*, 2012, **443–444**, 8–26.
154 (*a*) L. Su, L. Liu, J. Zhuang, H. Wang, Y. Li, W. Shen, Y. Xu and X. Bao, *Catal. Lett.*, 2003, **91**, 155–167; (*b*) N. Chu, J. Yang, C. Li, J. Cui, Q. Zhao, X. Yin, J. Lu and J. Wang, *Microporous Mesoporous Mater.*, 2009, **118**, 169–175.
155 A. Martinez, E. Peris, M. Derewinski and A. Burkat-Dulak, *Catal. Today*, 2011, **169**, 75–84.
156 N. B. Chu, J. Q. Wang, Y. Zhang, J. H. Yang, J. M. Lu and D. H. Yin, *Chem. Mater.*, 2010, **22**, 2757–2763.
157 Y. Wang, X. Wang, Z. Su, Q. Guo, Q. Tang, Q. Zhang and H. Wan, *Catal. Today*, 2004, **93–95**, 155–161.
158 (*a*) J. He, Y. Li, D. An, Q. Zhang and Y. Wang, *J. Nat. Gas Chem.*, 2009, **18**, 288–294; (*b*) Y. Li, D. An, Q. Zhang and Y. Wang, *J. Phys. Chem. C*, 2008, **112**, 13700–13708.
159 M. Rezaei, S. M. Alavi, S. Sahebdelfar and Z.-F. Yan, *J. Nat. Gas Chem.*, 2008, **17**, 278–282.
160 (*a*) J. Kang, K. Cheng, L. Zhang, Q. Zhang, J. Ding, W. Hua, Y. Lou, Q. Zhai and Y. Wang, *Angew. Chem.*, 2011, **123**, 5306–5309; (*b*) S. Sartipi, K. Parashar, M. Makkee, J. Gascon and F. Kapteijn, *Catal. Sci. Technol.*, 2013, **3**, 572–575; (*c*) S. Sarpiti, M. Alberts, M. J. Meijerink, T. C. Keller, J. Pérez-Ramirez, J. Gascon and F. Kapteijn, *ChemSusChem*, 2013, 1646–1650; (*d*) S. Sartini, M. Alberts, V. P. Santos, M. Nasalevich, J. Gascon and F. Kapteijn, *ChemCatChem*, 2014, **6**, 142–151.
161 (*a*) M. W. E. van den Berg, S. Polarz, O. P. Tkachenko, K. V. Klementiev, M. Bandyopadhyay, L. Khodeir, H. Gies, M. Muhler and W. Grünert, *J. Catal.*, 2006, **241**, 446–455; (*b*) M. W. E. van den Berg, S. Polarz, O. P. Tkachenko, K. Kahler, M. Muhler and W. Grünert, *Catal. Lett.*, 2009, **128**, 49–56.
162 (*a*) Q. Tang, H. Xu, Y. Zheng, J. Wang, H. Li and J. Zhang, *Appl. Catal., A*, 2012, **413–414**, 36–42; (*b*) K. Cho, H. S. Cho, L. C. de Menorval and R. Ryoo, *Chem. Mater.*, 2009, **21**, 5664–5673.
163 (*a*) M. Sugimoto, H. Katsuno, K. Takatsu and N. Kawata, *Zeolites*, 1987, **7**, 503–507; (*b*) M. Bjorgen, F. Joensen, M. S. Holm, U. Olsbye, K.-P. Lillerud and S. Svelle, *Appl. Catal., A*, 2008, **345**, 43–50; (*c*) J. Kim, M. Choi and R. Ryoo, *J. Catal.*, 2010, **269**, 219–228; (*d*) A. A. Rownaghi, F. Rezaei and J. Hedlund, *Microporous Mesoporous Mater.*, 2012, **151**, 26–33; (*e*) P. N. R. Vennestrom, M. Grill, M. Kustova, K. Egeblad, L. F. Lundegaard, F. Joensen, C. H. Christensen and P. Beato, *Catal. Today*, 2011, **168**, 71–79.
164 N. Armaroli and V. Balzani, *ChemSusChem*, 2011, **4**, 21–36.
165 J. Tollefson, *Nature*, 2010, **464**, 1262–1264.
166 H. F. Abbas and W. M. A. W. Daud, *Int. J. Hydrogen Energy*, 2010, **35**, 1160–1190.
167 D. P. Serrano, J. M. Coronado, V. A. de la Peña O'Shea, P. Pizarro and J. A. Botas, *J. Mater. Chem. A*, 2013, **1**, 12016–12027.
168 E. Reisner, *Eur. J. Inorg. Chem.*, 2011, 1005–1016.
169 A. Paracchino, V. Laporte, K. Sivula, M. Grätzel and E. Thimsen, *Nat. Mater.*, 2011, **10**, 456–461.
170 *Hydrogen and Syngas, Production and Purifcation Technologies*, ed. K. Lui, C. Song and V. Subramani, John Wiley & Sons, Inc., Hoboken, NJ, USA, 2010.
171 J. R. R. Nielsen, *J. Catal.*, 1973, **31**, 173–199.
172 G. Jones, J. G. Jakobsen, S. S. Shim, J. Kleis, M. P. Andersson, J. Rossmeisl, F. A. Pedersen, T. Bligaard, S. Helveg, B. Hinnemann, J. R. R-Nielsne, I. Chorkendorff, J. Sehested and J. N. Norskov, *J. Catal.*, 2008, **259**, 147–160.
173 J. H. Kim, D. J. Suh, T. J. Park and K. L. Kim, *Appl. Catal., A*, 2000, **197**, 191–200.
174 G. Li, L. Hu and J. M. Hill, *Appl. Catal., A*, 2006, **301**, 16–24.
175 J. G. Seo, M. H. Youn, S. Park, J. C. Jung, P. Kim, J. S. Chung and I. K. Song, *J. Power Sources*, 2009, **186**, 178–184.
176 Y. Bang, J. Lee, S. J. Han, J. G. Seo, M. H. Youn, J. H. Song and I. K. Song, *Int. J. Hydrogen Energy*, 2012, **37**, 11208–11217.
177 Y. Bang, S. J. Han, J. G. Seo, M. H. Youn, J. H. Song and I. K. Song, *Int. J. Hydrogen Energy*, 2012, **37**, 17967–17977.
178 J. Yoo, Y. Bang, S. J. Han, T. H. Kang, J. Lee and I. K. Song, *J. Mol. Catal. A: Chem.*, 2013, **380**, 28–33.
179 N. Wang, W. Chu, T. Zhang and X. S. Zhao, *Int. J. Hydrogen Energy*, 2012, **37**, 19–30.
180 M. Lindo, A. J. Vizcaíno, J. A. Calles and A. Carrero, *Int. J. Hydrogen Energy*, 2010, **35**, 5895–5901.

181 S. J. Han, Y. Bang, J. Yoo, J. G. Seo and I. K. Song, *Int. J. Hydrogen Energy*, 2013, **38**, 8285–8292.
182 S. J. Han, Y. Bang, J. Yoo, K. H. Kang, J. H. Song, J. G. Seo and I. K. Song, *Int. J. Hydrogen Energy*, 2013, **38**, 15119–15127.
183 Y. Bang, S. J. Han, J. Yoo, J. H. Choi, K. H. Kang, J. H. Song, J. G. Seo, J. C. Jung and I. K. Song, *Int. J. Hydrogen Energy*, 2013, **38**, 8751–8758.
184 J. F. C. Serra, M. T. Navarro, F. Rey and A. Chica, *Int. J. Hydrogen Energy*, 2012, **37**, 7101–7108.
185 J. S. Lee, G. B. Han and M. Kang, *Energy*, 2012, **44**, 248–256.
186 H. D. Kim, T. W. Kim, H. J. Park, K. E. Jeong, H. J. Chae, S. Y. Jeong, C. H. Lee and C. U. Kim, *Int. J. Hydrogen Energy*, 2012, **37**, 12187–12197.
187 J. A. Botas, D. P. Serrano, R. G. López, P. Pizarro and G. Gómez, *Int. J. Hydrogen Energy*, 2010, **35**, 9788–9794.
188 D. P. Serrano, J. A. Botas, P. Pizarro and G. Gómez, *Int. J. Hydrogen Energy*, 2013, **38**, 5671–5683.
189 L. Jin, H. Si, J. Zhang, P. Lin, Z. Hu, B. Qiu and H. Hu, *Int. J. Hydrogen Energy*, 2013, **38**, 10373–10380.
190 H. Tan, K. Li, S. Sioud, D. Cha, M. H. Amad, M. N. Hedhili and Z. A. A. Talla, *Catal. Commun.*, 2012, **26**, 248–252.
191 F. E. Osterloh, *Chem. Mater.*, 2008, **20**, 35–54.
192 M. D. H. Alonso, F. Fresno, S. Suárez and J. M. Coronado, *Energy Environ. Sci.*, 2009, **2**, 1231–1257.
193 K. Maeda and K. Domen, *J. Phys. Chem. Lett.*, 2010, **1**, 2655–2661.
194 R. M. N. Yerga, M. C. A. Galván, F. Vaquero, J. Arenales and J. L. G. Fierro, *Renewable Hydrogen Technol.: Prod., Purif., Storage, Appl. Saf.*, 2013, 43–61.
195 H. Yang, L. Guo, W. Yan and H. Liu, *J. Power Sources*, 2006, **159**, 1305–1309.
196 D. Jing and L. Guo, *Catal. Commun.*, 2007, **8**, 795–799.
197 S. Onsuratoom, S. Chavadej and T. Sreethawong, *Int. J. Hydrogen Energy*, 2011, **36**, 5246–5261.
198 H. Dang, X. Dong, Y. Dong, Y. Zhang and S. Hampshire, *Int. J. Hydrogen Energy*, 2013, **38**, 2126–2135.
199 (*a*) S. H. Liu and H. P. Wang, *Int. J. Hydrogen Energy*, 2002, **27**, 859–862; (*b*) D. Zhao, A. Rodriguez, N. M. Dimitrijevic, T. Rajh and R. T. Koodall, *J. Phys. Chem. C*, 2010, **114**, 15728–15734.
200 R. Peng, D. Zhao, M. M. Dimitrijevic, T. Rajh and R. T. Koodall, *J. Phys. Chem. C*, 2012, **116**, 1605–1613.
201 IEA, CO_2 emissions from fuel combustion 2012.
202 G. Centi and S. Perathoner, *Stud. Surf. Sci. Catal.*, 2004, **153**, 1–8.
203 M. Aresta, A. Dibenedetto, F. Nocita, C. Pastore, A. M. Venezia, F. Chirikalova, V. I. Kononenko, V. G. Shevchenko and I. A. Chupova, *Catal. Today*, 2006, **115**, 117–123.
204 T. Sakakura, J. C. Choi and H. Yasuda, *Chem. Rev.*, 2007, **107**, 2365–2387.
205 I. Omae, *Catal. Today*, 2006, **115**, 33–52.
206 P. G. Jessop, E. Joo and C. C. Tai, *Coord. Chem. Rev.*, 2004, **248**, 2425–2442.
207 G. Centi and S. Perathoner, *Catal. Today*, 2009, **148**, 191–205.
208 C. Song, *Catal. Today*, 2006, **115**, 2–32.
209 H. Arakawa, M. Aresta, J. N. Armor, M. A. Barteau, E. J. Beckman, A. T. Bell, J. E. Bercaw, C. Creutz, E. Dinjus, D. A. Dixon, K. Domen, D. L. DuBois, J. Eckert, E. Fujita, D. H. Gibson, W. A. Goddard, D. W. Goodman, J. Keller, G. J. Kubas, H. H. Kung, J. E. Lyons, L. E. Manzer, T. J. Marks, K. Morokuma, K. M. Nicholas, R. Periana, L. Que, J. R. Nielson, W. M. H. Sachtler, L. D. Schmidt, A. Sen, G. A. Somorjai, P. C. Stair, B. R. Stults and W. Tumas, *Chem. Rev.*, 2001, **101**, 953–996.
210 L. Lloyd, *Handbook of Industrial Catalysts*, Springer, New York, USA, 2011.
211 J. L. G. Fierro, *Metal Oxides: Chemistry and Applications*, CRC Taylor & Francis Pub., Boca Raton, FL, USA, 2006, ch. 18, p. 569.
212 H. Sano, *Energy Convers. Manage.*, 1995, **36**, 895–898.
213 L. Fan and K. Fujimoto, *J. Catal.*, 1994, **150**, 217–220.
214 X. L. Liang, X. Dong, G. D. Lin and H. B. Zhang, *Appl. Catal., B*, 2009, **88**, 315–322.
215 K. P. Yu, W. Y. Yu, M. C. Kuo, Y. C. Liou and S. H. Chien, *Appl. Catal., B*, 2008, **84**, 112–118.
216 T. Fujitani, M. Saito, Y. Kanai, Y. Watanabe, J. Nakamura and T. Uchijima, *Appl. Catal., A*, 1995, **125**, L199–L202.
217 J. Stoczyniskia, R. Grabowskia, P. Olszewskia, A. Kozlowskaa, J. Stoch and M. Lachowskab, *Appl. Catal., A*, 2006, **310**, 127–137.
218 S. E. Collins, D. L. Chiavassa, A. L. Bonivardi and M. A. Baltanás, *Catal. Lett.*, 2005, **103**, 83–88.
219 C. S. Song and K. M. Reddy, *Appl. Catal., A*, 1999, **176**, 1–10.
220 Y. Ohtsuka, T. Arai, S. Takasaki and N. Tsubouchi, *Energy Fuels*, 2003, **17**, 804–809.
221 E. Ghedini, F. Menegazzo, M. Signoretto, M. Manzoli, F. Pinna and G. Strukul, *J. Catal.*, 2010, **273**, 266–273.
222 Y. M. Yu, J. H. Fei, Y. P. Zhang and X. M. Zheng, *J. Fuel Chem. Technol.*, 2006, **34**, 700–705.
223 N. Kosizumi, X. Jiang, J. Kugai and C. Song, *Catal. Today*, 2012, **194**, 16–24.
224 M. Maestri, D. G. Vlachos, A. Beratta, G. Groppi and E. Tronconi, *J. Catal.*, 2008, **259**, 211–222.
225 X. Wu and S. Kawi, *Catal. Today*, 2009, **148**, 251–259.
226 L. Xu, H. Song and L. Chou, *Catal. Sci. Technol.*, 2011, **1**, 1032–1042.
227 L. Xu, H. Song and L. Chou, *Appl. Catal., B*, 2011, **108–109**, 177–190.
228 B. Sarkar, R. Tiwari, R. K. Singha, S. Suman, S. Ghosh, S. S. Acharyya, K. Mantri, L. N. S. Konathala, C. Penden and R. Bal, *Catal. Today*, 2012, **198**, 209–214.
229 L. Xu, H. Song and L. Chou, *Int. J. Hydrogen Energy*, 2012, **37**, 18001–18020.
230 Y. Takahashi and T. Yamazaki, *Fuel*, 2012, **102**, 239–246.
231 H. Liu, Y. Li, H. Wu, T. Miyake and D. He, *Int. J. Hydrogen Energy*, 2013, **38**, 15200–15209.
232 B. Li and S. Zhang, *Int. J. Hydrogen Energy*, 2013, **38**, 14250–14260.
233 S. Zeng, X. Fu, T. Zhou, X. Wang and H. Su, *Fuel Process. Technol.*, 2013, **114**, 69–74.

234 A. Y. Khodakov, W. Chu and P. Fongarland, *Chem. Rev.*, 2007, **107**, 1692–1744.
235 Y. H. Guo, C. Xia and B. S. Liu, *Chem. Eng. J.*, 2014, **237**, 421–429.
236 K. Nakagawa, M. Okamura, N. Ikenaga, T. Suzuki and T. Kobayashi, *Chem. Commun.*, 1998, 1025–1026.
237 I. Takahara and M. Saito, *Chem. Lett.*, 1996, 973–974.
238 K. T. Leth, A. K. Rovik, M. S. Holm, M. Brorson, H. J. Jakobsen, J. Skibsted and C. H. Christensen, *Appl. Catal., A*, 2008, **348**, 257–265.
239 T. V. M. Rao, Y. Yang and A. Sayari, *J. Mol. Catal. A: Chem.*, 2009, **301**, 152–158.
240 T. V. M. Rao, E. M. Zahidi and A. Sayari, *J. Mol. Catal. A: Chem.*, 2009, **301**, 159–165.
241 P. Michorczyk, J. Ogonowski, P. Kustrowski and L. Chmielarz, *Appl. Catal., A*, 2008, **349**, 62–69.
242 F. Zhang, R. Xu, Y. Yue, W. Yang, S. Gu, C. Miao, W. Hua and Z. Gao, *Microporous Mesoporous Mater.*, 2011, **145**, 194–199.
243 G. Wang, L. Zhang, J. Deng, H. Dai, H. He and C. T. Au, *Appl. Catal., A*, 2009, **355**, 192–201.
244 Y. Qiao, C. Miao, Y. Yue, Z. Xie, W. Yang, W. Hua and Z. Gao, *Microporous Mesoporous Mater.*, 2009, **119**, 150–157.
245 S. Udayakumar, M. K. Lee, H. L. Shim and D. W. Park, *Appl. Catal., A*, 2009, **365**, 88–95.
246 J. N. Appaturi and F. Adam, *Appl. Catal., B*, 2013, **136–137**, 150–159.
247 D. B. Nale, S. Rana, K. Parida and B. M. Bhanage, *Appl. Catal., A*, 2014, **469**, 340–349.
248 R. Zhang, A. A. Elzatahry, S. S. Al-Deyab and D. Zhao, *Nano Today*, 2012, **7**, 344–366.
249 X. Chen and S. S. Mao, *Chem. Rev.*, 2007, **107**, 2891–2959.
250 S. Wang, H. M. Ang and M. O. Tade, *Environ. Int.*, 2007, **33**, 694–705.
251 P. Van Der Voort, P. I. Ravikovitch, K. P. De Jong, A. V. Neimark, A. H. Janssen, M. Benjelloum, E. Van Bavel, P. Cool, B. M. Wechuysen and E. F. Vansant, *Chem. Commun.*, 2002, 1010–1011.
252 M. Kruk, M. Jaroniec, S. H. Joo and R. Ryoo, *J. Phys. Chem. B*, 2003, **107**, 2205–2213.
253 F. Bosc, P. L. Desmazes and A. Ayral, *J. Colloid Interface Sci.*, 2006, **304**, 545–548.
254 J. I. L. Chen, G. von Freymann, V. Kitaev and G. A. Ozin, *J. Am. Chem. Soc.*, 2007, **129**, 1196–1202.
255 L. Saadoun, J. A. Ayllon, J. Jiménez-Becerril, J. Peral, X. Domènech and R. Rodríguez-Clemente, *Mater. Res. Bull.*, 2000, **35**, 193–202.
256 X. Wang, J. C. Yu, C. Ho, Y. Hou and X. Fu, *Langmuir*, 2005, **21**, 2552–2559.
257 J. Yu, Y. Su and B. Cheng, *Adv. Funct. Mater.*, 2007, **17**, 1984–1990.
258 M. S. Hamdy, O. Berg, J. C. Jansen, T. Maschmeyer, J. A. Moulijm and G. Mul, *Chem. - Eur. J.*, 2006, **12**, 620–628.
259 A. M. Busuioc, V. Meynen, E. Beyers, P. Cool, N. Bilba and E. F. Vansant, *Catal. Commun.*, 2007, **8**, 527–530.
260 M. Tasbihi, U. L. Stangar, A. Ristic, V. Kaucic and N. N. Tusar, *J. Photochem. Photobiol., A*, 2010, **216**, 167–178.
261 W. Dong, Y. Sun, Q. Ma, L. Zhu, W. Hua, X. Lu, G. Zhuang, S. Zhang, Z. Guo and D. Zhao, *J. Hazard. Mater.*, 2012, **229–230**, 307–320.
262 R. Y. Zhang, B. Tu and D. Y. Zhao, *Chem. - Eur. J.*, 2010, **16**, 9977–9981.
263 S. Zhu, D. Zhang, Z. Chen, G. Zhou, H. Jiang and J. Li, *J. Nanopart. Res.*, 2010, **12**, 2445–2456.
264 F. He, J. Li, T. Li and G. Li, *Chem. Eng. J.*, 2014, **237**, 312–321.
265 M. Zhou, J. Yu and B. Cheng, *J. Hazard. Mater.*, 2006, **137**, 1838–1847.
266 A. A. Ismail, *Appl. Catal., B*, 2012, **117–118**, 67–72.
267 A. A. Ismail, *Microporous Mesoporous Mater.*, 2012, **149**, 69–75.
268 J. Choina, Ch. Fischer, G. U. Flechsig, H. Kosslick, V. A. Tuan, N. D. Tuyen, N. A. Tuyen and A. Schulz, *J. Photochem. Photobiol., A*, 2014, **274**, 108–116.
269 J. Nesic, D. D. Manojlovic, I. Andelkovic, B. P. Dojcinovic, P. J. Vulic, J. Krstic and G. M. Roglic, *J. Mol. Catal. A: Chem.*, 2013, **378**, 67–75.
270 P. S. S. Kumar, M. R. Raj and S. Anandan, *Sol. Energy Mater. Sol. Cells*, 2010, **94**, 1783–1789.
271 C. Zhan, F. Chen, H. Dai, J. Yang and M. Zhong, *Chem. Eng. J.*, 2013, **225**, 695–703.
272 X. Yan, X. Zong, G. Q. Lu and L. Wang, *Prog. Nat. Sci.*, 2012, **22**, 654–660.
273 Z. Hu, L. Xu and J. Chen, *Mater. Lett.*, 2013, **106**, 421–424.
274 Y. Shiraishi, Y. Teshima and T. Hirai, *J. Phys. Chem. B*, 2006, **110**, 6257–6263.
275 S. Rodriguez, S. Uma, I. N. Martyanov and K. J. Klabunde, *J. Photochem. Photobiol., A*, 2004, **165**, 51–58.
276 S. Rodríguez, K. T. Ranjit, S. Uma, I. N. Martyanov and K. J. Klabunde, *J. Catal.*, 2005, **230**, 158–165.
277 S. Rodríguez, S. Uma, I. N. Martyanov and K. J. Klabunde, *J. Catal.*, 2005, **233**, 405–410.
278 E. C. C. Baly, I. M. Heilbron and W. F. Barker, *J. Chem. Soc. Trans.*, 1921, **119**, 1025–1035.
279 M. Tahir and N. A. S. Amin, *Renewable Sustainable Energy Rev.*, 2013, **25**, 560–579.
280 A. Fujishima and K. Honda, *Nature*, 1972, **238**, 37–38.
281 T. Inoue, A. Fujishima, S. Konishi and K. Honda, *Nature*, 1979, **277**, 637–638.
282 J. S. Hwang, J. S. Chang, S. E. Park, K. Ikeue and M. Anpo, *Top. Catal.*, 2005, **35**, 311–319.
283 N. Ulagappan and H. Frei, *J. Phys. Chem. A*, 2000, **104**, 7834–7839.
284 W. Lin and F. Frei, *J. Am. Chem. Soc.*, 2005, **127**, 1610–1611.
285 M. Tahir and N. A. S. Amin, *Appl. Catal., A*, 2013, **467**, 483–496.
286 Y. Li, W. N. Wang, Z. Zhan, M. H. Woo, C. Y. Wu and P. Biswas, *Appl. Catal., B*, 2010, **100**, 386–392.
287 Y. Wang, B. Li, C. Zhang, L. Cui, S. Kang, X. Li and L. Zhou, *Appl. Catal., B*, 2013, **130–131**, 277–284.

288 Y. Wang, F. Wang, Y. Chen, D. Zhang, B. Li, S. Kang, X. Li and L. Cui, *Appl. Catal., B*, 2014, **147**, 602–609.
289 C. Copéret, M. Chabanas, R. P. Saing-Arroman and J. M. Basset, *Angew. Chem., Int. Ed.*, 2003, **42**, 156–181.
290 K. D. Dubois, H. He, C. Liu, A. S. Vorushilov and G. Li, *J. Mol. Catal. A: Chem.*, 2012, **363–364**, 208–213.
291 S. B. Yoon, B. Fang, M. Kim, J. Ho Kim and J.-S. Yu, in *Frontiers of Nanoscience, Nanostructured Materials*, ed. G. Wilde, Elsevier, Amsterdam, the Netherlands, 2009, vol. 1, pp. 173–231.
292 R. M. Ormerod, *Chem. Soc. Rev.*, 2003, **32**, 17–28.
293 A comparison between the different fuel cell types can be found in: S. Mekhilef, R. Saidurb and A. Safaria, *Renewable Sustainable Energy Rev.*, 2012, **16**, 981–989.
294 S. Giddey, S. P. S. Badwal, A. Kulkarni and C. Munnings, *Prog. Energy Combust. Sci.*, 2012, **38**, 360–399.
295 J.-J. Hwang, *Renewable Sustainable Energy Rev.*, 2013, **19**, 220–229.
296 M. W. Ellis, M. R. Von Spakovsky and D. J. Nelson, *Proc. IEEE*, 2001, **89**, 1808–1818.
297 N. V. Long, Y. Yang, C. M. Thi, N. V. Minh, Y. Cao and M. Nogami, *Nano Energy*, 2013, **2**, 636–676.
298 S. Sharma and B. G. Pollet, *J. Power Sources*, 2012, **208**, 96–119.
299 (*a*) J. B. Xu and T. S. Zhao, *RSC Adv.*, 2013, **3**, 16–24; (*b*) J. Liang, S. Z. Qiao, G. Q. Lu and D. Hulicova-Jurcakova, in *Novel Carbon Adsorbents*, ed. Juan. M. D. Tascón, Elsevier, Oxford, 2012, pp. 549–581; (*c*) E. Antolini, *Appl. Catal., B*, 2009, **88**, 1–24.
300 Y.-J. Wang, D. P. Wilkinson and J. Zhang, *Chem. Rev.*, 2011, **111**, 7625–7651.
301 S. Zhang, Y. Shao, G. Yin and Y. Lin, *J. Mater. Chem. A*, 2013, **1**, 4631–4641.
302 L. Calvillo, V. Celorrio, R. Moliner, A. B. Garcia, I. Caméan and M. J. Lazaro, *Electrochim. Acta*, 2013, **102**, 19–27.
303 J. R. C. Salgado, V. A. Paganin, E. R. Gonzalez, M. F. Montemor, I. Tacchini, A. Ansón, M. A. Salvador, P. Ferreira, F. M. L. Figueiredo and M. G. S. Ferreira, *Int. J. Hydrogen Energy*, 2013, **38**, 910–920.
304 J. Cao, Z. Chen, J. Xu, W. Wang and Z. Chen, *Electrochim. Acta*, 2013, **88**, 184–192.
305 R. Silva, D. Voiry, M. Chhowalla and T. Asefa, *J. Am. Chem. Soc.*, 2013, **135**, 7823–7826.
306 R. Li, H. Mao, J. Zhang, T. Huang and A. Yu, *J. Power Sources*, 2013, **241**, 660–667.
307 (*a*) M. Yang, R. Guarecuco and F. J. DiSalvo, *Chem. Mater.*, 2013, **25**, 1783–1787; (*b*) M. Yang, Z. Cui and F. J. DiSalvo, *Phys. Chem. Chem. Phys.*, 2013, **15**, 7041–7044; (*c*) M. Yang, Z. Cui and F. J. DiSalvo, *Phys. Chem. Chem. Phys.*, 2013, **15**, 1088–1092; (*d*) Z. Cui, R. G. Burns and F. J. DiSalvo, *Chem. Mater.*, 2013, **25**, 3782–3784.
308 (*a*) A. Kumar and V. K. Ramani, *Appl. Catal., B*, 2013, **138–139**, 43–50; (*b*) C.-P. Lo, G. Wang, A. Kumar and V. Ramani, *Appl. Catal., B*, 2013, **140–141**, 133–140.
309 (*a*) Q. Wang, G. Wang, K. Sasaki, T. Takeguchi, T. Yamanaka, M. Sadakane and W. Ueda, *J. Power Sources*, 2013, **241**, 728–735; (*b*) J. Zhang, J.-p. Tu, G.-h. Du, Z.-m. Dong, Q.-m. Su, D. Xie and X.-l. Wang, *Electrochim. Acta*, 2013, **88**, 107–111; (*c*) H. Hua, C. Hu, Z. Zhao, H. Liu, X. Xie and Y. Xi, *Electrochim. Acta*, 2013, **105**, 130–136; (*d*) M. P. Gurrola, M. Guerra-Balcázar, L. Álvarez-Contreras, R. Nava, J. Ledesma-García and L. G. Arriaga, *J. Power Sources*, 2013, **243**, 826–830.
310 R. Zolfaghari, F.-R. Ahmadun, M. R. Othman, W. R. W. Daud and M. Ismail, *Mater. Chem. Phys.*, 2013, **139**, 262–269.
311 K. K. Tintula, A. Jalajakshi, A. K. Sahu, S. Pitchumani, P. Sridhar and A. K. Shukla, *Fuel Cells*, 2013, **13**, 158–166.
312 M. M. Bruno, M. A. Petruccelli, F. A. Viva and H. R. Corti, *Int. J. Hydrogen Energy*, 2013, **38**, 4116–4123.
313 S. Song, K. Wang, Y. Liu, C. He, Y. Liang, R. Fu, D. Wu and Y. Wang, *Int. J. Hydrogen Energy*, 2013, **38**, 1405–1412.
314 (*a*) F. Li, K.-Y. Chan, H. Yung, C. Yang and S. W. Ting, *Phys. Chem. Chem. Phys.*, 2013, **15**, 13570–13577; (*b*) S.-J. Park, B.-J. Kim and S.-Y. Lee, *J. Colloid Interface Sci.*, 2013, **405**, 150–156.
315 (*a*) A. M. Baena-Moncada, G. A. Planes, M. S. Moreno and C. A. Barbero, *J. Power Sources*, 2013, **221**, 42–48; (*b*) Q.-X. Li, H.-M. Mao, J.-G. Li and Q.-J. Xu, *J. Fuel Cell Sci. Technol.*, 2013, **10**, 051006; (*c*) C. Y. Wong, S.-K. Chen, A.-Y. Lo, C.-M. Tseng, C.-Y. Lin and S.-B. Liu, *Int. J. Hydrogen Energy*, 2013, **38**, 12984–12990.
316 C. Alegre, M. E. Gálvez, E. Baquedano, R. Moliner, E. Pastor and M. J. Lázaro, *J. Phys. Chem. C*, 2013, **117**, 13045–13058.
317 D. Banham, F. Feng, K. Pei, S. Ye and V. Birss, *J. Mater. Chem. A*, 2013, **1**, 2812–2820.
318 S. Shrestha, S. Asheghi, J. Timbro and W. E. Mustain, *Appl. Catal., A*, 2013, **464–465**, 233–242.
319 (*a*) K. Vaarmets, J. Nerut, E. Härk and E. Lust, *Electrochim. Acta*, 2013, **104**, 216–227; (*b*) K. Vaarmets, S. Sepp, J. Nerut, E. Härk, I. Tallo and E. Lust, *J. Solid State Electrochem.*, 2013, **17**, 1729–1741.
320 (*a*) J. Tang, T. Wang, X. Sun, Y. Guo, H. Xue, H. Guo, M. Liu, X. Zhang and J. He, *Microporous Mesoporous Mater.*, 2013, **177**, 105–112; (*b*) M. Lei, T. Z. Yang, W. J. Wang, K. Huang, R. Zhang, X. L. Fu, H. J. Yang, Y. G. Wang and W. H. Tang, *Int. J. Hydrogen Energy*, 2013, **38**, 205–211; (*c*) C. Rüdiger, J. Brumbarov, F. Wiesinger, S. Leonardi, O. Paschos, C. Valero Vidal and J. Kunze-Liebhäuser, *ChemCatChem*, 2013, **5**, 3219–3223.
321 (*a*) J. Zeng, C. Francia, C. Gerbaldi, V. Baglio, S. Specchia, A. S. Aricò and P. Spinelli, *Electrochim. Acta*, 2013, **94**, 80–91; (*b*) L. Samiee, F. Shoghi and A. Vinu, *Appl. Surf. Sci.*, 2013, **265**, 214–221.
322 (*a*) J. Y. Cheon, C. Ahn, D. J. You, C. Pak, S. H. Hur, J. Kim and S. H. Joo, *J. Mater. Chem. A*, 2013, **1**, 1270–1283; (*b*) X. Bo and L. Guo, *Electrochim. Acta*, 2013, **90**, 283–290; (*c*) J. Tang, T. Wang, X. Sun, Y. Hu, Q. Xie, Y. Guo, H. Xue and J. He, *Electrochim. Acta*, 2013, **90**, 53–62.
323 J. H. Kim, S. Y. Kwon, D. Bhattacharjya, G. S. Chai and J.-S. Yu, *J. Catal.*, 2013, **306**, 133–145.
324 (*a*) J. Yan, H. Meng, F. Xie, X. Yuan, W. Yu, W. Lin, W. Ouyang and D. Yuan, *J. Power Sources*, 2014, **245**,

772–778; (*b*) J.-e. Park, Y. J. Jang, Y. J. Kim, M.-s. Song, S. Yoon, D. H. Kim and S.-J. Kim, *Phys. Chem. Chem. Phys.*, 2014, **16**, 103–109; (*c*) J.-S. Lee, K. Jo, T. Lee, T. Yun, J. Cho and B.-S. Kim, *J. Mater. Chem. A*, 2013, **1**, 9603–9607.

325 B. O'Regan and M. Grätzel, *Nature*, 1991, **353**, 737.

326 A. Yella, H.-W. Lee, H. N. Tsao, C. Yi, A. K. Chandiran, Md. K. Nazeeruddin, E. W.-G. Diau, C.-Y. Yeh, S. M. Zakeeruddin and M. Grätzel, *Science*, 2011, **334**, 629–634.

327 An overview of the state-of-the-art conversion efficiencies in DSCs can be found in: H. M. Upadhyaya, S. Senthilarasu, M.-H. Hsu and D. K. Kumar, *Sol. Energy Mater. Sol. Cells*, 2013, **119**, 291–295.

328 G. Hodes and A. Zaban, in *Frontiers of Nanoscience, Nanostructured Materials*, ed. G. Wilde, Elsevier, Amsterdam, the Netherlands, 2009, vol. 1, pp. 232–269.

329 J. Burschka, N. Pellet, S.-J. Moon, R. Humphry-Baker, P. Gao, M. K. Nazeeruddin and M. l. Grätzel, *Nature*, 2013, **499**, 316–319.

330 T. Peng, W. Sun, X. Sun, N. Huang, Y. Liu, C. Bu, S. Guo and X.-Z. Zhao, *Nanoscale*, 2013, **5**, 337–341.

331 G. Wang, S. Kuang, D. Wang and S. Zhuo, *Electrochim. Acta*, 2013, **113**, 346–353.

332 S.-j. Xu, Y.-f. Luo, W. Zhong and Z.-h. Xiao, *New Carbon Mater.*, 2013, **28**, 254–261.

333 E. Ramasamy and J. Lee, *Chem. Commun.*, 2010, **46**, 2136–2138.

334 E. Ramasamy, J. Chun and J. Lee, *Carbon*, 2010, **48**, 4563–4565.

335 P. Srinivasu, S. P. Singh, A. Islam and L. Han, *Int. J. Photoenergy*, 2011, 617439.

336 (*a*) A. Kay and M. Grätzel, *Sol. Energy Mater. Sol. Cells*, 1996, **44**, 99–117; (*b*) K. Imoto, K. Takahashi, T. Yamaguchi, T. Komura, J. Nakamura and K. Murata, *Sol. Energy Mater. Sol. Cells*, 2003, **79**, 459–469; (*c*) T. N. Murakami, S. Ito, Q. Wang, M. K. Nazeeruddin, T. Bessho, I. Cesar, P. Liska, R. H. Bakar, P. Comte, P. Pechy and M. Grätzel, *J. Electrochem. Soc.*, 2006, **153**, A2255–A2261.

337 H. Alama and S. Ramakrishna, *Nano Energy*, 2013, **2**, 190–212.

338 *Waste Heat Recovery: Technologies and Opportunities in U.S. Industry*, U.S. Department of Energy, 2008.

339 W. Liu, X. Yan, G. Chen and Z. Ren, *Nano Energy*, 2012, **1**, 42–56.

340 G. A. Slack, in *CRC Handbook of Thermoelectrics*, ed. M. Rowe, CRC, Boca Raton, FL, 1995, pp. 407–440.

341 A. Shakouri and S. Li, *Proceedings of International Conference on Thermoelectrics*, Baltimore, September 1999.

342 Y. Zhang, T. Day, M. L. Snedaker, H. Wang, S. Krämer, C. S. Birkel, X. Ji, D. Liu, G. J. Snyder and G. D. Stucky, *Adv. Mater.*, 2012, **24**, 5065–5070.

343 (*a*) B. Qiu and X. Ruan, *Appl. Phys. Lett.*, 2010, **9**, 183103–183107; (*b*) J.-H. Lee, G. A. Galli and J. C. Grossman, *Nano Lett.*, 2008, **8**, 3750–3754; (*c*) Y. He, D. Donadio, J.-H. Lee, J. C. Grossman and G. Galli, *ACS Nano*, 2011, **5**, 1839–1844.

344 M.-H. Hong, S.-Y. Jung, T.-J. Ha, W.-S. Seo, Y. S. Lim, S. Shin, H. H. Cho and H.-H. Park, *Surf. Coat. Technol.*, 2013, **231**, 370–373.

345 S.-Y. Jung, T.-J. Ha, C.-S. Park, W.-S. Seo, Y. S. Lim, S. Shin, H. H. Cho and H.-H. Park, *Thin Solid Films*, 2013, **529**, 94–97.

346 S.-Y. Jung, T.-J. Ha, W.-S. Seo, Y. S. Lim, S. Shin, H. H. Cho and H.-H. Park, *J. Electron. Mater.*, 2011, **40**, 652–656.

347 T.-J. Ha, H.-H. Park, S.-Y. Jung, S.-J. Yoon, J.-S. Kim and H. W. Jang, *Thin Solid Films*, 2010, **518**, 7196–7198.

348 M.-H. Hong, C.-S. Park, S. Shin, H. H. Cho, W.-S. Seo, Y. S. Lim, J.-K. Lee and H.-H. Park, *J. Nanomater.*, 2013, 172504.

349 M.-H. Hong, C.-S. Park, W.-S. Seo, Y. S. Lim, J.-K. Lee and H.-H. Park, *J. Nanomater.*, 2013, 131537.

350 S. Walia, S. Balendhran, H. Nili, S. Zhuiykov, G. Rosengarten, Q. H. Wang, M. Bhaskaran, S. Sriram, M. S. Strano and K. Kalantar-zadeh, *Prog. Mater. Sci.*, 2013, **58**, 1443–1489.

351 J. Fang, C. B. Kang, Y. Huang, S. H. Tolbert and L. Pilon, *J. Phys. Chem. C*, 2012, **116**, 12926–12933.

352 H. Lee, D. Vashaee, D. Z. Wang, M. S. Dresselhaus, Z. F. Ren and G. Chen, *J. Appl. Phys.*, 2010, **107**, 094308.